EXPERIMENTAL ASSESSMENT OF AGGREGATES

by

Nicholas Robert Trimble

A thesis submitted in partial fulfillment
of the requirements for the degree

of

Master of Science

in

Civil Engineering

MONTANA STATE UNIVERSITY
Bozeman, Montana

July 2007

APPROVAL

of a thesis submitted by

Nicholas Robert Trimble

This thesis has been read by each member of the thesis committee and has been found to be satisfactory regarding content, English usage, format, citations, bibliographic style, and consistency, and is ready for submission to the Division of Graduate Education.

Dr. Robert L. Mokwa

Approved for the Department of Civil Engineering

Dr. Brett W. Gunnink

Approved for the Division of Graduate Education

Dr. Carl A. Fox

STATEMENT OF PERMISSION TO USE

In presenting this thesis in partial fulfillment of the requirements for a master's degree at Montana State University, I agree that the Library shall make it available to borrowers under rules of the Library.

Copying is allowable only for scholarly purposes, consistent with "fair use" as prescribed in the U.S. Copyright Law. Requests for permission for extended quotation from or reproduction of this thesis in whole or in parts may be granted only by the copyright holder.

Nicholas Robert Trimble

July 2007

ACKNOWLEDGEMENTS

The author extends his appreciation to family and friends for their support throughout the course of preparing this thesis. The author would also like to thank Bob Mokwa and Eli Cuelho for their valuable advice, guidance, and patience throughout the testing and writing that went into the preparation of this thesis.

Recognition is also extended to Montana Department of Transportation personnel in obtaining soil samples from around the state, and to Mike Mullings for conducting all R-value tests.

Acknowledgement of financial support for this research is extended to the Western Transportation Institute and the Montana Department of Transportation.

TABLE OF CONTENTS

TABLE OF CONTENTS - CONTINUED

LIST OF FIGURES

Figure Page

LIST OF FIGURES - CONTINUED

Figure Page

LIST OF FIGURES - CONTINUED

Figure Page

LIST OF FIGURES - CONTINUED

Figure Page

LIST OF TABLES

Table Page

ABSTRACT

An extensive suite of geotechnical laboratory tests were conducted to quantify differences in engineering properties of three crushed aggregates commonly used on Montana highway projects. The material types are identified in the Montana Supplemental Specifications as crushed base course (CBC, 1.5 to 2-inch maximum particle sizes) and crushed top surfacing (CTS, 0.75-inch maximum particle size). All aggregates were open-graded and contained relatively few fines. Results from R-value tests and direct shear (DS) tests performed on large samples (12-in by 12-in) indicate the CBC aggregates generally exhibited higher strength and stiffness than the CTS aggregates.

Drainage capacity was quantified by conducting multiple saturated constant head permeability (k) tests on 10-inch-diameter samples of each material type. Hydraulic properties of the materials examined in this study did not correlate well with aggregate type, but were found to correlate with pore properties. The fine fraction void ratio was correlated to k. It is derived from gradation and density, both parameters that are commonly tested in roadway construction projects. This could allow roadway designers to incorporate an estimate of k into their design, and could also allow quick comparisons of aggregate samples and the development of aggregate specifications.

X-ray CT scanning was performed to acquire pore size distributions of the materials. No differences between aggregate types could be discerned from the pore size distributions, but a strong correlation between the pore size of 80% passing and k was discovered. Additionally, an equation was presented for thresholding 2D X-ray CT soil images. This equation could be applied in future studies to help reduce the subjectivity of the thresholding process.

INTRODUCTION

Highway base courses are typically constructed using crushed and processed aggregate. Roadway designers currently have a number of options for specifying the base course material on Montana Department of Transportation (MDT) highway projects. The engineering characteristics of these various options have not been thoroughly investigated or quantified by MDT; consequently, the designer must rely on experience and habitual practices. This approach often leads to inconsistencies in design and occasionally misunderstandings between designers, contractors, and materials personnel in regards to aggregate specifications.

Three of the most commonly specified crushed and processed aggregates specified by MDT were examined in this study. Two of these materials were crushed base courses (CBC) and the other grade was crushed top surfacing (CTS). Based on particle size gradations, the three options for untreated base course examined here are: i) CBC Type A Grade 5, ii) CBC Type A Grade 6, and iii) CTS Type A Grade 2. The maximum allowable particle size for Grade 6 and 5 are 1.5 inches and 2 inches, respectively, while CTS Grade 2 has a maximum particle size of 0.75 inches. CTS materials have smaller maximum particle sizes than CBC materials because they are intended for different uses. CBC materials are used as full depth base course aggregate layers, while CTS materials are typically used in relatively thin lifts over the CBC aggregate layer to provide a smooth flat surface for the placement of asphalt concrete.

A series of laboratory tests were performed to quantify differences in the most important engineering properties of these three materials. The specific properties

examined in this study were: compaction, durability, strength, stiffness, and drainage capacity. These properties were quantified by synthesizing and analyzing results from the following laboratory tests:

- Particle size gradation,
- Modified Proctor density,
- Relative density (maximum and minimum index densities),
- Specific gravity,
- Los Angeles abrasion/degradation,
- R-value,
- Direct shear,
- Permeability, and
- X-ray computed tomography.

Several of these tests were performed for basic classification purposes. The equipment and procedures corresponding to each of these tests are considered standardized. These basic classification and materials tests included particle size gradation, modified Proctor density, relative density, specific gravity, and R-value tests. Because these tests are standardized, there is little discussion of the equipment, procedures, or interpretation of results in this report. The primary purpose of these tests was for classification and general characterization of the materials.

Direct shear and permeability testing are standardized by both ASTM and AASHTO, but not for the large particle sizes utilized in this study. Over-sized testing apparatus were utilized in each case; consequently, more detailed discussions of testing conditions and procedures are presented herein. These tests were a key aspect of this study because strength and drainage are both vitally important to the performance of base course aggregates and ultimately the pavement structure as a whole. Maximizing strength and stiffness yields less rutting, smaller pavement deflections, and ultimately

less cracking of the pavement surface. Maximizing drainage yields less water in the pavement structure; this reduces the damaging effects of water in the structural layers of roadways. Maximization of both of these properties ultimately translates into longer pavement service live.

X-ray computed tomography (CT) scanning was performed to attain pore size distributions, which cannot be attained using more traditional methods for aggregate materials with large pore sizes. Results from this testing were used to examine and quantify the relationship between permeability and pore size distribution. X-ray CT is not commonly used in soil analysis and there are no standardized testing procedures; consequently, a thorough discussion of background information and test conditions are presented.

MATERIALS

In Montana, untreated base courses generally consist of Crushed Base Course (CBC) aggregates. These CBC aggregates are specified by gradation in Section 701.02.4 of the Montana Supplemental Specifications. MDT has three different grading options for CBC aggregates. These grading options range from a maximum particle size of 2 inches down to a maximum particle size of 1.5 inches. As requested by MDT, this study utilizes the two most commonly specified base course aggregate gradations: Grade 6 and Grade 5. CBC-6A and CBC-5A aggregates have maximum particle sizes of 1.5 inches and 2 inches, respectively. The Type A designation indicates that they are untreated.

On some projects, a finer-grained leveling course is substituted for the top 0.15 feet of CBC. This leveling course has a smaller maximum particle size and is used in place of CBC at the top of the base course layer to provide a smooth level surface for the placement of asphalt concrete. Aggregates used for this purpose are termed Crushed Top Surfacing (CTS) aggregates, as specified in Section 701.02.6 of the Montana Supplemental Specifications. Like CBC aggregates, CTS aggregates are specified according to gradation. MDT has five different grading options for CTS aggregates. These grading options range from a maximum particle size of 1 inch down to a maximum particle size of 0.375 inch. As requested by MDT, this study utilized the 0.75-inch maximum particle size material, which is denoted by MDT as CTS Grade 2 Type A. The gradation specification limits for the three aggregates used in this study (CBC-6A, CBC-5A, and CTS-2A) are shown in Table 1.

Table 1. Material Specification Limits

Sieve Size	CBC-6A	CBC-5A	CTS-2A
2 in		100	
1 ½ in	100	94-100	
3/4 in	74-96	70-88	100
3/8 in	40-76	50-70	
No. 4	24-60	34-58	40-70
No. 10			25-55
No. 40	6-34	6-30	
No. 200	0-8	0-8	2-8

Note: specification limits are given in percent by weight passing square mesh sieves.

Fifteen different aggregate samples were originally proposed in this study, consisting of five samples of each base course category, each from a different source. The actual number of samples (14) was modified from the prescribed number due to the limited availability of CBC-5A samples. At the time of this study, only three CBC-5A samples were available from MDT. Consequently, an additional CBC-6A sample was added to the testing scheme to keep the total number of samples near the originally prescribed quantity. The modified materials schedule used in this study consisted of fourteen aggregates from a variety of locations across Montana, as shown in Figure 1.

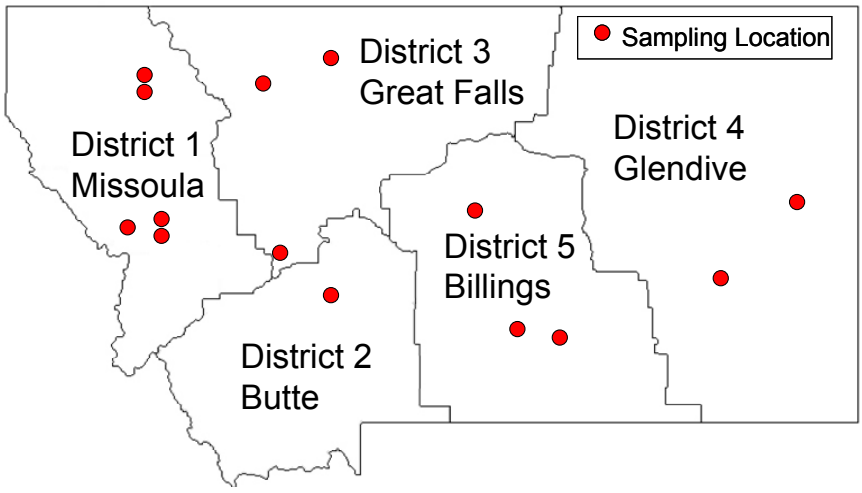

Figure 1. Location map showing origin of samples.

Table 2 shows the abbreviations for each material that will be used throughout this report. Samples that are of different aggregate type yet labeled under the same town name did not come from the same source pit, only from the same regional area. If each aggregate type were sampled from the same pit in each town some variability would have been eliminated. However, this would have required more samples to be tested increasing time and cost. Additionally, the samples used here were the only ones available at the time of sample collection.

Table 2. Materials Schedule

Aggregate Type		Abbreviation
CBC-6A	Butte	6A-Butte
	Missoula	6A-Missoula
	Glendive	6A-Glendive
	Billings	6A-Billings
	Great Falls	6A-Great Falls
	Kalispell	6A-Kalispell
CBC-5A	Missoula	5A-Missoula
	Great Falls	5A-Great Falls
	Kalispell	5A-Kalispell
CTS-2A	Missoula	2A-Missoula
	Billings	2A-Billings
	Glendive	2A-Glendive
	Lewistown	2A-Lewistown
	Havre	2A-Havre

Photographs of 6A, 5A, and 2A aggregates are presented in Figure 2, Figure 3, and Figure 4, respectively. All photos were taken at approximately the same scale, and a graduated scale in inches is shown at the bottom of each photo. The following

differences in particle size and gradation between the CBC type aggregates and the CTS type aggregates can be visually discerned by comparing Figure 2, Figure 3, and Figure 4.

- All aggregates are relatively well graded.
- 2A aggregates have a smaller maximum particle size (0.75 inches), while the 6A and 5A aggregates have larger maximum particle sizes (1.5 and 2 inches).
- The 5A aggregates appear to be slightly gap graded with some larger particles and an abundance of sand-size particles, while the 6A aggregates appear to have a better distribution and range of particle sizes.

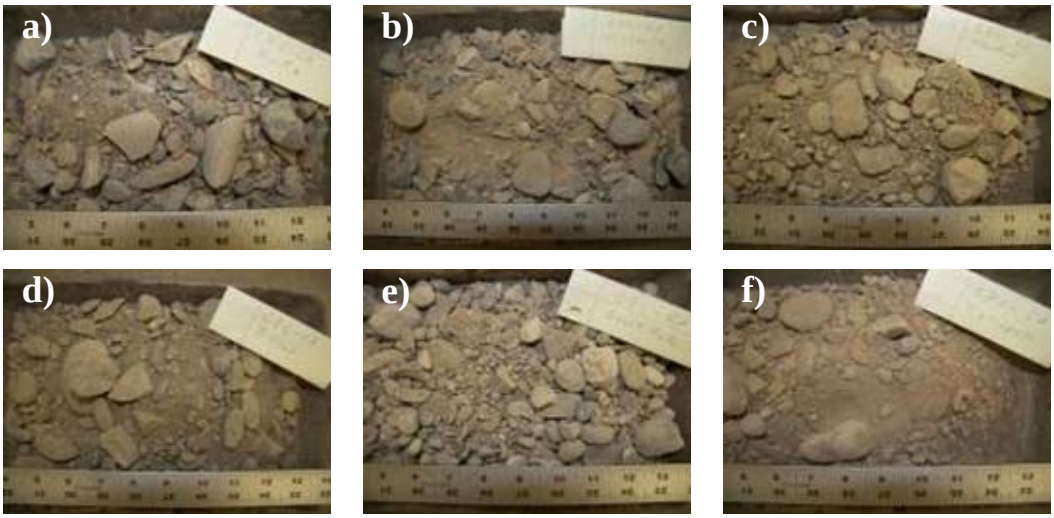

Figure 2. Pictures of CBC-6A samples from a) Butte, b) Missoula, c) Glendive, d) Billings, e) Great Falls, and f) Kalispell.

Figure 3. Pictures of CBC-5A samples from a) Missoula, b) Great Falls, and c) Kalispell.

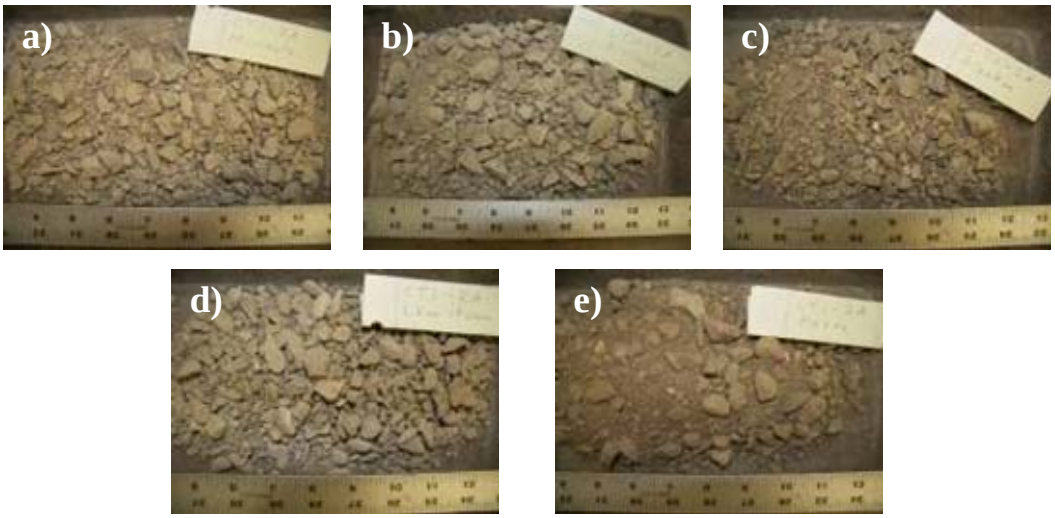

Figure 4. Pictures of CTS-2A samples from a) Missoula, b) Billings, c) Glendive, d) Lewistown, and e) Havre.

AGGREGATE MATERIALS TESTING

Aggregate materials testing includes any soils testing that would normally be performed on a base course aggregate on a MDT roadway construction project. This chapter begins with a description of the statistical testing that was used to evaluate results where averages for each aggregate type were examined. Soils tests that could be termed "index tests" are then presented (particle size distribution, modified Proctor compaction, relative density, and specific gravity). The Los Angeles abrasion and R-value tests are also commonly performed by the MDT materials laboratory for many roadway construction projects.

Statistical Evaluation of Results

The primary focus of this project is to determine relative differences in important engineering properties between three different aggregate types. Statistical analyses of average values based on aggregate type were conducted using the two sample t-test to determine if apparent trends in measured laboratory test results represent true differences between aggregate types. The following statistical symbols are used throughout this report:

- μ = average (also known as the mean)
- σ = standard deviation
- COV = coefficient of variation (σ/μ)

The two sample t-test is a statistical test used to determine if the averages of two data sets are statistically different based on a mathematical evaluation of data scatter. It can further be used to determine the relationship between the two averages; i.e., whether

one average is greater than, less than, or equal to the other. Three separate comparisons are required to determine the relationship between each set of test results (i.e., 6A versus 5A, 6A versus 2A, and 5A versus 2A).

The output of interest from this statistical test is the p-value parameter, which ranges from 0 to 1 based on the methodology used in this study. p-values from the two sample t-test can be used to indicate how two average values compare to each other taking into account data scatter and the number of data points. In this investigation, results from the two sample t-test were interpreted as follows:

- p-values between 0 and 0.15 indicated that one average was statistically less than another average;
- p-values between 0.85 and 1.0 indicated that one average is statistically greater than another average; and
- p-values between 0.15 and 0.85 indicated the two averages being compared are not statistically different, which is denoted here with an equal sign (see Figure 5).

This latter outcome may be because the averages were truly the same, or that the standard deviations are relatively large compared to the difference between the averages. In either case, no statistically significant differences can be discerned between the two averages. The two sample t-test does not inherently include cut-off p-values for evaluating the relationship between data sets; rather appropriate cutoff values must be selected by the user. The cut-off p-values of 0.15 and 0.85 were selected by the researchers in this study using judgment based on the relatively large variability that is typically observed in geotechnical test data.

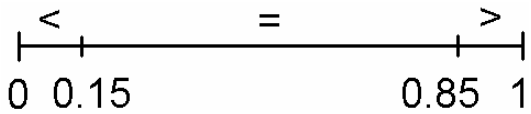

Figure 5. p-value ranges utilized in this study for the two sample t-test.

Particle Size Distribution

Grain size analyses were completed on each of the 14 samples in general accordance with AASHTO Test Method T311 and MDT Test Method MT202. Particle size distributions were compared to MDT specified upper and lower gradation limits, which are described in Sections 701.02.4 and 701.02.6 of the Montana Supplemental Specifications. Screen sizes used for gradation analyses were selected based on MDT specifications, as shown in Table 3. Figure 6 shows a comparison plot of the specification limits for the three aggregate types compared in this study.

Table 3. Sieve Sizes Utilized in this Study

Sieve Opening		**Standard Sieve Size**
(in)	**(mm)**	
2	50	-
1.5	37.5	-
1	25	-
0.75	19	-
0.5	12.5	-
0.375	9.5	-
0.187	4.75	No. 4
0.079	2	No. 10
0.017	0.425	No. 40
0.003	0.075	No. 200

A dash indicates that a standard sieve size does not exist for this sieve opening size.

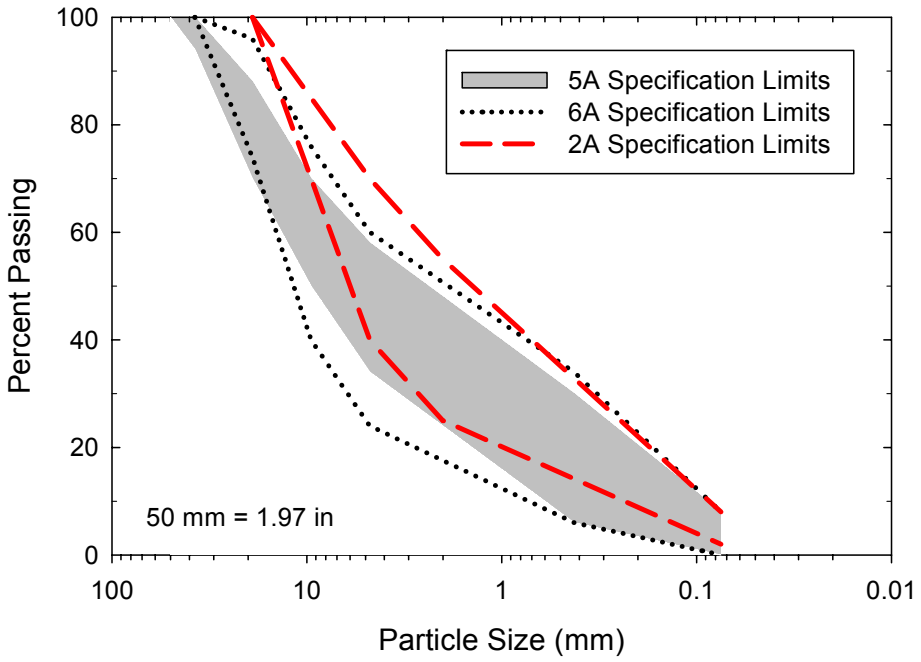

Figure 6. MDT specification limits for CBC-5A, CBC-6A, and CTS-2A.

Grain size analyses were performed by two separate labs. One set of analyses was performed at the Montana State University (MSU) geotechnical laboratories, and another set was completed by MDT. MSU grain size distributions are shown in Figure 7 through Figure 9, and copies of MDT grain size distributions are provided in Appendix A. Gradation plots compare favorably for the two sets of analyses, with only one notable difference; the MSU gradations show less fine material than the MDT grain size distributions. One explanation of the discrepancy between the results is that the MDT lab performed a wash test on the minus No. 4 size particles, while the MSU lab did not. Wash testing was not performed at the MSU lab because these materials contained relatively few fines and it was thought that washing would have a relatively minor impact on the results. The slight differences in results could also partially be attributed to

variations in methodologies used to fill the multiple sample bags at the source location, and particle segregation that may occur during sampling, splitting, and testing.

Nearly all samples were within MDT specification for both sets of gradations. Only two samples fall outside of specification for both sets of gradations. These two samples are 5A-Kalispell and to a much lesser extent 6A-Missoula. Several other samples fall slightly outside of specification depending on which set of gradations is consulted, but these discrepancies are relatively minor. All of these discrepancies are so minor that all aggregates in this study would likely be approved for use on MDT construction projects.

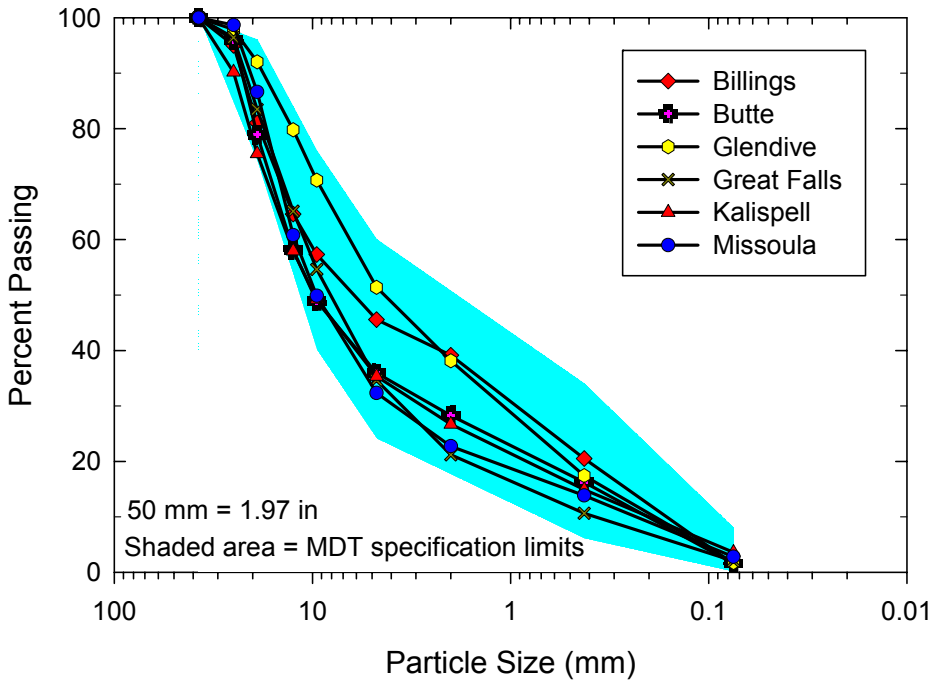

Figure 7. CBC-6A gradation results from the MSU soils lab.

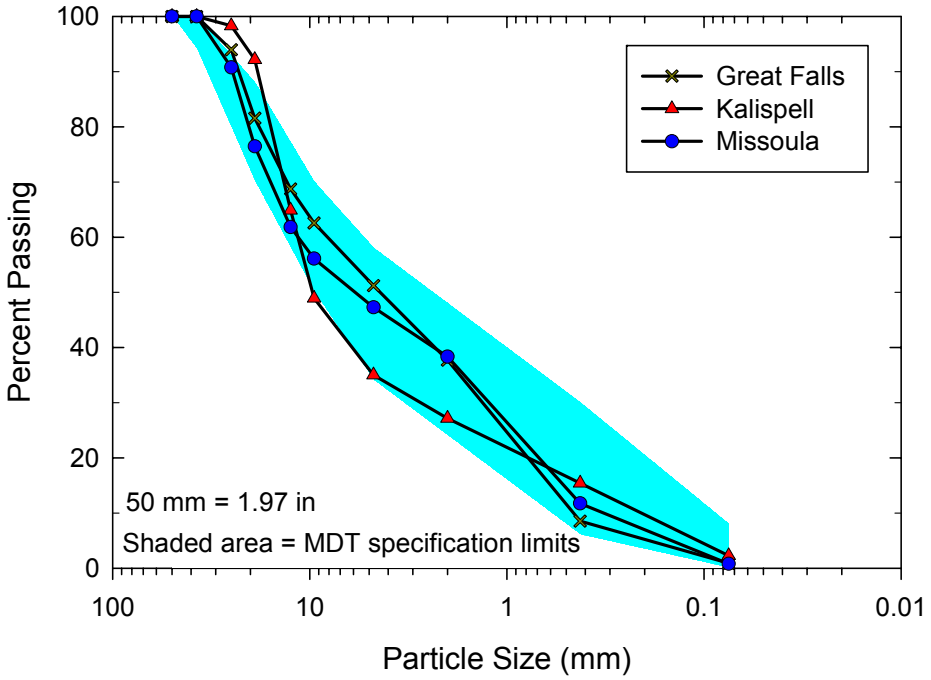

Figure 8. CBC-5A gradation results from the MSU soils lab.

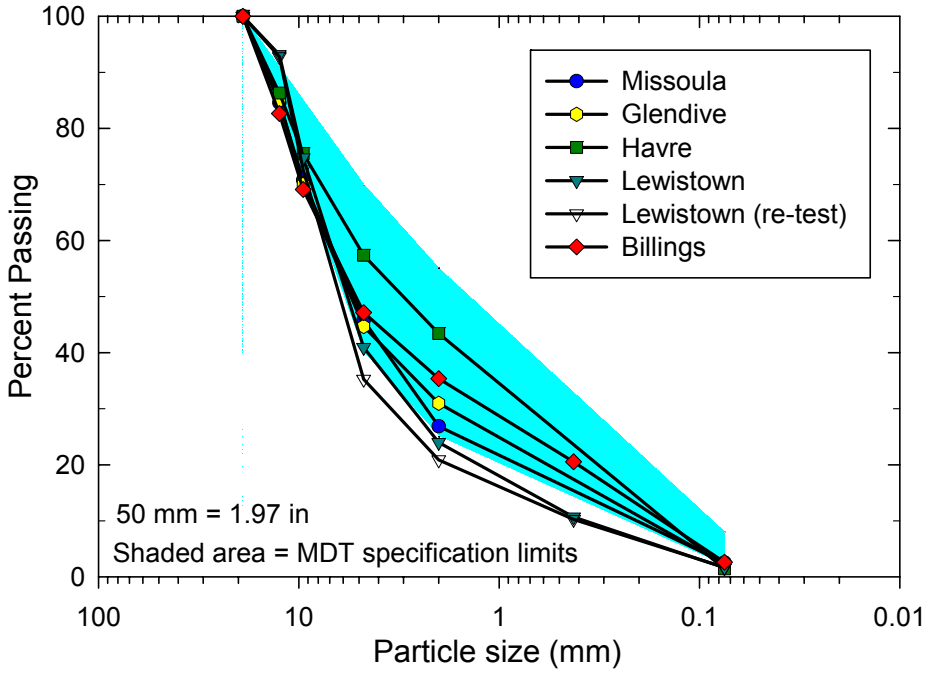

Figure 9. CTS-2A gradation results from MSU soils lab.

Modified Proctor Compaction

Modified Proctor testing was conducted in general accordance with AASHTO Test Method T180 and MDT Test Method MT230. Because the 2A aggregates had a maximum particle size of 0.75 inches, no screening of oversize particles was necessary with the 6-inch-diameter Proctor mold. Material greater than the 0.75-inch sieve was screened off for testing of the 6A and 5A materials and replaced with an equal weight of material between the No. 4 and 0.75-inch sieve sizes, as specified in MT230. When testing the 6A and 5A materials, several difficulties were encountered in obtaining results that were accurate and repeatable enough for research purposes. These difficulties included excessive amounts of water and fines washing out of the bottom of the Proctor mold, excessive movement of particles when the hammer was applied to the sample, and variations in measured densities depending on the approach used to level-off the top surface of the test specimen. The combined effect of these factors led to wide variation in the results. This variation is generally attributed to the open graded nature of the 6A and 5A aggregates.

ASTM Test Method D2049 specifies that relative index density testing is appropriate for materials with less than 12% passing the No. 200 sieve. In addition, as described in AASHTO Test Methods T99 and T180, the Proctor test is not necessarily applicable for use on cohesionless soils. All aggregate samples evaluated in this study have less than 12% fines and are cohesionless. Consequently, densities obtained from maximum and minimum index density testing (ASTM D4253 and ASTM D4254) were

used in place of Proctor densities for evaluating relative densities of prepared samples in this study.

Accurate modified Proctor data was gathered for the 2A samples, even though testing was not completed on 6A or 5A samples. Modified Proctor maximum dry densities (for the 2A samples) were similar in magnitude to dry densities determined using the saturated maximum index density method, as shown in Figure 10. Density measurements are provided in terms of void ratio (e) in Figure 10, which can be related to dry unit weight (γ_d) using Equation (1), as follows:

$$\gamma_d = \frac{G_s \gamma_w}{1+e} \tag{1}$$

where, G_s = specific gravity, γ_w = unit weight of water, and e = void ratio.

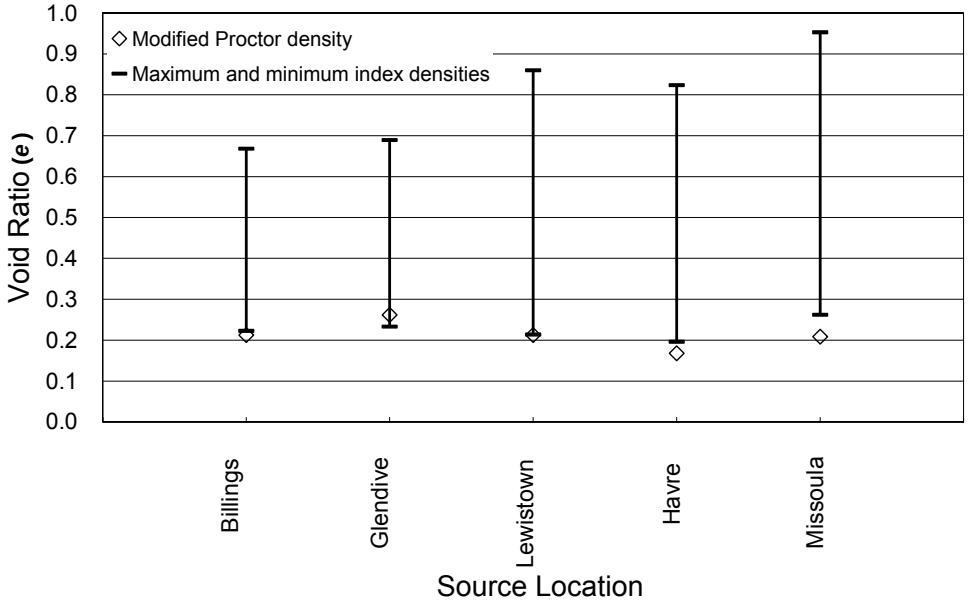

Figure 10. CTS-2A modified Proctor and maximum index density comparison.

This indicates that either method (saturated maximum index density or modified Proctor) for determining maximum density would be acceptable for the 2A aggregates. For consistency, maximum dry densities obtained using the maximum index density test were used in this study for all three aggregate types. It is expected that if accurate Proctor densities could be obtained for 5A and 6A aggregates, they would likely also correspond to maximum dry densities measured using the maximum index density test because these aggregates are similar in structure to 2A aggregates.

Relative Density

Relative density testing was conducted in general accordance with ASTM Test Method D4253 (Maximum Index Density and Unit Weight of Soils Using a Vibratory Table) and ASTM Test Method D4254 (Minimum Index Density and Unit Weight of Soils and Calculation of Relative Density). ASTM D4253 provides the option of conducting either dry or saturated testing. It was observed in this study that saturated testing yielded significantly lower minimum void ratios (higher maximum densities) than dry testing. Consequently, all maximum index density results reported herein are based on tests performed under saturated conditions. The size of the mold used for testing was governed by the ASTM specification, which is based on the maximum particle size of the sample. The 5A and 6A samples were tested in the 10-inch-diameter (volume = 0.500 ft^3) mold, while 2A samples were tested in the 6-inch-diameter (volume = 0.100 ft^3) mold. Relative density can be calculated in terms of either void ratio or dry density as:

$$D_r = \frac{e_{\max} - e}{e_{\max} - e_{\min}} = \left[\frac{\rho_d - \rho_{d(\min)}}{\rho_{d(\max)} - \rho_{d(\min)}} \right] \left[\frac{\rho_{d(\max)}}{\rho_d} \right] \qquad (2)$$

where, D_r = relative density, e_{max} = maximum void ratio, e_{min} = minimum void ratio, e = in-situ void ratio, ρ_d = in-situ density, $\rho_{d(max)}$ = maximum index density, and $\rho_{d(min)}$ = minimum index density.

Maximum and minimum index density results are summarized in Figure 11 in terms of void ratio. This figure shows maximum and minimum void ratios, as well as the associated void ratio spread ($e_{max}-e_{min}$) for each aggregate. The majority of specimens compacted to an e_{min} between 0.20 and 0.25, with three exceptions. The 5A-Kalispell sample had the lowest e_{min} value (0.17), while the 6A-Missoula and 6A-Glendive samples were on the high end with e_{min} values of 0.29 and 0.27, respectively.

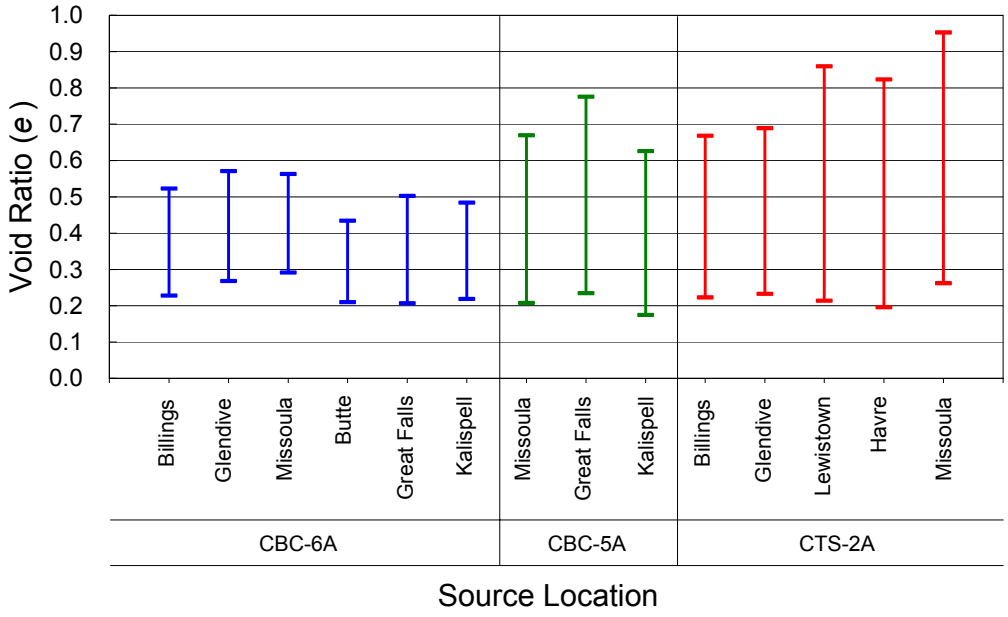

Figure 11. Maximum and minimum index density test results.

Specific Gravity

Specific gravity (G_s) tests were conducted on the 14 aggregate samples in general accordance with AASHTO Test Method T100 (Specific Gravity of Soils) and AASHTO Test Method T85 (Specific Gravity and Absorption of Coarse Aggregate). Specific gravity was determined by taking a weighted average from the fine and coarse fractions of each soil sample. Aggregate type is not expected to have any relation to G_s. Additionally, different aggregate types that have the same location label may not have corresponding G_s values because samples did not necessarily come from the same pit only the same region. Values ranging from 2.66 to 2.76 were obtained for the samples tested in this study; well within the typical range reported for these material types (Das 2002). Specific gravity results are summarized in Table 4.

Table 4. Specific Gravity Results

Aggregate Type		Specific Gravity
CBC-6A	Great Falls	2.73
	Billings	2.71
	Glendive	2.71
	Missoula	2.72
	Butte	2.68
	Kalispell	2.69
CBC-5A	Great Falls	2.73
	Missoula	2.70
	Kalispell	2.69
CTS-2A	Havre	2.66
	Glendive	2.76
	Missoula	2.76
	Lewistown	2.71
	Billings	2.72

Los Angeles Abrasion

Los Angeles (LA) abrasion tests were conducted in general accordance with AASHTO Test Method T96 and MDT Test Method MT209 (Resistance to Degradation of Small-Size Coarse Aggregate by Abrasion and Impact in the Los Angeles Machine). LA abrasion tests are used to quantify the relative durability of aggregates. Aggregate durability is thought to depend on mineralogy so no relation to aggregate type was expected. Results from LA abrasion testing are summarized in Table 5. The 2A-Havre and 5A-Missoula samples fell outside of the MDT specification limit of 40 percent loss, with LA abrasion loss percentages of 48.2 and 61.9, respectively. All other samples fell within the MDT specification limit for durability.

The loss value for the 2A-Havre sample is about 8 percent greater than the specification limit, and the loss for 5A-Missoula is about 22 percent greater than the limit. It was noted during direct shear testing that the larger particles of the 5A-Missoula sample contained conglomerations of smaller particles that broke apart under load. It is likely that these weaker particles contributed to the high loss obtained using the LA impact device.

Table 5. Los Angeles Abrasion Results

Aggregate Type		Percent Loss
CBC-6A	Great Falls	27.3
	Billings	23.5
	Glendive	22.3
	Missoula	15.3
	Butte	19.0
	Kalispell	15.5
CBC-5A	Great Falls	19.0
	Missoula	61.9
	Kalispell	13.2
CTS-2A	Havre	48.2
	Glendive	15.3
	Missoula	13.1
	Lewistown	24.1
	Billings	16.9

Resistance Value

The Resistance R-value and Expansion Pressure of Compacted Soils test (commonly referred to as the R-value test) is used by MDT to evaluate the strength and stability of subgrade and base materials. The test is standardized by AASHTO Test Method T190 and ASTM Test Method D2844. Testing was completed by MDT at their Helena materials testing lab. R-value test output is a number ranging from 0 to 100, with 0 representing viscous liquid slurry with no shear resistance, and 100 representing a rigid solid. The R-value test is conducted using a stabilometer, which is shown schematically in Figure 12. Testing involves applying a constant vertical pressure to the sample and measuring the corresponding increase in horizontal (fluid) pressure. The R-value is calculated based on the ratio of vertical pressure applied to the amount of fluid pressure measured.

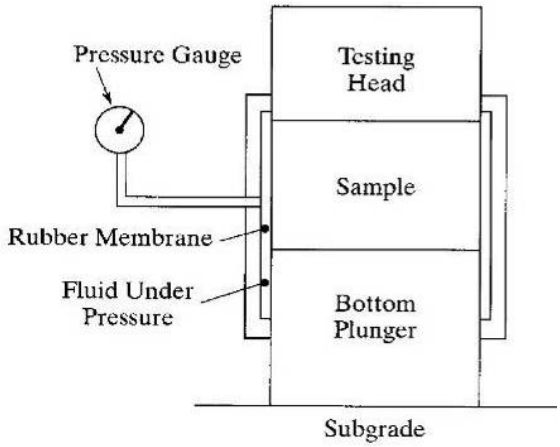

Figure 12. Schematic Diagram of a Stabilometer (from Huang 2004).

All soils in this study are classified as A-1-a in the AASHTO soil classification system. Published correlations suggest that R-values for A-1-a soils would likely range from approximately 70 to greater than 80 (PCA 1966, Van Til et al. 1972). R-value results are summarized in Figure 13, and data sheets for the R-value tests are provided in Appendix B.

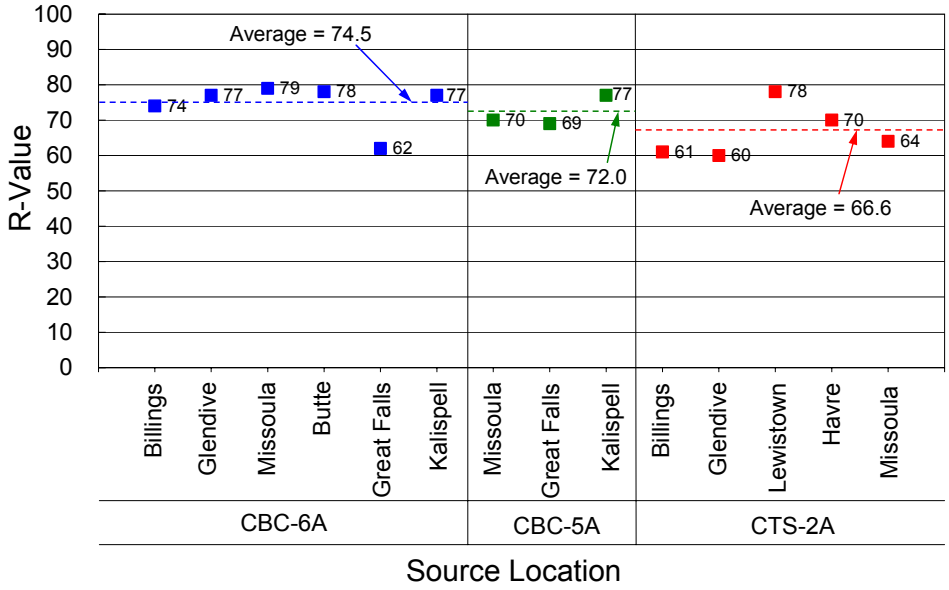

Figure 13. R-value test results.

As shown in Figure 13, slight differences in average R-values were observed between the different aggregate types. A series of two sample t-tests were performed to determine if differences in the average values were statistically significant. Results from this statistical evaluation are shown in Table 6. Based on the statistical testing, the average 2A R-value (66.6) was less than both the average 6A R-value (74.5) and the average 5A R-value (72.0). There is no statistically significant difference between the average 6A and average 5A R-values. From a practical viewpoint, the relative differences are not significant based on the accuracy of the test.

Table 6. Average R-value Statistical Evaluation

Relationship			**p-value**
6A μ=74.5	=	5A μ=72.0	0.740
6A μ=74.5	>	2A μ=66.6	0.950
5A μ=72.0	>	2A μ=66.6	0.873

DIRECT SHEAR

Direct shear testing was performed to supplement R-value testing by providing another means of quantifying shear strength parameters of the aggregate samples. Tests were performed in general accordance with AASHTO Test Method T236. A 12-inch by 12-inch Brainard-Kilman direct shear testing apparatus was used to accommodate the large maximum particle size of the aggregate samples. Shear resistance was measured using an S-type load cell and lateral displacement was measured using a linear variable displacement transducer (LVDT). Figure 14 shows some of the main components of the direct shear device.

Background

The direct shear test is used to obtain average macro strength properties of a soil sample by measuring the load required to induce shear failure along a predetermined plane. A flat shear failure plane is commonly assumed because there is no practical way to measure the shape of the actual failure plane in a direct shear test, which has been shown by Atkinson and Bransby (1978) to be elliptical. Localized strains in the sample are not measured, and high stress concentrations near the sample boundaries can lead to non-uniform stress conditions (Holtz and Kovacs 1981). Consequently, the average strain is calculated from displacement, and the average stress is calculated from the load.

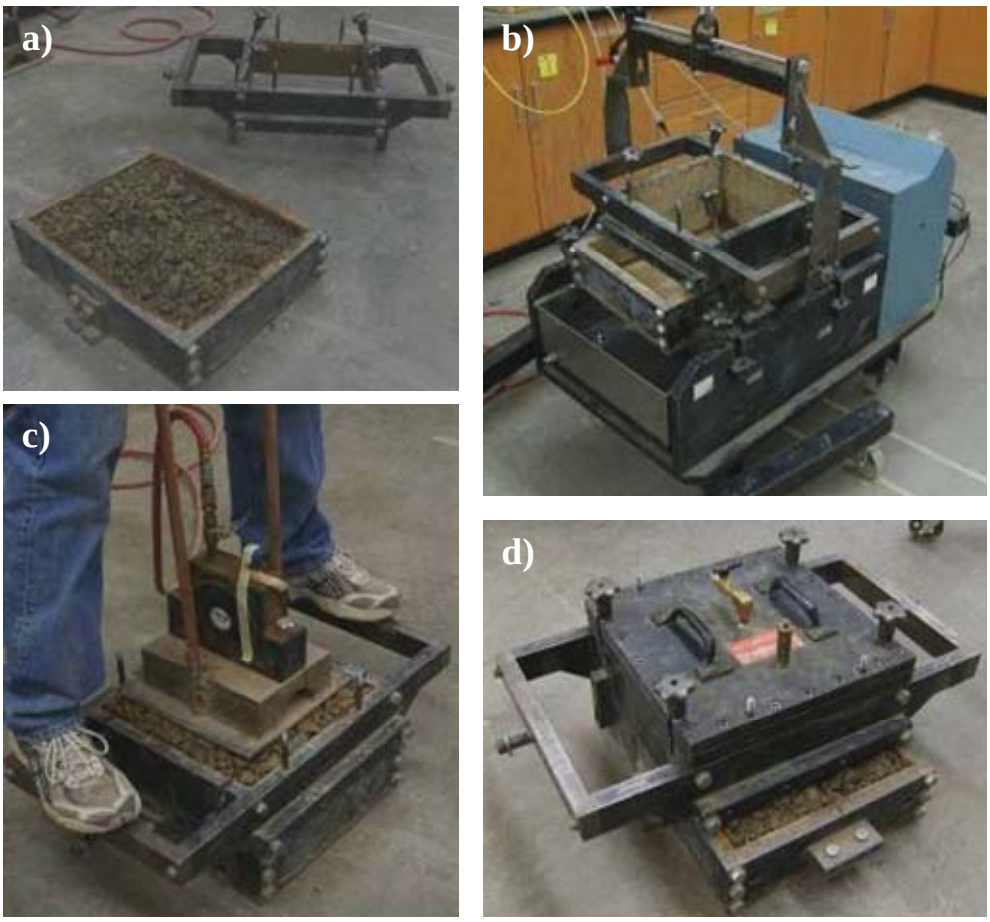

Figure 14. Direct shear testing apparatus a) mold halves, b) mold placed in load frame with a crane, c) vibratory compactor, and d) assembled mold halves with air bladder and cover plate attached to top.

The direct shear machine is a reasonable, practical device for quantifying stresses that cause failure on a specific (horizontal) failure plane (Atkinson and Bransby 1978). This test was selected as a method for quantifying strength and stiffness because it provides a repeatable approach for quantifying relative differences between the aggregate types examined in this study. The test was also selected because it is relatively easy to perform compared to the triaxial test; especially for aggregates containing large particle sizes, like those utilized in this study.

Testing Conditions

Testing conditions are presented here to document the details of equipment setup and sample preparation that are not specified for the over-size samples utilized in this study.

Apparatus and Sample Preparation

Soil was placed into the shear box in 1.3-inch compacted lifts. Compaction was performed at 4% moisture using a 57-pound pneumatic vibratory compactor with a 100 in^2 contact area (Figure 14c). Normal stress (pressure) was applied to the sample using a pressurized rubber air bladder, which was located on the inside of the shear box lid (Figure 14d). The samples were sheared at a constant rate of 0.05 in/min to a maximum horizontal displacement of 3.8 inches. The horizontal displacement rate was slow enough to ensure full drainage (effective stress conditions).

Compacted Density of Samples

In the field, large vibratory drum compactors pass over a material multiple times to impart weight and vibration to the underlying geomaterials. This process was simulated in the laboratory using a weighted vibratory plate. Vibration and impact compaction energy were applied until observable particle movement ceased, which generally occurred after approximately 1 minute of compaction for each soil layer. This method of compaction provided high densities with minimal compaction non-uniformities. All samples were compacted using an initial water content of 4% to help minimize particle segregation and achieve high densities.

The dry density of each direct shear sample was determined using mass-volume relationships after each sample was compacted into the direct shear mold. Relative density (D_r) was calculated for each compacted sample using Equation (2). There is some variation in D_r between aggregate types because of the differences in particle gradation, particle shape, and maximum particle size. Overall, good repeatability was achieved using this method of compaction, as evidenced by the relatively small spread of compacted void ratios, as shown by the dashed symbols in Figure 15.

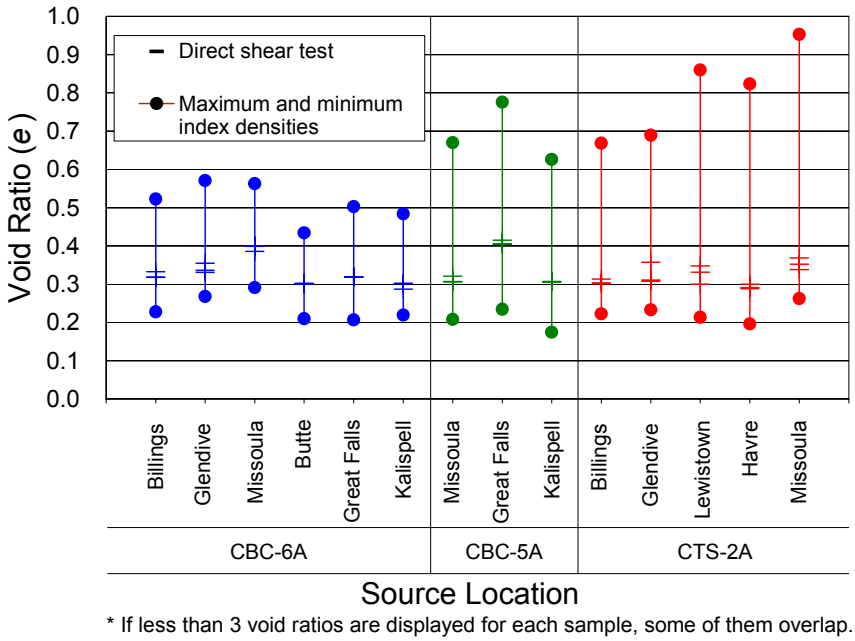

Figure 15. Void ratio (e) for each direct shear test compared to e_{max} and e_{min}.

Results

Several parameters were obtained from direct shear testing including initial stiffness (k_i), ultimate secant stiffness (k_u), and ultimate strength (σ_u). Mohr-Coulomb failure envelopes were determined from the ultimate strength of each material at different

normal stresses. Values of k_i reported here are defined as the slope of the linear elastic portion of the stress-displacement curve, which occurs at low displacements. Ultimate secant stiffness is defined as the slope of a line drawn from the origin to the shear stress at 8% strain, where the strain is averaged over the entire length of the sample. Percent strain in this context is thus defined as the measured displacement divided by sample width. σ_u was determined at 8% strain or the peak stress, whichever occurred first. An example illustrating how these values were determined for the 6A-Missoula, 10 psi sample, is shown in Figure 16. Shear stress versus horizontal displacement plots for all three normal stresses are provided in Appendix C for each material.

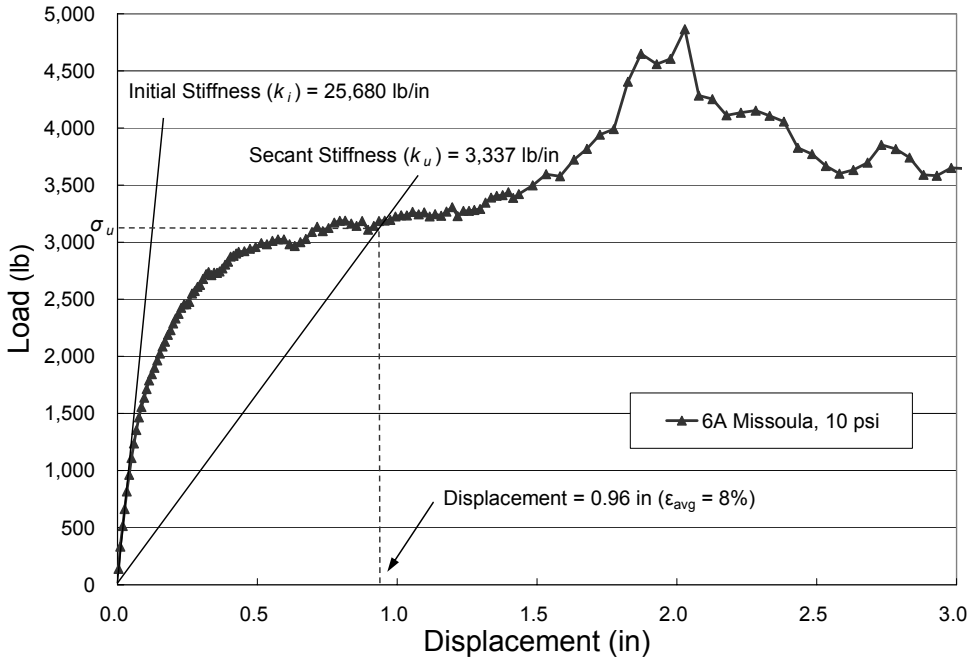

Figure 16. Example of strength parameter (k_i, k_u, and σ_u) determination.

Friction Angle

The effective angle of internal friction (ϕ') was determined by testing three separately compacted samples (each with virgin material) at normal stresses of 5, 10, and 15 psi. In the field, these aggregates likely experience relatively low normal stresses because of the small overburden loads that are typical of highway pavement sections. Normal pressures of 5, 10, and 15 psi were used to simulate the low normal pressures typical of in-situ conditions. The spread of 5 psi between normal pressures is a practical measure necessary to provide accurate Mohr-Coulomb failure envelopes. Mohr-Coulomb failure envelopes are presented in Figure 17, Figure 18, and Figure 19 for the 6A, 5A, and 2A samples, respectively. Effective friction angles shown in the plots are based on best fit lines drawn through the origin.

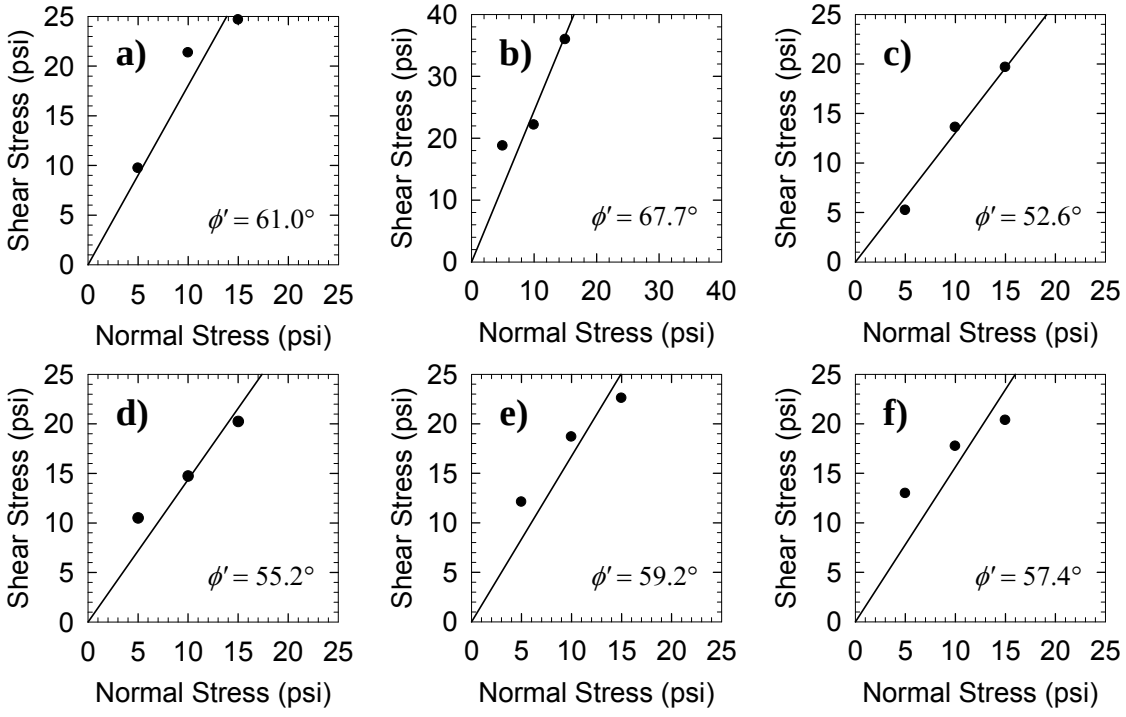

Figure 17. Mohr-Coulomb failure envelopes for 6A samples: a) Butte, b) Missoula, c) Glendive, d) Billings, e) Great Falls, and f) Kalispell.

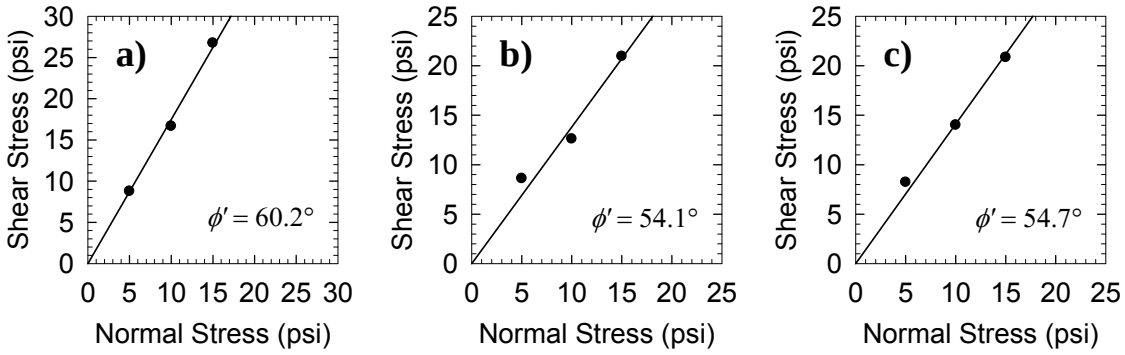

Figure 18. Mohr-Coulomb failure envelopes for 5A samples: a) Missoula, b) Great Falls, and c) Kalispell.

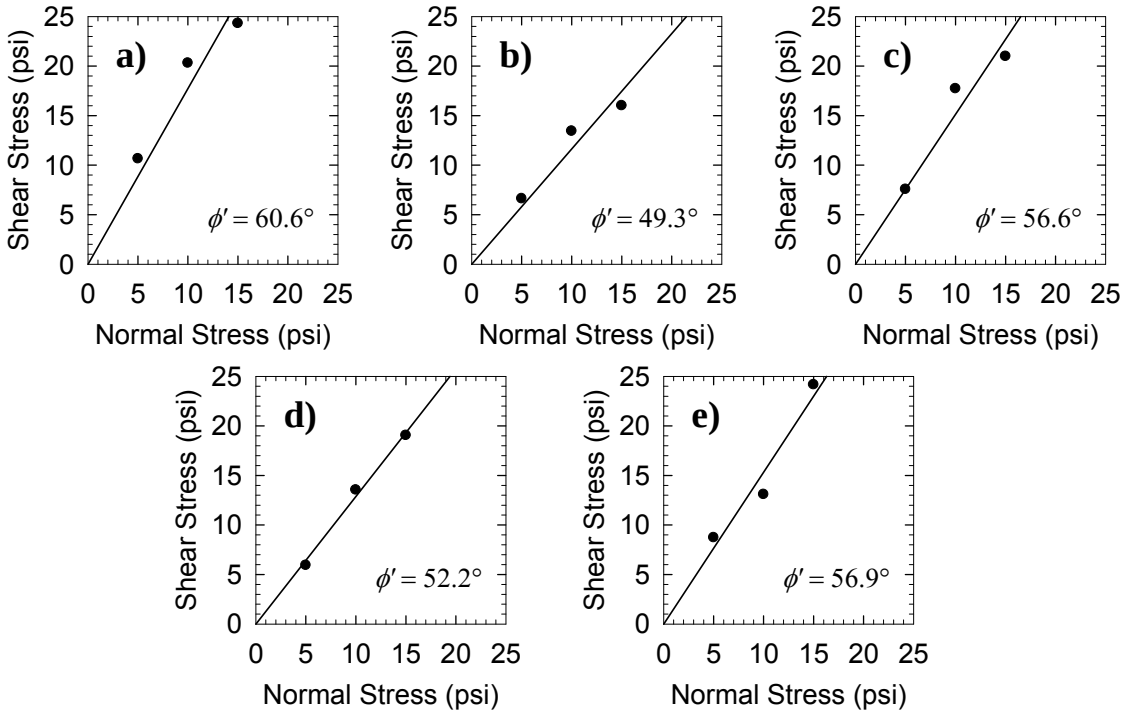

Figure 19. Mohr-Coulomb failure envelopes for 2A samples: a) Missoula, b) Billings, c) Glendive, d) Lewistown, and e) Havre.

Measured ϕ' values were in the range of 49° to 68°, which represents a relatively large spread. Figure 20 provides a direct comparison of ϕ' values for the three aggregate types. A series of two sample t-tests were performed on the average ϕ' values to

determine the statistical significance of the scatter or spread in results. The results of this statistical evaluation are summarized in Table 7, which indicates that the average 6A effective friction angle (58.8°) is larger than the average 2A friction angle (55.1°). When the spread of data is taken into account, there is not a significant difference in the ϕ' values between the 6A and 5A materials or between the 5A and 2A materials.

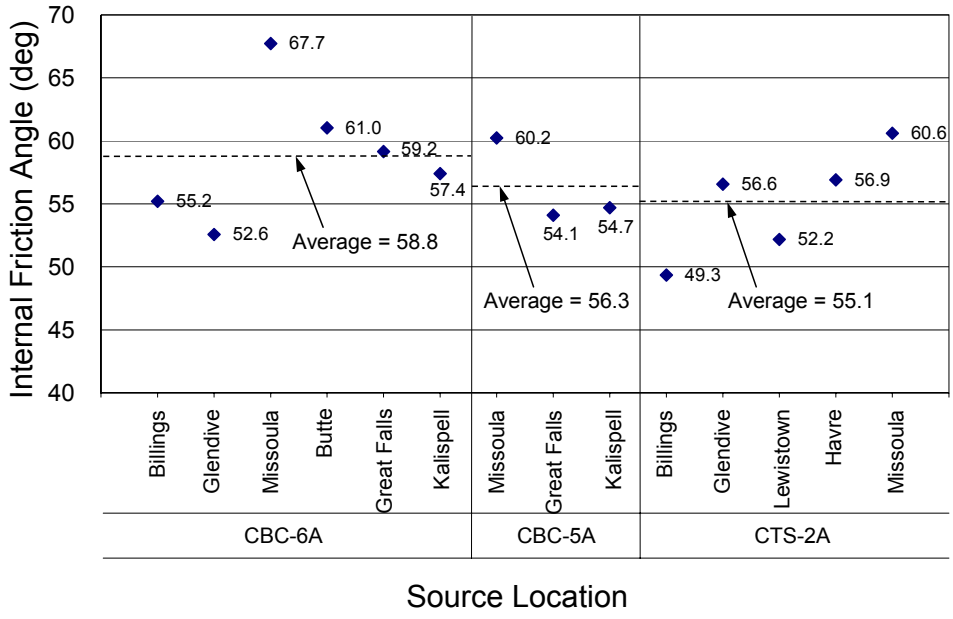

Figure 20. Internal friction angles (ϕ') for each aggregate.

Table 7. Average Internal Friction Angle (ϕ')Statistical Evaluation

Relationship			p-value
6A μ=58.8	=	5A μ=56.3	0.791
6A μ=58.8	>	2A μ=55.1	0.882
5A μ=56.3	=	2A μ=55.1	0.660

Initial Stiffness

Failure of roadway materials is generally defined by relatively small deformations, which are related to the initial portion of the stress-displacement curve. The initial stiffness, k_i, is defined as the slope of the stress-displacement curve at low displacements, where the curve is relatively linear, as shown in Figure 16.

Values of k_i for all of the samples tested are compared in Figure 21. These values generally ranged from 10,000 lb/in to 30,000 lb/in. As expected, most aggregates exhibited increasing k_i with increasing normal stress. There were some minor exceptions to this trend, which may be attributed to small variations in the test pressures and variations in sample collection methodology, compaction non-uniformities, and minor particle segregation during sampling and sample preparation.

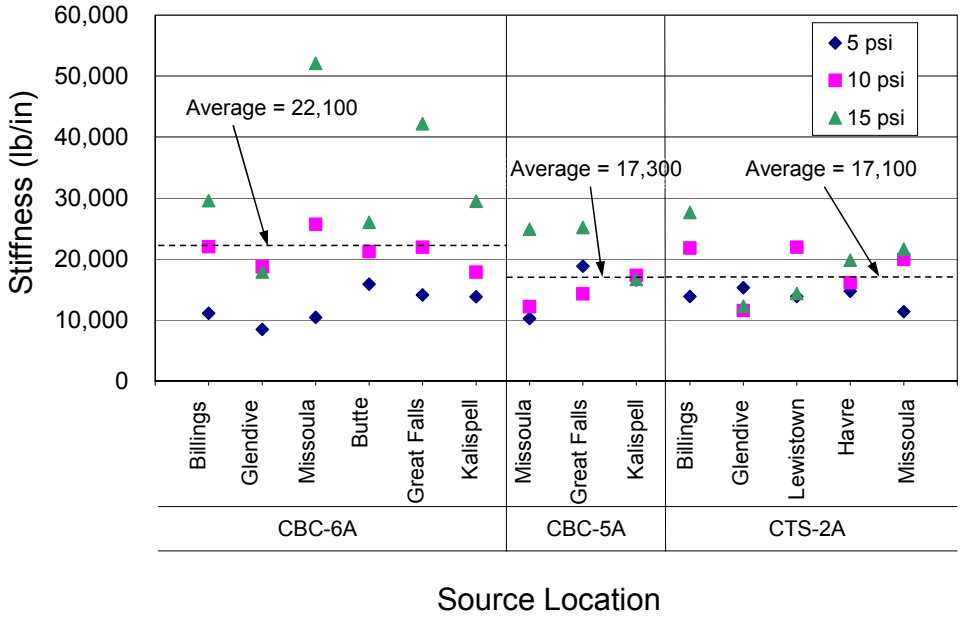

Figure 21. Initial stiffness (k_i) results.

A series of two sample t-tests were performed to determine if the apparent trends in average k_i values were statistically significant. The results of the statistical evaluation are summarized in Table 8. The average k_i of the 6A aggregate type (22,100 lb/in) is statistically greater than the average k_i of the 2A aggregate type (17,100 lb/in) and the 5A aggregate type (17,300 lb/in). There is no significant difference between the average k_i of the 5A and 2A aggregate types.

Table 8. Average Initial Stiffness (k_i) Statistical Evaluation

Relationship			p-value
6A μ=22.1	>	5A μ=17.3	0.931
6A μ=22.1	>	2A μ=17.1	0.953
5A μ=17.3	=	2A μ=17.1	0.552

Secant Stiffness

Ultimate secant stiffness (k_u) values were determined for each aggregate to evaluate the soil behavioral characteristics at large strains. Ultimate secant stiffness is defined here as the slope of a line drawn from the origin to the shear stress at 8% strain on a shear stress-displacement curve, as shown in Figure 16. Ultimate secant stiffness may not be as relevant as k_i because roadway base course aggregates would likely not experience 8% strain during normal service. However, k_u is an additional, meaningful parameter that can be used for quantifying strength and stiffness differences between aggregate types.

As shown in Figure 22, k_u values generally ranged from 1,000 lb/in to 3,500 lb/in. All aggregates exhibited increasing k_u values with increasing normal stresses. The 6A-Missoula sample exhibited significantly higher secant stiffness than all of the other samples. A series of two sample t-tests were performed to compare average k_u values based on aggregate type. Results of this statistical evaluation are presented in Table 9.

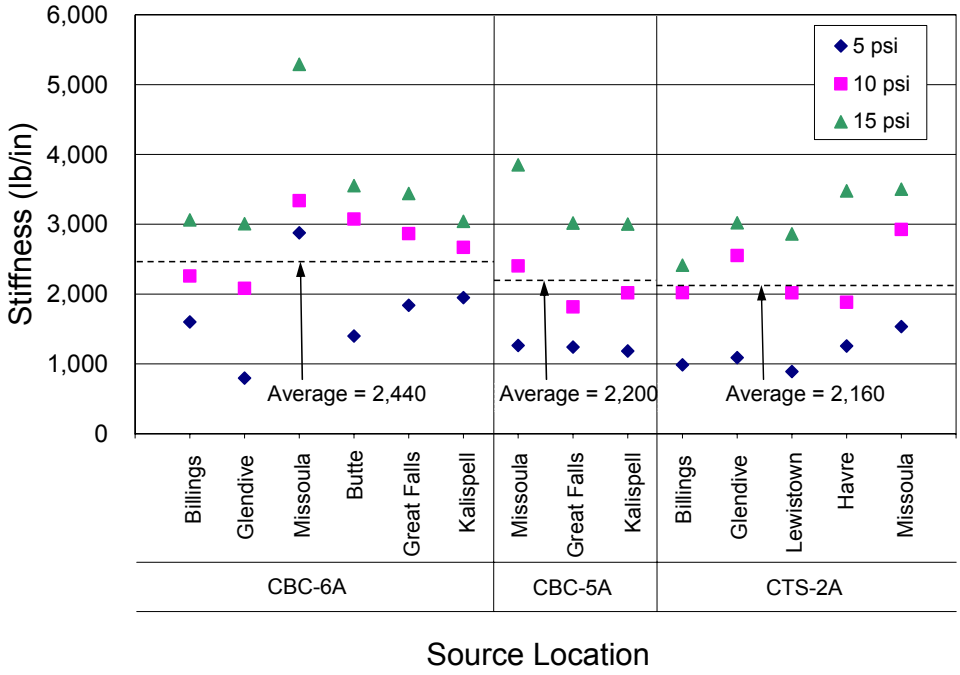

Figure 22. Secant stiffness (k_u) results.

Table 9. Average Secant Stiffness (k_u) Statistical Evaluation

Relationship			p-value
6A μ=2.44	>	5A μ=2.20	0.878
6A μ=2.44	>	2A μ=2.16	0.934
5A μ=2.20	=	2A μ=2.16	0.538

The average k_u of the 6A aggregate type (2,440 lb/in) is greater than the average of the 2A aggregate type (2,160 lb/in) and the 5A aggregate type (2,200 lb/in). There is no significant difference between the average k_u of the 5A and 2A aggregates. This indicates that at relatively large displacements, these aggregates all exhibit relatively similar stress-displacement behavior, with the 6A aggregate type exhibiting only a small potential advantage over the other aggregates. Trends observed in the k_u results are similar to the k_i results.

Summary

Sample preparation techniques and testing procedures were adapted for an over-sized 12-inch by 12-inch direct shear box. Results for all three parameters determined in direct shear testing are summarized in Table 10. These results indicate that, in general, the 6A aggregates were the strongest and stiffest examined in this study, followed by the 5A, and then the 2A aggregates.

Table 10. Summary of Direct Shear Results

k_i	k_u	ϕ'
6A > 5A	6A > 5A	6A = 5A
6A > 2A	6A > 2A	6A > 2A
5A = 2A	5A = 2A	5A = 2A

PERMEABILITY

Drainage capacity was quantified through saturated constant head hydraulic conductivity (permeability) testing. Permeability (*k*) tests were performed in general accordance with ASTM Test Method D2434 and AASHTO Test Method T215 (Permeability of Granular Soils - Constant Head). Constant head testing was utilized (as opposed to falling head) to limit the amount of hydraulic head applied to the samples thus ensuring laminar flow conditions. Darcy's Law was used to compute *k*, as follows:

$$k = \frac{QL}{tHA} \tag{3}$$

where, k = permeability, Q = volume of water passed through the specimen, L = length of the specimen, t = elapsed time corresponding to Q, H = total head across the specimen, and A = cross sectional area of the specimen perpendicular to the flow direction.

Testing the least permeable layer of a soil sample in the laboratory is a commonly accepted method for quantifying the speed with which a fluid will pass through porous media. Permeability is a highly variable soil property that can vary significantly with small variations in compaction and gradation. To minimize testing errors, average *k* values were obtained for each sample by conducting three separate tests, using virgin aggregate each time. Experimental results were compared to empirical estimation equations and published typical ranges to verify laboratory test results, and to evaluate the prediction methods themselves to determine if any performed well for the aggregates in this study.

Testing Conditions

Testing conditions are presented here to document the details of equipment setup, sample preparation, and testing procedures that are not specified for the over-size samples utilized in this study.

Apparatus

A custom-built large-diameter permeameter was utilized for this testing. The permeameter specimen mold has a diameter of 10 inches and an approximate height of 10 inches. The permeameter utilizes a unique Mariotte tube and integral upper reservoir arrangement to maintain constant pressure head and complete saturation of the soil sample and testing apparatus throughout the experiment. A photograph and schematic diagram of the permeameter are shown in Figure 23.

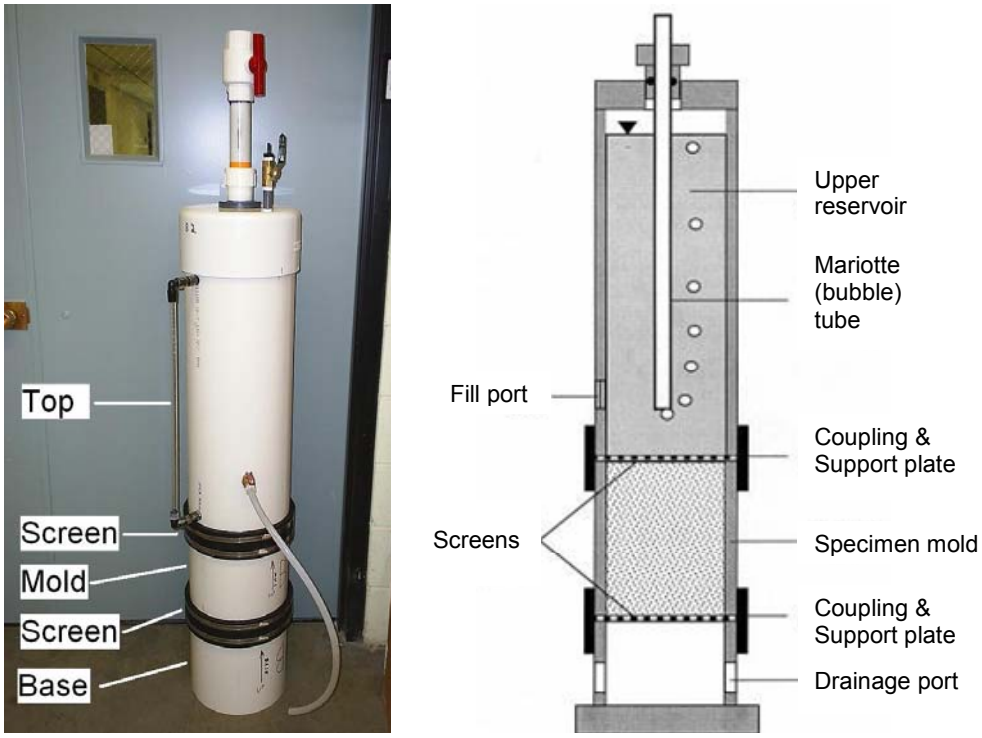

Figure 23. Photograph and schematic diagram of permeameter setup.

There are several notable improvements in this custom-built device over a traditional constant head permeability testing apparatus. The apparatus used in this study completely submerges the specimen in the tail water tank, which ensures the specimen remains saturated throughout the test. There is no head loss between the head water tank and specimen because there are no tubes, valves, or fittings between the headwater and specimen. Only a screen and support plate separates the supply water from the specimen. The upper reservoir is used to supply water to the sample and can be precisely measured using a manometer, which eliminates the need to collect and measure the tail water. Additionally, the use of a Mariotte tube to maintain constant head eliminates the waste of overflow head water, which is inherent in traditional permeameter devices.

The specimen support plates are shown in Figure 24. The support plates consist of 0.25 inch thick galvanized steel plates that have 0.25 inch holes throughout to permit the unrestricted flow of water. Two square mesh screens, oriented at 45° relative to each other, were placed between the sample and the support plates to reduce the washing of finer particles out of the specimen during testing. The screens were placed at 45° relative to each other to further reduce the opening size of the sieves, thereby reducing the movement of fines.

A 0.125-inch thick soft neoprene rubber liner with 450 psi tensile strength and 10A durometer hardness was attached to the inside of the specimen mold with silicone adhesive to reduce edge effects, as suggested by Thornton and Toh (1995). The liner was installed to alleviate high stress concentrations that may occur at the contact points of the larger particles on the smooth rigid interior wall of the mold, and to maintain a more uniform and representative distribution of particles near the sample edges. The liner was

used for all tests performed in this study. Any effect imparted on the measured *k* from the presence of the liner was assumed to be the same for all samples.

Figure 24. Support plate for bottom of specimen mold.

Sample Preparation

Virgin aggregate samples were compacted into the 10-inch tall specimen mold in five lifts using 15 drops from a modified Proctor hammer (with a 10-lb weight and 18-inch drop). Relatively low energy was utilized for compaction (2,600 lb-ft/ft^3) to minimize damage to the bottom screens. Impact was selected as the compaction mechanism to minimize particle segregation. Samples were compacted at 4% water content to further reduce particle segregation and to help achieve high densities.

Preventing particle segregation during placement and compaction is important in *k* testing because a heterogeneous fine particle distribution can have a large effect on the measured permeability (Moulton 1980). Careless sample preparation and compaction techniques can lead to inaccurate results. Even if extreme care is taken, the measured value of permeability will likely only be within one order of magnitude of the true value

(Bowles 1992). Every effort was made in the preparation, placement, and compaction of samples to minimize particle segregation and to ensure consistency between test specimens.

Samples were compacted in the permeameter specimen mold, screens put in place, and then saturated. De-aired water was used to minimize the potentially adverse effects of air bubbles in the system. De-aired water was obtained by filling buckets with tap water that was above room temperature and allowing air bubbles to rise to the surface. Over time, the warm water was allowed to cool to room temperature. This process ensured that the air holding capacity of the water was at equilibrium with the ambient air conditions, such that no air bubbles would develop during saturation or testing. It is recognized that the water utilized here was not completely de-aired, but de-airing the water any further would have been difficult because of the large quantity of water used in each test. Furthermore, additional de-airing would have had minor effect on the results.

A small negative pressure (vacuum) was applied to the reservoir tube to draw in head water and to help saturate the soil specimen. While applying the vacuum through the vacuum port at the top of the reservoir tube, the side port was opened to allow water to fill the upper reservoir. This also created a slight negative hydraulic gradient across the sample thereby causing water to be drawn up through the specimen. This helped to saturate the specimen because the negative pressure forced entrapped air bubbles out of the sample. The negative pressure was kept small to avoid washing fines from the specimen into the upper reservoir.

ASTM D2434 recommends applying a 20-inch Hg vacuum to the specimen for 15 minutes to remove air adhering to soil particles, and then full vacuum during saturation.

In this study, it was found that even relatively low vacuum had a tendency to wash finer particles out of the samples. The ASTM specification cited above was developed for finer grained materials in which the washing of fines is not likely a problem. Due to the granular cohesionless nature and high permeabilities of the aggregates in this study, only a small amount of vacuum was applied during this process. Samples were filled under low vacuum at a rate of approximately 0.6 gpm. This slow filling rate and low vacuum was selected to provide a balance between the removal of air bubbles entrapped in the sample and the control of fines migration.

Approximately 35 to 40 gallons of water were prepared for each test. This included water for filling the tail water container, saturating the sample, and filling the upper reservoir. The saturation procedure is briefly outlined below:

1. Assemble permeameter base and specimen mold with all screens in place.
2. Place the assembly in the tail water tub (35 gallon plastic barrel).
3. Slowly fill tail water tub until the water level almost reaches the top of the specimen mold, as shown schematically in Figure 25.
4. Provide sufficient time for water to saturate the specimen mold. The time required for full saturation varied depending on aggregate properties. Open graded samples saturated in several minutes, while densely graded samples with high fine particle contents required several hours. In Figure 25, arrows indicate the direction of water flow into the drain holes in the base of the permeameter (bottom tube) and then upward into the specimen.

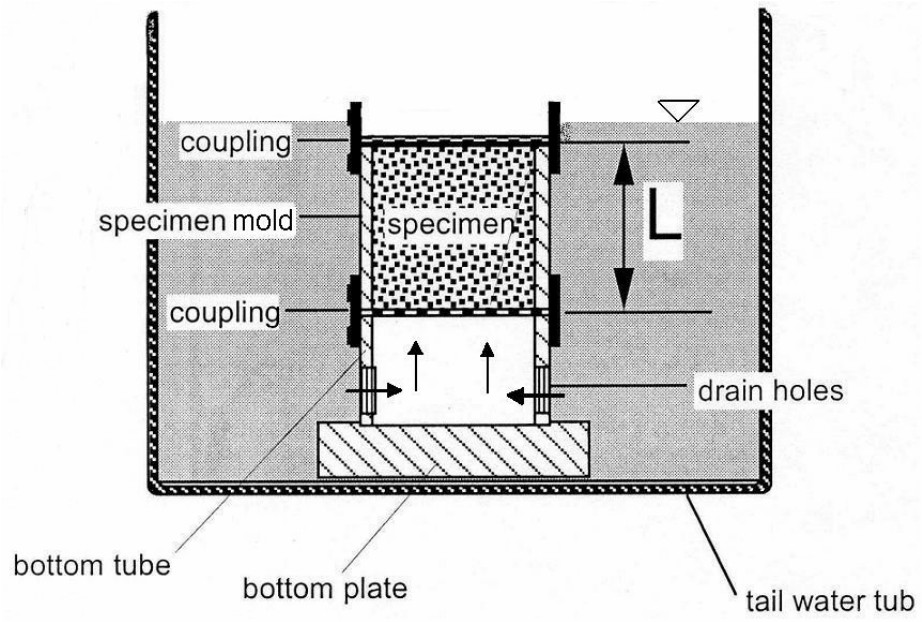

Figure 25. Schematic diagram of permeameter base and specimen mold.

Testing Procedure

After the sample is fully saturated, the upper reservoir is attached to the specimen mold and filled with water. The procedure for filling the reservoir and running a test is outlined below:

1. Install the upper reservoir using the coupling near the top of the specimen mold, as shown in Figure 26, and adjust the height of the Mariotte tube to control the hydraulic gradient through the sample.
2. Open the side port and the vacuum port.
3. Plug the top of the Mariotte tube.
4. Apply a small amount of vacuum to the vacuum port. This will draw water into the side port from the tailwater tub. Leave vacuum on until the upper reservoir is completely full of water. Additional water will need to be added to the tailwater tub as it is drawn into the upper reservoir.
5. Close the vacuum and side ports after the upper reservoir is completely filled with water.
6. Unplug the Mariotte tube to initiate the flow of water through the sample.

7. Allow the system to approach steady state conditions.
8. Record the water level and *start* time.
9. Record the water level and *stop* time just before the water reaches the bottom of the Mariotte tube.

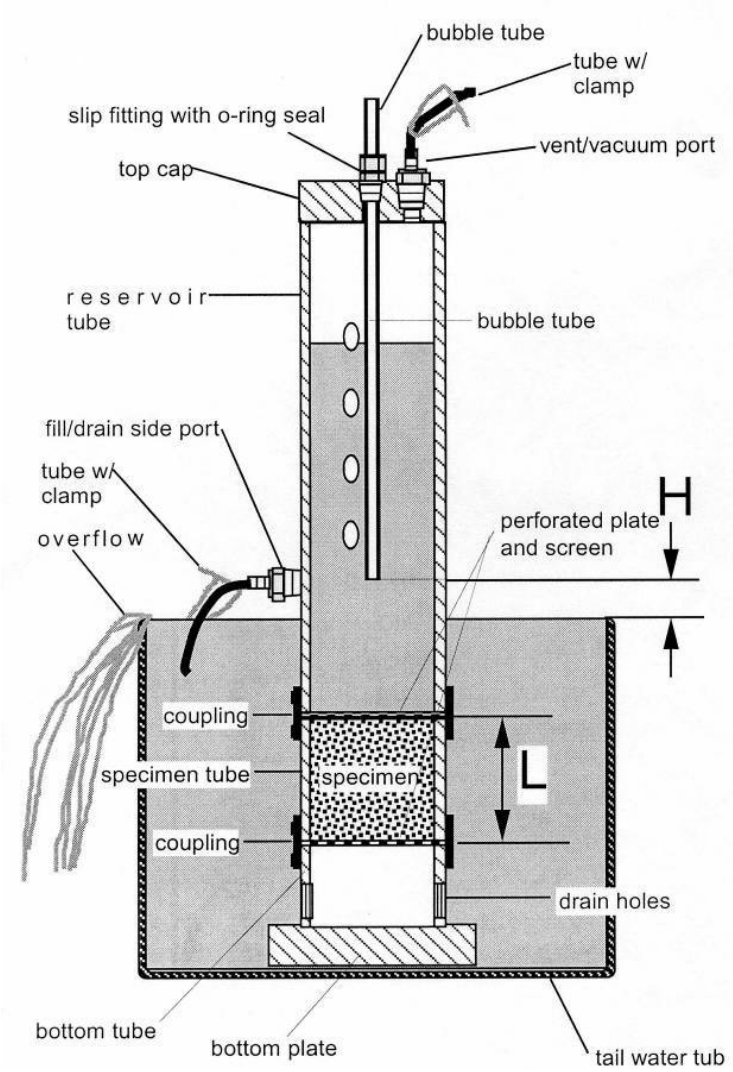

Figure 26. Schematic diagram of permeameter fully assembled.

The permeameters used in this study were opaque. Consequently, a manometer was used to measure the change in water height. This is in contrast to a clear reservoir

tube, which could be graduated on the surface. When the reservoir is completely filled, the water level is above the range measurable by the manometer. The difference in water level from where the reservoir is completely full to where the water level can be measured by the manometer is approximately 7 inches, which corresponds to a volume of approximately 2.3 gallons of water. Each test was started by allowing this initial volume of water to drain through the sample to allow the system to approach steady state conditions.

ASTM D2434 and AASHTO T215 suggest that *k* testing should not be started until the system completely reaches steady state conditions. However, for the wide range of particle sizes examined in this study, it was observed that running excessively large quantities of water through the specimen before testing is started could be counter-productive. Excessive seepage, especially at high gradients could change the results of the test because fines could be washed out of the specimen. It was determined that using a carefully controlled hydraulic gradient and a water volume of 2.3 gallons allowed the system to approach steady state successfully because only minor changes in *k* were noted after this initial volume of water drained through a sample.

Relatively low hydraulic gradients were used on all samples to ensure that the assumptions inherent in Darcy's Law were not violated and to provide consistency between tests. ASTM D2434 recommends applying gradients of 0.2 to 0.3 ft/ft to coarse grained soils and gradients of 0.3 to 0.5 ft/ft to finer soils. All of the aggregate samples examined in this study were predominately coarse-grained; consequently, a hydraulic gradient of 0.26 ft/ft was employed.

Results

Saturated permeabilities were determined for each aggregate in this study by conducting three independent *k* tests (each using virgin aggregates). Results for each *k* test are summarized in Figure 27, and average results for each aggregate type are shown in Table 11. The COV values shown in Table 11 are relatively large, which is attributed to the inherently highly variable nature of this parameter. (Values of *k* are presented in this section using units of cm/s as is typical practice in the United States. Whenever practically possible, US Customary units are also presented.)

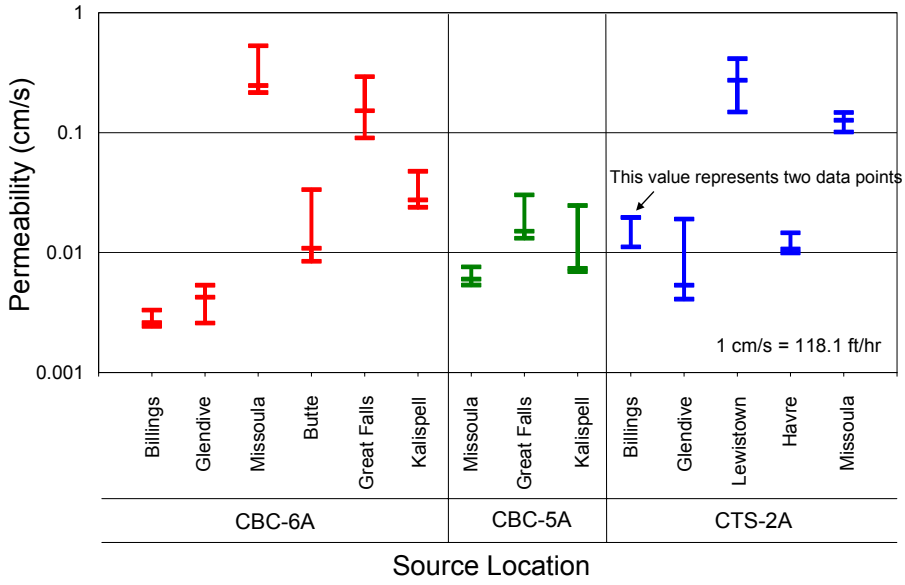

Figure 27. Summary of permeability (*k*) test results.

Table 11. Average Permeability (*k*) Values Based on Aggregate Type

Aggregate Type	Average *k*		Standard Deviation, σ		COV
	(ft/hr)	(cm/s)	(ft/hr)	(cm/s)	
6A	11.1	0.094	16.9	0.143	1.52
5A	1.5	0.013	1.1	0.009	0.69
2A	10.4	0.088	14.2	0.120	1.36

A series of two sample t-tests were performed to facilitate the evaluation of average *k* values. The results of this statistical evaluation are presented in Table 12. The average *k* values for each aggregate type were all in the same order of magnitude, ranging from 0.094 to 0.013 cm/s (11.1 to 1.5 ft/hr). The statistical evaluation indicates that 6A and 2A aggregates both have higher average permeabilities than the 5A aggregates. There is no statistically significant difference between the average permeabilities of the 2A and 6A samples.

Table 12. Average Permeability (*k*) Statistical Evaluation

Relationship			**p-value**
6A μ=11.1	>	5A μ=1.5	0.986
6A μ=11.1	=	2A μ=10.5	0.552
5A μ=1.5	<	2A μ=10.5	0.015

The measured permeability values fell within typical reported ranges based on general soil type. Measured values of *k* for the aggregates in this study varied from 0.002 to 0.529 cm/s (0.23 to 62.5 ft/hr), similar to the approximate ranges reported by Holtz and Kovacs (1981) for clean sands and gravels.

Estimating Permeability from Grain Size

Background

For course grained materials like those in this study, particle size information is commonly used for correlation with *k*. These correlation equations can be unreliable

when applied to soils other than those they were developed for (Carrier 2003); consequently, there is no widely accepted *k* estimation equation. Several of these grain size-*k* correlation equations were evaluated in this study to determine their effectiveness for use with crushed and processed base course aggregates and for comparison with laboratory measured permeabilities to further evaluate their reasonableness.

Permeability correlation equations developed for sands and gravels rely on data obtained from geotechnical index testing to estimate *k*. Although the parameters used to determine *k* vary from equation to equation, they generally rely on particle size and/or void space measurements of the soil. Table 13 summarizes the six empirical equations that were evaluated using data measured in this study.

Table 13. Empirical Permeability Correlation Equations

Name	Year	Equation	Validity
Hazen	1911	$k = C_H d_{10}^2$	Sands between 0.1 and 3.0 mm
Terzaghi	1925	$k = \frac{C}{\mu_0}\frac{\mu_0}{\mu_T}\left[\frac{n-0.13}{(1-n)^{1/3}}\right]^2 d_{10}^2$	Sands with non-uniform grain size and shape
Moulton	1980	$k = \frac{0.00219*10^5 (d_{10})^{1.478} n^{6.654}}{(P_{200})^{0.597}}$	Roadway subbase aggregates
Shahabi et al.	1984	$k = 1.2 C_u^{\,0.735} d_{10}^{0.89} \frac{e^3}{1+e}$	Medium to fine sand
Chapuis	2004	$k = 2.4622\left[d_{10}^2 \frac{e^3}{1+e}\right]^{0.7825}$	Saturated sands and gravels
Chapuis	2004	$k = \frac{C_H d_{10}^2 e^3 (1+e_{\max})}{e_{\max}^3 (1+e)}$	Extended Hazen equation for use on sand or gravel

Notes: C_H = empirical coefficient, d_{10} = grain size corresponding to 10% passing, C/μ_o = empirical coefficient, μ_o = dynamic viscosity of water at 10° C, μ_T dynamic viscosity of the permeant (water) at the temperature of interest, n = porosity, P_{200} = percent of material passing the No. 200 sieve, C_u = coefficient of uniformity, e = void ratio, and e_{max} = maximum void ratio.

Empirical correlation equations for estimating k are best suited for materials that are similar to those used to develop the equation. The Hazen (1911) equation was developed for clean filter sands at or near their minimum density (ρ_{min}) with uniformity coefficients (C_u) of less than 5. The empirical coefficient, C_H, in this equation is generally considered to vary between 0.8 and 1.5. However, Carrier (2003) has shown that the magnitude of C_H can vary over several orders of magnitude when applied to different granular materials. Hazen's equation is not expected to perform very well for the aggregates in this study because they contain effective particle sizes (d_{10}) larger than the sand that Hazen used to develop his equation, and C_u values greater than 5.

The Terzaghi (1925) equation takes multiple factors into account including viscosity of the permeant (water) at different temperatures, d_{10}, and n. The empirical coefficient in this equation, C/μ_o, varies from 460 for angular sands to 800 for rounded sands. A value of 460 was used here due to the crushed nature of the aggregates being examined. This equation was developed for sands with non-uniform grain size and shape. It is more versatile than Hazen's equation because it accounts for more factors that influence k. It is unknown if the Terzaghi equation can be successfully applied to soils containing particle sizes larger than sand.

The Moulton (1980) equation was developed for roadway subbase aggregates. It takes multiple factors into account including n and P_{200}. This equation utilizes multiple factors and was developed for materials similar to those used in this study; consequently, this equation is expected to perform well.

The Shahabi et al. (1984) and Chapuis (2004) equations are both variants of the Kozeny-Carman equation, which is given by:

$$k\left(\frac{\mu}{\gamma_p}\right) = \frac{1}{k_0 T^2 S_0^2}\left(\frac{e^3}{1+e}\right) \quad (4)$$

where, μ = the dynamic viscosity of the permeant, γ_p = is the unit weight of the permeant, k_o = the pore shape factor, T = the tortuosity factor, and S_o = particle shape factor (Kozeny 1927, Carman 1937).

This equation is widely recognized as a reasonable predictor of k in porous media such as gravels, sands, and silts (Carrier 2003). The Kozeny-Carman equation is based on hydraulic principles and takes into account pore shape and size, particle shape and size, and the tortuosity of the flow path. These parameters are difficult to quantify because there is no practical way of measuring the tortuosity of the pore space, and most aggregates contain widely varying pore and particle sizes and shapes, as compared to the single value the equation accounts for.

Many variations of the Kozeny-Carman equation have been developed that utilize different methods of experimentally correlating the pore shape/tortuosity/particle shape term ($k_o T^2 S_o^2$) to more readily measured parameters. The equations presented here from Shahabi et al. (1984) and Chapuis (2004) are both based on the Kozeny-Carman equation. Shahabi et al. (1984) assumed that the $k_o T^2 S_o^2$ term depends on d_{10} and C_u, while Chapuis (2004) assumed that this term depends solely on d_{10}. The researchers each used different regression techniques and data sets to develop their equations.

Chapuis (2004) also developed what is known as the “extended Hazen” equation, which is essentially another variant of the Kozeny-Carman equation. The extended Hazen equation is nearly the same as the Hazen equation except that it includes a

correction factor for the void ratio. Hazen's equation was developed for loose filter sands. The term "loose" implies that these sands were at or near e_{max}. The correction factor was developed by Chapuis (2004) using the e relationship from the Kozeny-Carman equation to adjust the k of a sample that is at an e other than its e_{max}.

Results

The empirical correlation equations presented in this study utilize grain size data from mechanical sieve analyses. Two sets of estimated permeabilities are presented; one set utilizes MSU grain size data, and the other set utilizes MDT grain size data. Figure 28 shows a comparative plot of the predicted and measured k values for the 6A aggregate type utilizing MSU and MDT grain size data. Differences in k estimations between the MSU and MDT grain size data are evident in the 6A-Great Falls sample where predicted values of k are almost an order of magnitude apart from each other. This exemplifies the dependence of these estimation equations on the finer fraction of the grain size data.

Figure 29 and Figure 30 show comparative plots of the predicted and measured permeabilities for the 5A and 2A aggregate types, respectively. Permeability estimations utilizing MDT gradation data could not be created for the 5A-Kalispell sample because the MDT gradation did not include grain size data with small enough particle sizes to utilize the estimation equations.

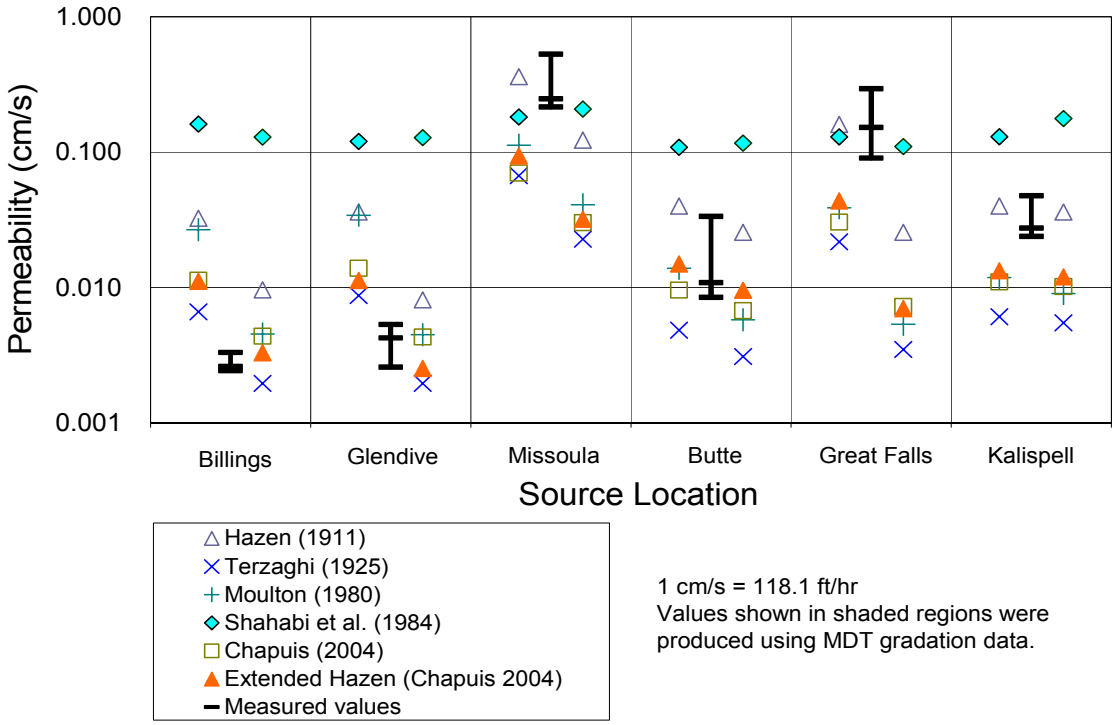

Figure 28. Calculated permeabilities for the 6A aggregates.

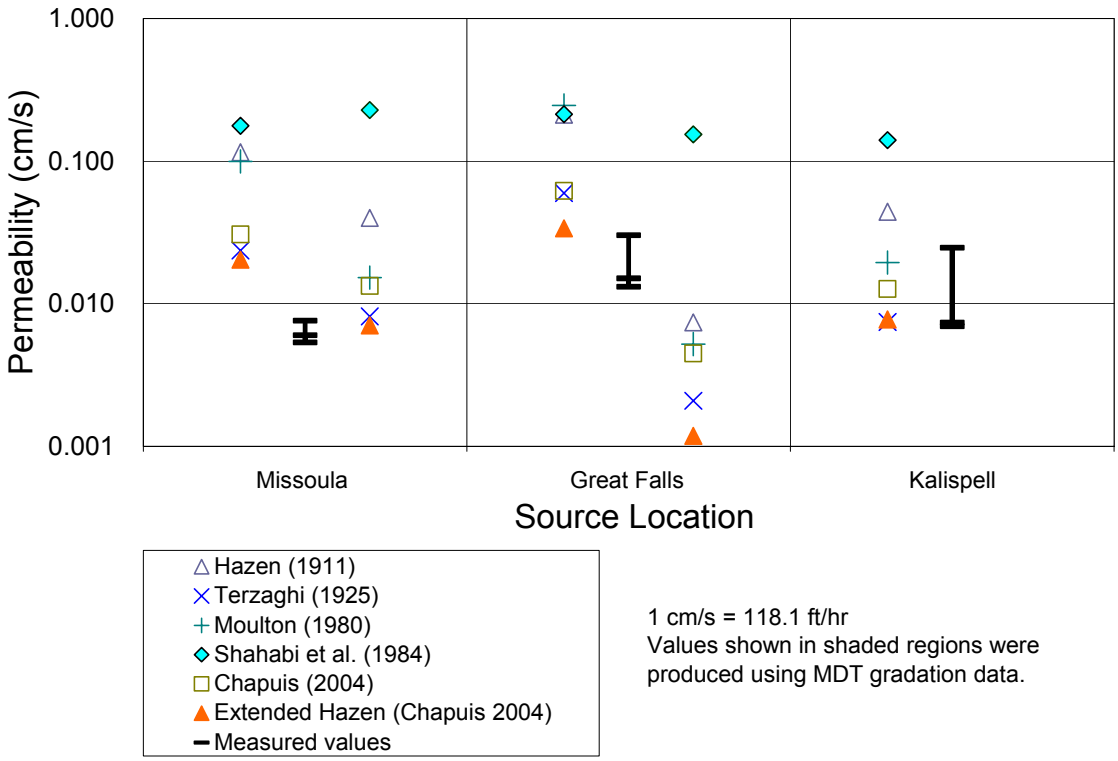

Figure 29. Calculated permeabilities for the 5A aggregates.

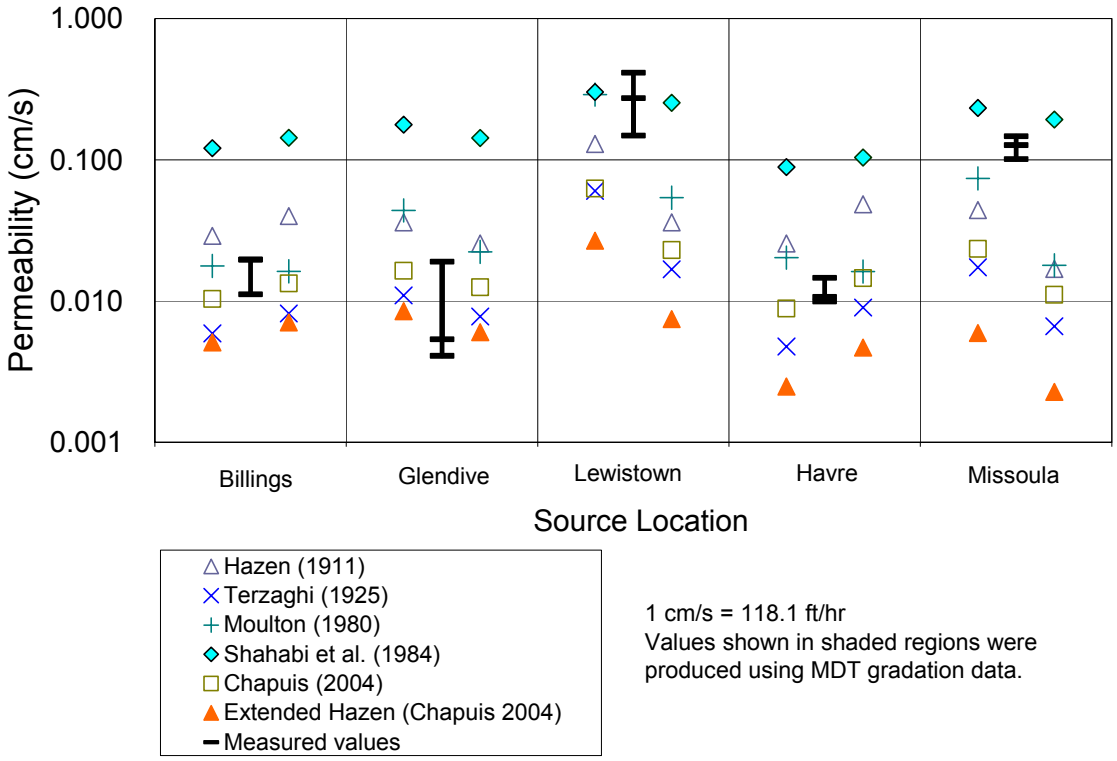

Figure 30. Calculated permeabilities for the 2A aggregates.

Ranges of permeability predicted by the correlation equations varied widely, as summarized in Table 14. In many cases, the highest and lowest predicted values of *k* bracketed the measured *k* values. This is true of 6A-Butte, 6A-Kalispell, 5A-Great Falls, 5A-Kalispell, 2A-Billings, and 2A-Havre. The *k* predictions from the Hazen (1911) and Moulton (1980) equations both tended to fall at or near the upper end of the estimations, while the *k* predictions from the Terzaghi (1925) and extended Hazen (Chapuis, 2004) equations both fell at or near the lower end of the estimations. The equations from Chapuis (2004) and Moulton (1980) tended to fall somewhere in between these high and low values.

Table 14. Ranges of Predicted Permeability Based on Aggregate Type

Prediction Equation	**CBC-6A (cm/s)**	**CBC-5A (cm/s)**	**CTS-2A (cm/s)**
Hazen (1911)	0.021-0.002	0.078-0.044	0.083-0.031
Terzaghi (1925)	0.015-0.004	0.016-0.007	0.039-0.007
Moulton (1980)	0.077-0.010	0.057-0.020	0.172-0.017
Shahabi et al. (1984)	0.195-0.113	0.203-0.140	0.278-0.097
Chapuis (2004)	0.045-0.008	0.022-0.013	0.043-0.012
Extended Hazen (Chapuis, 2004)	0.063-0.007	0.014-0.008	0.017-0.004
Measured Values	0.529-0.002	0.030-0.005	0.273-0.004

* Note; The predicted permeability ranges are based on averages from both the MSU and MDT data.

The equation developed by Shahabi et al. (1984) generally over predicted *k* for the aggregates in this study. This equation was not very sensitive to its inputs because predicted values of *k* did not change significantly even when there were notable changes in grain size distribution.

The estimated permeabilities generally rise and fall in a similar manner to the measured values for each aggregate type as shown in Table 14, Figure 28, Figure 29, and Figure 30. These trends coupled with the bracketing effect of the predicted *k* values on the measured values indicates that the measured *k* values are reasonable based on past studies by others.

Void Ratio-Permeability Relationships

In addition to particle size and particle size distribution, *k* is affected by pore size, pore shape, and tortuosity. These pore characteristics are in turn affected by the state of

compaction. For cohesionless soils, the state of compaction is often quantified on a macro basis by void ratio (e). The permeameter samples in this study were each compacted using the same compaction energy and methodology; however, because of differences in particle size, shape, and distribution, the compacted void ratios varied slightly between samples. Because of the dependency of k on void structure, a relationship between e and k was explored. When all soil samples are examined together, there is not a very strong correlation between e and k, as shown in Figure 31. This indicates that k cannot be predicted solely on the basis of compacted density or e.

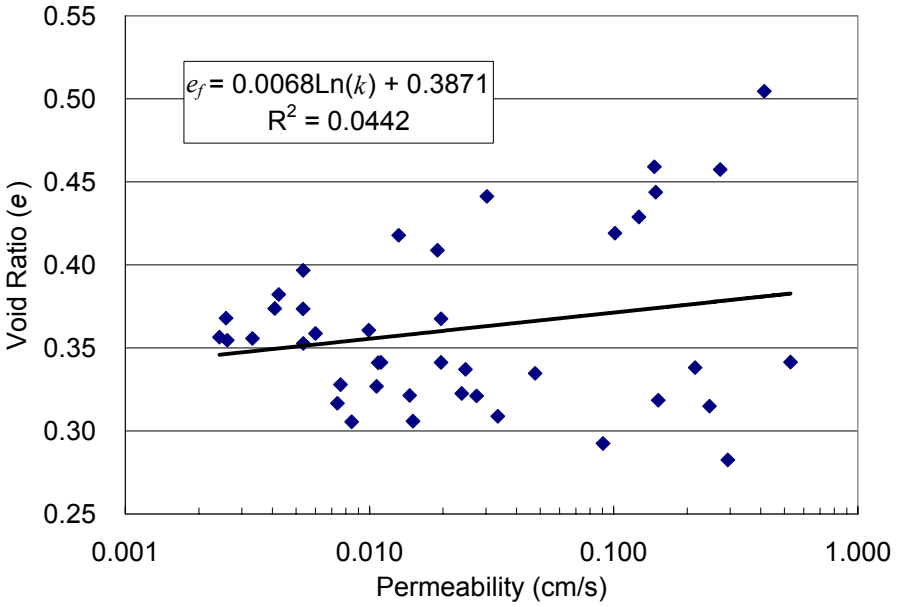

Figure 31. Void ratio versus permeability for all aggregates in this study.

The value of e commonly used to calculate k is the average e determined from weight-volume relationships using total weight and total volume data. Cote and Konrad (2003) proposed that because k is known to highly depend on smaller particles, it could

be better correlated by considering only the finer fraction of a base course aggregate. The average e is a function of both fine fraction (e_f) and coarse fraction (e_c) void ratios. Volumetric relationships illustrating e, e_c, and e_f are shown in Figure 32. By isolating only e_f, a more accurate prediction of k may be possible. The cutoff size between fine and coarse fractions depends on the material size and particle distribution – the cutoff is not necessarily the No. 200 sieve size.

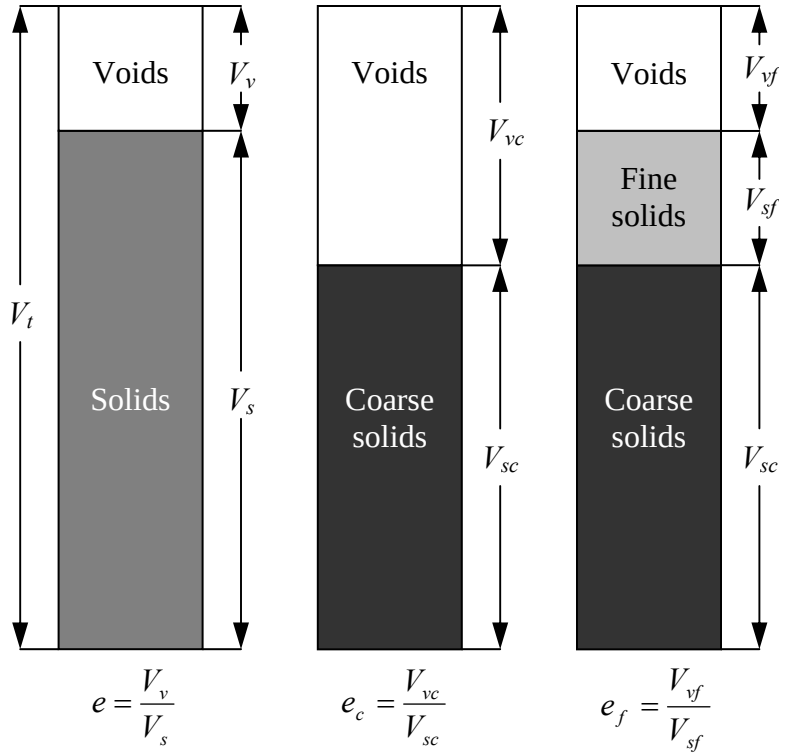

Figure 32. Phase diagrams illustrating e, e_c, and e_f for the same soil (Modified from Cote and Konrad 2003).

The following equation for calculating e_f has been modified from Cote and Konrad (2003):

$$e_f = \frac{e}{F} = \frac{V_v}{FV_s} = \frac{G_s\gamma_w - \gamma_d}{F\gamma_d} \quad (5)$$

where, V_v = volume of voids, V_s = volume of solids, e = void ratio, e_f = void ratio of the finer fraction, F is the percent fines based on the No. 10 sieve, γ_d = dry unit weight, G_s = specific gravity, and γ_w = unit weight of water.

Equation (5) requires the assumption that fine particles are evenly distributed in the void space of the coarse particle skeleton. This assumption is valid for aggregates with enough fine particles to fill the coarse particle void space, as shown in Figure 33b. The validity of this assumption is called into question for aggregates that have insufficient fine particles to completely fill the coarse fraction void space. This is difficult to quantify and could account for minor errors or inconsistencies in the data.

Based on a parametric study of sieve sizes, the No. 10 sieve was selected as the cut-off size between fine and coarse for determining the percent of fine material for use in Equation (5). A comparison of e_f versus k is shown in Figure 34. The utilization of e_f provides a significantly better correlation than e, although there is still some scatter in the data.

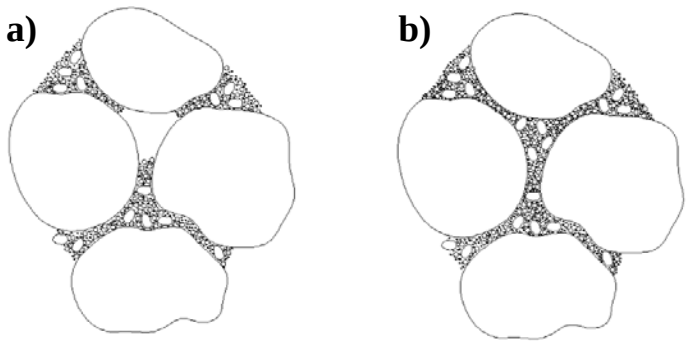

Figure 33. Conceptual schematic views of a) uneven fines distribution and b) even fines distribution.

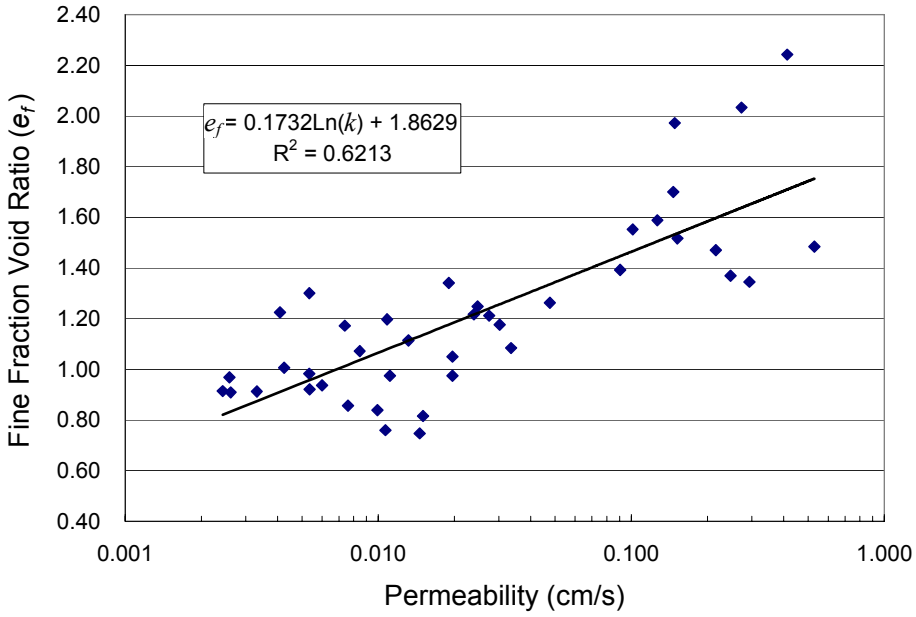

Figure 34. Fine fraction void ratio (e_f) versus permeability.

Several other correlations were examined using C_u, C_c, and d_{10}; however, none of these other parameters were effective at reducing R^2. This suggests that hydraulic properties of an aggregate rely more heavily on pore parameters than particle parameters. According to Equation (5), e_f is a function of e and F, which is derived from the grain size distribution (percent fines based on the No. 10 sieve). Aggregate compaction is often specified as some percentage of a maximum laboratory determined density or unit weight. Combining the logarithmic regression shown in Figure 34 with Equation (5) yields an equation that can be used for estimating k for base course materials used by MDT from readily assumed or measured parameters, and is shown as:

$$\ln k = \frac{1}{0.17F}\left[\frac{G_s\gamma_w}{RC\gamma_{d\max}} - 1\right] - 10.77 \qquad (6)$$

where, k is the permeability in cm/s, F is the percent material finer than the No. 10 sieve, G_s is the specific gravity, γ_w is the unit weight of water in pcf, $\gamma_{d\ max}$ is the maximum unit weight in pcf, and RC is the relative compaction.

This equation could be useful for comparing the hydraulic properties of base course aggregates, for estimating the hydraulic properties of materials that are out of specification, or to determine the maximum amount of material passing the No. 10 sieve to achieve a particular minimum k.

Equation (6) can be re-arranged to compute F (the maximum amount of material passing the No. 10 sieve) if G_s, $\gamma_{d\ max}$, the required RC, and the required minimum k are all known. This is a useful application of the equation for developing material specifications, and is presented as:

$$F = \left[\frac{1}{0.17\ln k + 1.83}\right]\left[\frac{G_s\gamma_w}{RC\gamma_{d\max}} - 1\right] \qquad (7)$$

The following steps outline the calculation procedure:

1. Determine $\gamma_{d\ max}$ from either maximum index density or modified Proctor testing.
2. Assume a value for RC. MDT commonly uses 0.95 to 0.98.
3. Measure G_s in the lab, or assume a value of about 2.7.
4. Select a minimum value of k. This value should be selected so that it is practically achievable, and will provide adequate drainage capacity.
5. Table 15 shows AASHTO (1993) design guide recommended minimum permeabilities.
6. Substitute the above parameters into Equation (7) to determine the maximum amount of material passing the No. 10 sieve.

Table 15. 1993 AASHTO Base Course Minimum Permeability Recommendations

Quality of Drainage	Minimum Permeability		Time to Drain
	ft/hr	cm/s	
Excellent	41.67	0.353	2 hours
Good	3.54	0.030	1 day
Fair	0.46	0.004	1 week
Poor	0.02	0.0002	1 month
Very poor	0.0008	0.00007	Water will not drain

Following is an example calculation.

1. $\gamma_{d\,max}$ is determined from maximum index density testing to be 138 pcf.
2. The required degree of *RC* is assumed to be 0.98, as is commonly used by MDT for the base course.
3. G_s is determined from laboratory testing to be 2.70.
4. A minimum value of *k* is assumed to be 0.01 cm/s because it is practical and achievable for these materials based on Figure 34, and will provide fair to good drainage based on the minimum values provided in Table 15.
5. The values are substituted into Equation (7) and *F* is calculated.

$$F = \left[\frac{1}{0.17\ln(0.01)+1.83}\right]\left[\frac{(2.70)(62.4)}{(0.98)(138)}-1\right] = \left[\frac{1}{1.047}\right]\left[\frac{168.48}{135.24}-1\right] = 0.235 \quad (8)$$

Solution: For this material, there can be a maximum of 23.5% of material passing the No. 10 sieve to ensure the desired minimum k is achieved.

Summary

Major achievements of the permeability testing are listed below:

- Sample preparation techniques and testing procedures were adapted for a custom-built over-sized permeameter.
- Results were obtained that are reasonable based on published typical permeability ranges and permeability estimation equations.
- Permeability was shown to depend more on e_f than aggregate type.

X-RAY COMPUTED TOMOGRAPHY

The primary goal of X-ray computed tomography (CT) scanning in this study was to non-destructively acquire and subsequently measure 2-dimensional (2D) slice images of aggregate samples to estimate/measure their properties. The soil properties of interest were the void ratio (*e*), grain size distribution, and pore size distribution. Grain size distributions were previously measured using traditional geotechnical techniques, and *e* can be calculated from weight-volume relationships. These same properties were estimated from X-ray CT data in order to test/confirm the applicability of the MSU X-ray CT scanning system for these purposes. The pore size distribution was measured to discern differences between aggregate types and to further the understanding of the internal structure/behavior of crushed and processed aggregates. In addition, image thresholding methods were developed to further refine soils image processing techniques.

The MSU X-ray CT scanner and scanning software exclusively use SI units. For this reason, SI units will be the primary units presented in the following X-ray CT sections.

History & Applications

X-ray CT was first developed in the late-1970's for use in the medical field to obtain 2D and 3D images of internal body organs and tissues. X-ray beam power was limited to approximately 125 kV with relatively short exposure times to minimize tissue damage. X-ray CT technology was adapted for industrial uses in the 1980's. Uninhibited by exposure time and power limitations inherent in medical scanning, X-ray beam

powers in excess of 400 kV were possible. This allowed for significantly better resolutions than those attainable by medical scanners, and facilitated a wide variety of applications for X-ray CT. These applications included the internal imaging of irreplaceable paleontology specimens (Conroy and Vannier 1984) and one-of-a-kind meteorites (Arnold et al. 1982). In the mid-1980's and early-1990's, X-ray CT applications in the geo-sciences were also developed. As X-ray CT scanners evolved and improved over the years, so have the vastness of applications of this technology. Ketcham and Carlson (2001) noted that the applications of X-ray CT to the geo-sciences were still only in their infancy as of the time of publishing.

X-ray CT has been used in the geotechnical and geologic fields to study a wide variety of topics. Steude et al. (1994) provides a comprehensive list of the early uses of industrial X-ray CT. Several more recent examples are provided by Ketcham and Carlson (2001) and Alramahi and Alshibli (2006). Several of the most recently studied geotechnical topics include the formation and propagation of shear bands in sand during triaxial testing (Alshibli et al. 2000, Desrues et al. 1996), and various flow and moisture properties of soil and rock (Fukahori 2003, Cislerova 2002). Researchers have attempted to use computer software to model flow properties of soil and asphalt cores using 3D X-ray CT particle and compaction information (Kutay et al. 2006). Unfortunately, this software is highly complex and is still in developmental stages.

Alternative methods for acquiring 2D slice images of soil or rock cores, such as serial sectioning, are destructive (Ketcham and Carlson 2001). The serial sectioning process involves impregnating a soil sample with low viscosity epoxy and physically cutting the object into thin slices and measuring those slices. This process is expensive,

time consuming, and can alter the internal features of a soil sample. X-ray CT can also be expensive initially due to the high capital cost of equipment. Additionally, X-ray CT is considerably faster than serial sectioning once equipment is set-up and calibrated, and X-ray CT provides digitized results that can be easily measured and stored, which makes it suitable for quantitative analyses.

The non-destructive nature of X-ray CT represents a significant advantage over traditional methods of acquiring 2D internal slice images of soil and rock cores. Non-destructive testing allows multiple tests to be run on one sample without changing the structure of that sample. Similarly, the same sample can be tested while undergoing small incremental changes, like changes in water content or stress state, to quantify the effect of these changes.

Acquiring Images: How it Works

X-ray CT scanning consists of basically two phases: image acquisition and image reconstruction. The MSU X-ray CT scanner is a 3rd generation scanner based on a classification system proposed by Ketcham and Carlson (2001). The MSU Scanner is capable of both centered and off-set geometries, though centered geometry is almost exclusively used. A schematic diagram of the major system components is shown in Figure 35. The scanning system consists of: i) an X-ray source that produces a fanned beam of X-rays, ii) lead collimator plates that shape the rough X-ray fan beam to a more precise thin fan of X-rays, iii) the object being scanned that rests on a rotating table, iv) another set of lead collimator plates to shape the X-ray fan beam, v) a phosphor screen, which converts X-ray beams into visible light, and vi) a digital camera for capturing

images of the illuminated phosphor screen during scanning. The variation in the amount of light given off at different locations along the phosphor screen is directly proportional to the extent that the X-ray beam has been attenuated by the object.

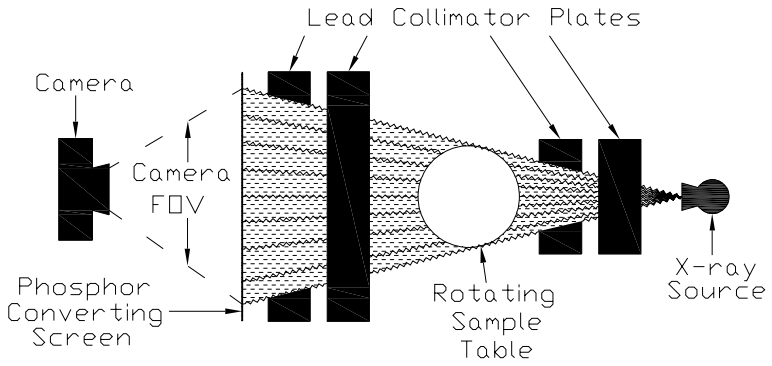

Figure 35. Schematic plan view of MSU 3rd generation CT scanner.

One camera image for a particular orientation of the object is termed a “view”, which appears as a thin strip of pixels of varying brightness. A simplified “view” of several concentric circles of varying density is shown in Figure 36a. Many views must be acquired at different degrees of rotation to produce one final 2D slice image of an object. The smaller the degree of rotation between views, the higher resolution the final 2D slice image will be.

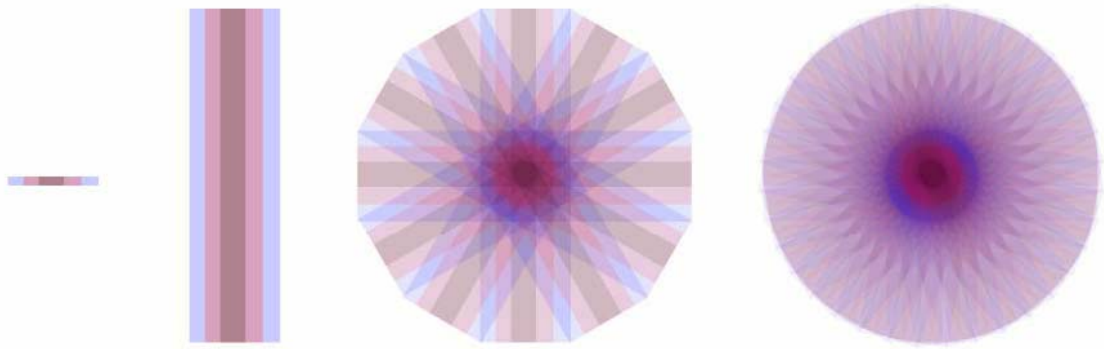

a) **b)** **c)** **d)**

Figure 36. Image reconstruction: a) single view, b) projection of single view, c) overlayed and rotated projected views, and d) same as c with more projected views (from Nielson and Mokwa 2004).

After images are acquired, they must be reconstructed. The first step in image reconstruction is projection. In this step, each view is projected to the full diameter of the spacimen, as shown in Figure 36b. Projected views are then rotated to the angle in which they were acquired and overlain on top of one another, as shown in Figure 36c and Figure 36d. Figure 37 shows different reconstructions of the same object each using different numbers of views. It can be seen in these 2D slice images that the clarity of the object is dramatically increased by increasing the number of views used to reconstruct the 2D slice image. Increasing the number of views is analogous to decreasing the degree of rotation between subsequent views.

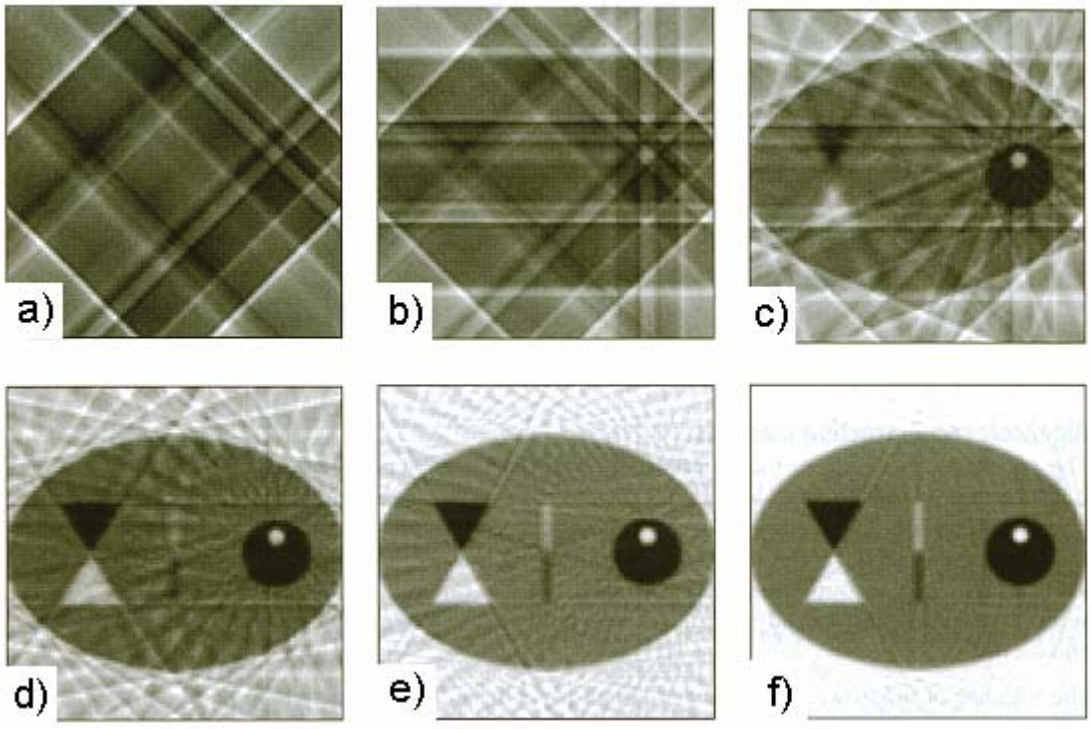

Figure 37. 2D slice CT images reconstructed using: a) two views, b) four views, c) eight views, d) 16 views, e) 32 views, and f) 64 views (from Russ 2002).

Apparatus and Scanner Setup

X-ray CT scanning was completed using MSU's custom built scanner, which is capable of 1/8 degree increment rotations and 160 kV of power. The X-ray CT scanner is fully automated and computer controlled using software developed by Synergistic Detector Designs. MSU's X-ray CT scanner required setup and adjustment to produce the highest resolution images possible for the aggregate samples.

The camera's field-of-view (FOV) (shown in Figure 35) can have a large impact on the resolution of X-ray CT images. If the camera's FOV is relatively small, fine

details will be captured in the resulting images, and if the camera's FOV is relatively large, detail is lost but larger objects can be scanned.

Particles of the 6A and 5A soil samples larger than 19.1 mm (0.75 inches) were screened and removed to reduce the sample container size, thereby reducing the camera's FOV and improving the resolution. Modification of the 2A samples was not necessary. The same container size was utilized for all samples so that all images had the same resolution, and maintained the same container diameter to maximum particle size (*d:p*) ratio. A container diameter of 76.2 mm (3 inches) was selected, which provided a *d:p* ratio of 4:1, and a resolution of approximately one pixel = 0.080 mm.

Nine scans were completed on each cylindrical sample at a spacing of one scan every 9.00 mm. Scans were not taken within 38 mm of the top or bottom of the container to avoid heterogeneities near these boundaries. Multiple scans were taken of each sample so that properties measured from each scan location could be averaged together to account for variations across the sample due to unavoidable minor segregation. The number of scans was limited to nine to keep scanning time within reason, while still providing accurate results. Each scan took approximately two hours, for a total of more than 20 hours required to fully scan each sample.

The highest power setting (160 kV) on the MSU X-ray CT scanner was used with camera exposure times of approximately 3.6 seconds. High power was necessary to fully penetrate samples because of the high density of the soil and rock samples being scanned and the relatively large size of the sample containers. Camera exposure times were set as long as possible to achieve the highest resolution possible, while preventing the saturation of pixels in the resulting digital images.

The increment of sample rotation between the acquisition of each view effects the resolution. The MSU X-ray CT scanner is capable of producing 1/8 degree increment scans. However, 1/4 degree scans were utilized in this study because the increase in resolution realized in 1/8 degree scanning was negligible, and 1/4 degree scans required significantly less acquisition and processing time. Scanning at 1/4 degree increments produced 1,440 views requiring reconstruction to produce one final 2D slice image of the soil sample.

These settings provided the highest resolution achievable by the MSU X-ray CT scanner with the samples being tested. Nielson and Mokwa (2004) provide additional details regarding soil sample imaging using the MSU X-ray CT scanner.

Sample Preparation

Meticulous care was taken during the preparation, placement, and compaction of samples to minimize segregation. All samples were compacted in four evenly sized lifts of approximately 400 grams each. Each lift received 20 drops from a 24.4-N rammer from a height of 152.4 mm, which equates to 409.9 kN-m/m^3 of compaction energy. Samples were prepared dry so that only two phases (solid and gas) were present in the samples for X-ray CT scanning, as compared to the three phases that would have to be discerned in X-ray CT images if samples were compacted moist.

Image Processing

All image processing was completed using ImageJ image analysis software, which was developed by the National Institutes of Health and is available at no charge

from http://rsb.info.nih.gov/ij. Image processing of 2D X-ray CT images involves the following basic steps: despeckling, thresholding, and measuring/analysis.

Despeckling

After image acquisition and re-construction, all 2D slice images were despeckled. This process smoothes the images by removing some of the noise present. This is accomplished in the software by measuring pixel intensities in a 3x3 grid around a given pixel and assigning this center pixel the median value of the surrounding pixels (Russ 2002). This process is completed for each pixel in the digital image. The despeckling command can be found in ImageJ in the following menus: Process – Noise – Despeckle. Despeckled images of the aggregate samples are provided in Appendix D.

Thresholding

The next image processing step is referred to as thresholding. Each pixel in an 8-bit X-ray CT image represents some grayscale value from 0 to 255, where 0 represents white or void space and 255 represents black or solid space. In order to take meaningful measurements, each pixel must be deemed either void or solid space. A cut-off threshold grayscale value must be determined to assign all pixels the distinction of either void or solid. Figure 38 shows two images, one before thresholding and one after. The corresponding histogram of pixel intensities is shown in Figure 38c. This histogram has the threshold value used to produce the image in Figure 38b indicated on the x-axis. The original image has a wide variety of pixel intensities, while the thresholded image has only white (0, void) or black (255, solid) pixels. The thresholding command can be found in ImageJ in the following menus: Image – Adjust – Threshold.

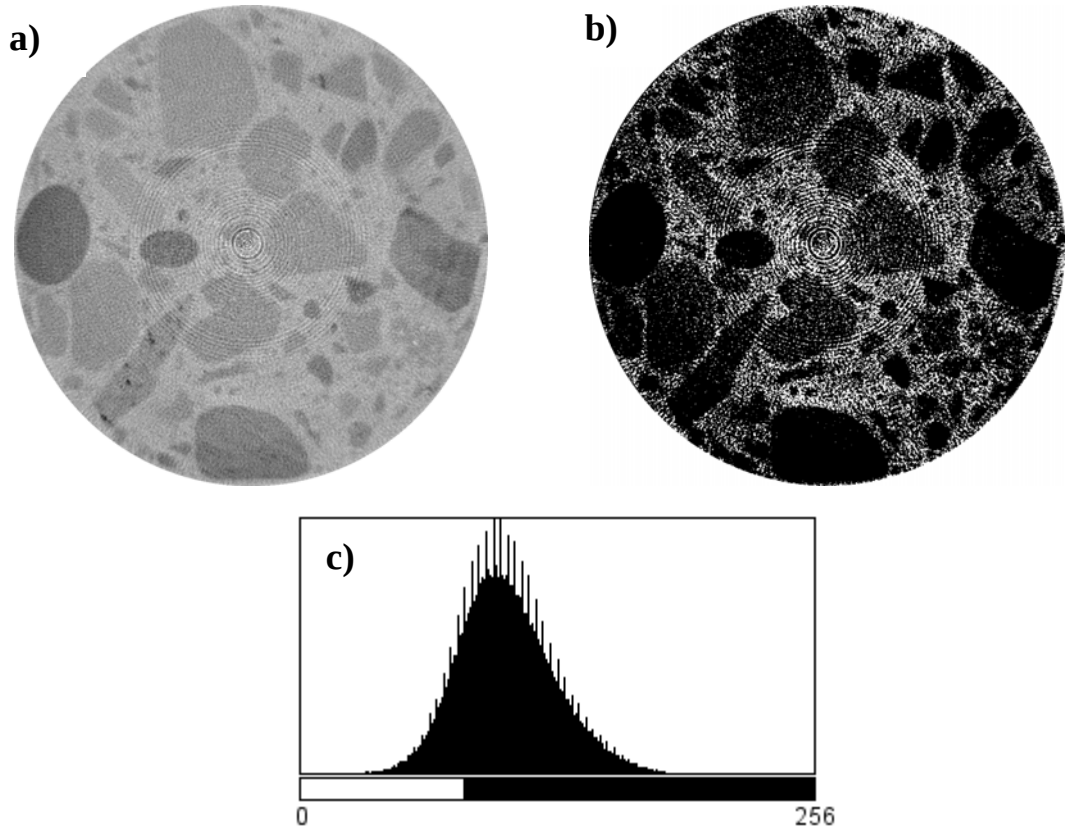

Figure 38. Thresholding example: a) original image, b) thresholded image, and c) pixel intensity histogram with threshold value indicated on the x-axis.

There are no well established guidelines for determining the threshold value for soil X-ray CT images. Images are commonly thresholded in a subjective manner by visually adjusting the threshold value until void and solid space appear to match the original image, which leads to variance between the thresholding of different images and between different operators. In scanning soil samples with particles of varying density and size, a threshold value that visually makes all known solid objects completely black may also misclassify some of the solid space as void, as shown in Figure 39. The image in Figure 39b still exhibits some void pixels in areas that are actually solid space, as indicated by the circles, despite the fact that very few void pixels can be seen in the rest

of the image. This phenomenon occurs because the measured void and solid pixel intensities partially overlap, which can at least partially be attributed to partial volume effects.

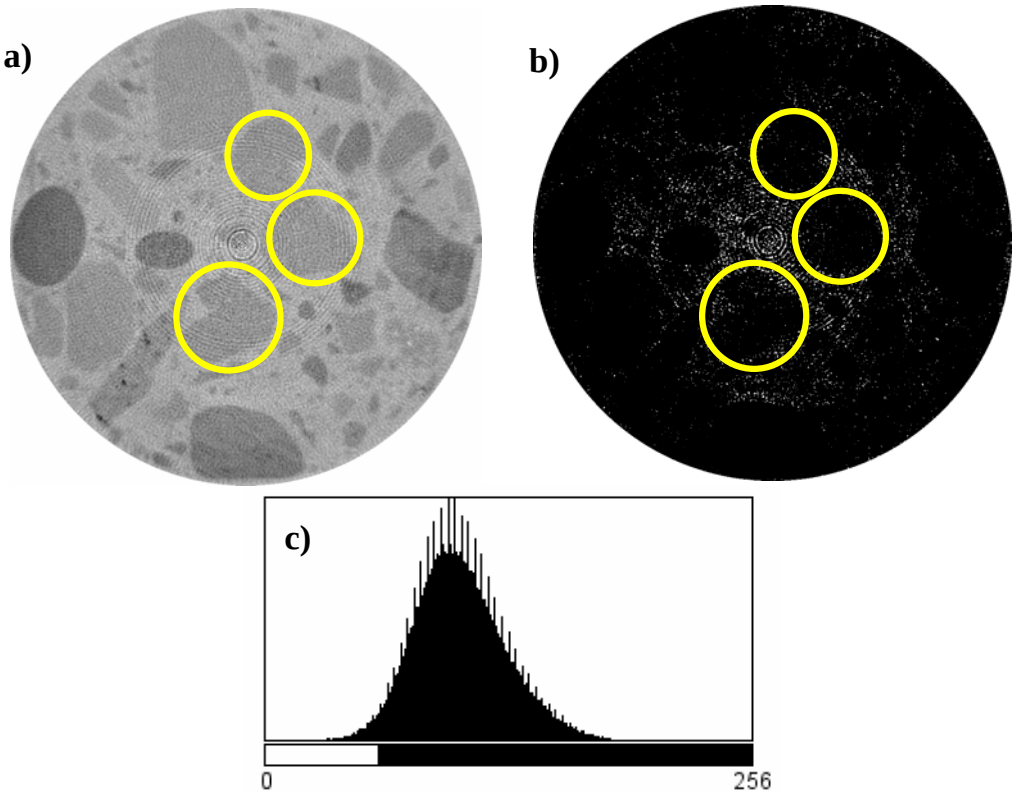

Figure 39. Thresholding example where void pixels in identified solid areas are minimized: a) original image, b) thresholded image, and c) pixel intensity histogram with threshold value indicated on the x-axis.

Each pixel in a 2D X-ray CT image represents a specific quantification of area. In this study, one pixel = 0.080 mm. If this area is occupied by several different materials, the resulting measured pixel intensity will represent some average of these different materials. In other words, if an image is acquired with several small particles (with some

air space in between them) in one pixel, then the pixel intensity produced will not represent solid or void, but rather some average of the two.

One of the subordinate goals of this research was to develop a more objective means of thresholding soil X-ray CT images. It is hypothesized that choosing a threshold value based on the histogram of grayscale pixel intensities will produce a more accurate and consistent final thresholded image. Pixel intensity histograms typically have a nearly normal distribution, with occasional slightly positive or negative skews (Figure 39c). The following statistical terms will be used in subsequent discussions:

- Average, $\mu = \frac{1}{N}\sum_{i=1}^{N} x_i$
- Mode, *M*, the most frequently occurring value in a histogram
- Standard deviation, $\sigma = \sqrt{\frac{1}{N}\sum_{i=1}^{N}(x_i - \mu)^2}$
- Pearson's 1st skewness coefficient, $s = 3\frac{\mu - M}{\sigma}$

Several options were weighed in developing a formula for determining threshold values. The following two formulas were carefully considered after a parametric study was conducted to determine the primary factors for consideration:

$$T = \mu - 0.6\sigma \quad (9)$$

$$T = M - 0.6\sigma \quad (10)$$

where, T = threshold value. The value of 0.6 was determined by trial and error and provided reasonable results for the soil images in this study. Initially, Equation (9) and Equation (10) were both used to determine threshold values for five of the soil samples (2A-Billings, 6A-Billings, 5A-Great Falls, 6A-Kalispell, and 6A-Missoula). Values of *e*

produced using these two thresholding equations were compared to the weight-volume determined *e* values. Equation (10) generally produced more accurate results, as shown in Figure 40. Equation (9) did not seem to be very sensitive to inputs because it produced values of *e* that were between 0.3 and 0.4 for all images/samples.

An in-depth sensitivity analysis was outside the scope of this study, but the following recommendation is provided for future work in this area. The values of *e* produced by Equation (10) appears to be inversely related to *s*. Therefore, it is hypothesized that incorporating some factor of *s* into Equation (10), possibly in place of the constant value of 0.6, may produce better results.

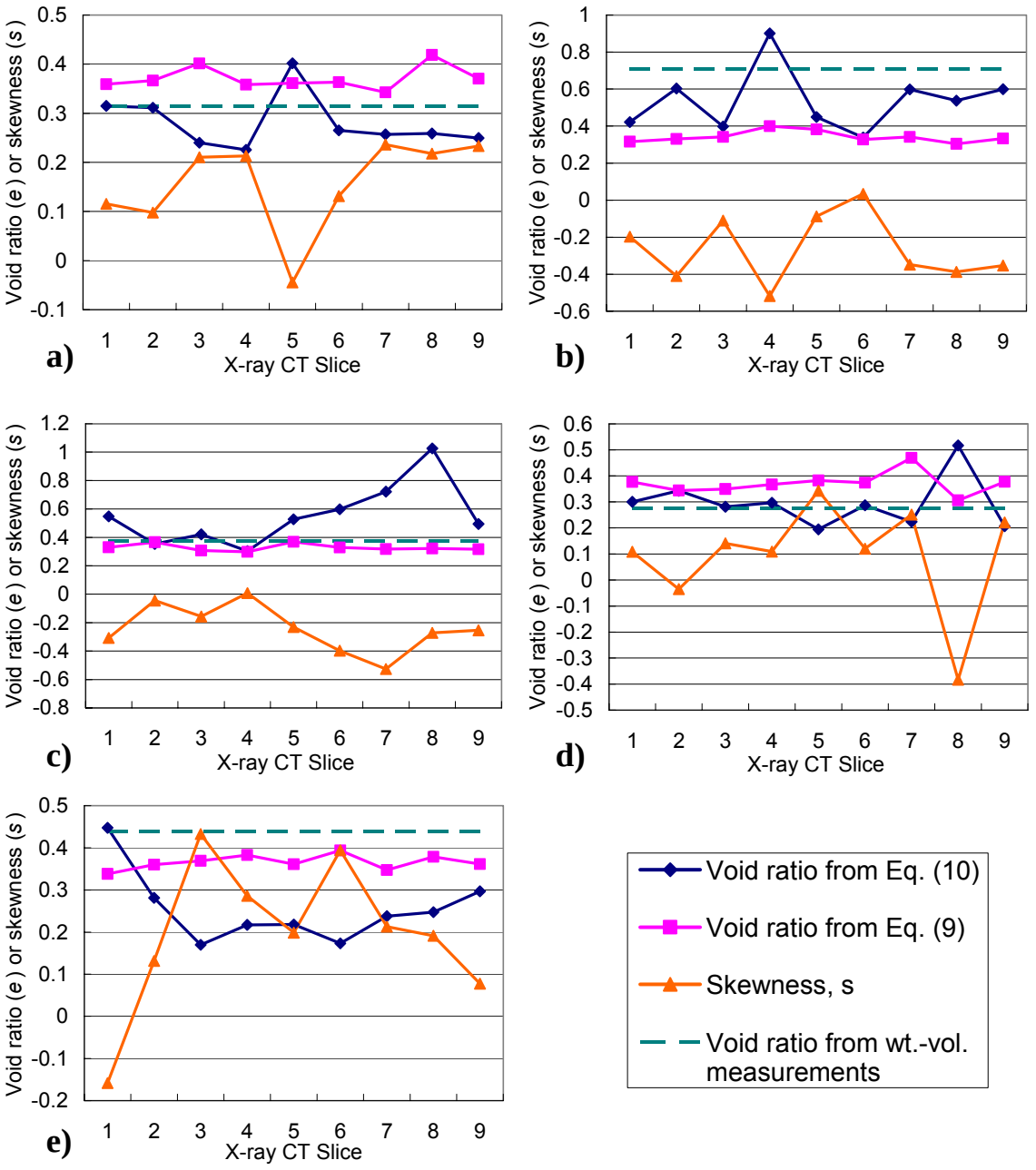

Figure 40. Threshold sensitivity plots for: a) 2A-Billings, b) 6A-Missoula, c) 6A-Billings, d) 6A-Kalispell, and e) 5A-Great Falls.

Void Ratio Analysis

Void ratio (e) was calculated from the 2D thresholded images by counting the number of void and the number of solid pixels in each image. From these pixel counts, values of e can be calculated using the following equation:

$$e = \frac{Number\ of\ void\ pixels}{Number\ of\ solid\ pixels} \tag{11}$$

Calculated e values for each of the nine images were averaged together for each aggregate sample. Values of e determined from the X-ray CT images are compared to e values determined from weight-volume relationships in Figure 41. Values of e estimated from X-ray CT images generally exhibited relatively small variances between the nine images measured for each sample. There are three exceptions (6A-Billings, 6A-Missoula, and 2A-Lewistown) that exhibited relatively large variations in CT estimated e values between different slices of the same sample. In two other samples (5A-Missoula and 2A Missoula), the weight-volume measured e did not fall in the range of the X-ray CT estimated values.

High variance or inaccuracies in the X-ray CT measured e values are attributed to the segregation of particles during placement and compaction, as well as thresholding techniques. Known inaccuracies in the measured images include partial volume effects and ring artifacts. Ring artifacts (Figure 38 and Figure 39) proved difficult to remove from the images, and are likely the result of a number of factors related to changes in the way the phosphor converting screen responds to changes in beam strength during a single CT scan. These changes in beam strength could be due to environmental conditions, such

as temperature or humidity, or variations in beam hardness as the sample rotates (Ketcham and Carlson 2001). Beam hardness causes the edges of an object to appear brighter than the center because lower energy X-rays are attenuated more easily than higher energy ones. Consequently, the average energy of the beam is changed after passing through an object.

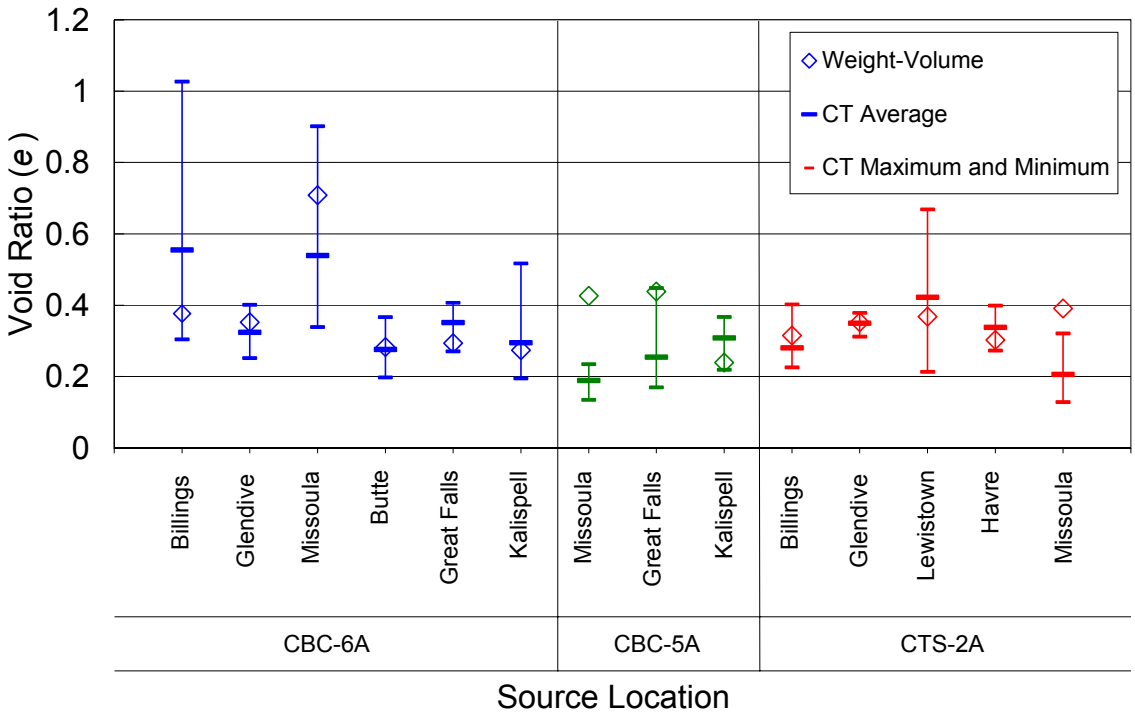

Figure 41. X-ray CT and weight-volume void ratio comparison.

Grain Size Analysis

Grain size distributions were calculated from the thresholded 2D X-ray CT images using granulometry and stereology. Granulometry and stereology are image processing and statistical methods used to determine grain or pore size distributions from 2D soil images.

The granulometry procedure involves many steps of “opening” an image and then measuring it. In 2D image processing, the process of opening an image results in the smallest particles being eliminated from the image. Before and after each opening, the number of solid pixels is counted. The difference in solid pixels before and after the opening indicates the number of particles that were contained in the size that was eliminated from the image. Openings are performed that remove increasingly large particle sizes, until all particles have been removed from the image.

The data collected in the granulometry procedure is collected from 2D images; however, grain size distributions are representative of 3D objects. Stereology is defined as the science of estimating 3D properties from 2D images. A series of statistical procedures are used to adjust granulometry data such that it approximately represents 3D objects. Mokwa and Nielson (2004) present additional details regarding granulometry and stereology procedures.

Before the granulometry and stereology analysis was performed, additional image processing was conducted to improve the accuracy of the results. During thresholding, it was visually apparent that some solid space was misclassified as void space (Figure 38b). To improve the accuracy of the process, images were closed one time to eliminate the smallest pore sizes. This resulted in the elimination of much of the misclassified void space. Remaining visually apparent misclassified void space was removed by hand. Example images from before and after this closing are shown in Figure 42. This additional step produced more accurate grain size distributions for larger particle sizes, but also reduced the resolution and consequently produced less accurate grain size distributions for smaller particle sizes.

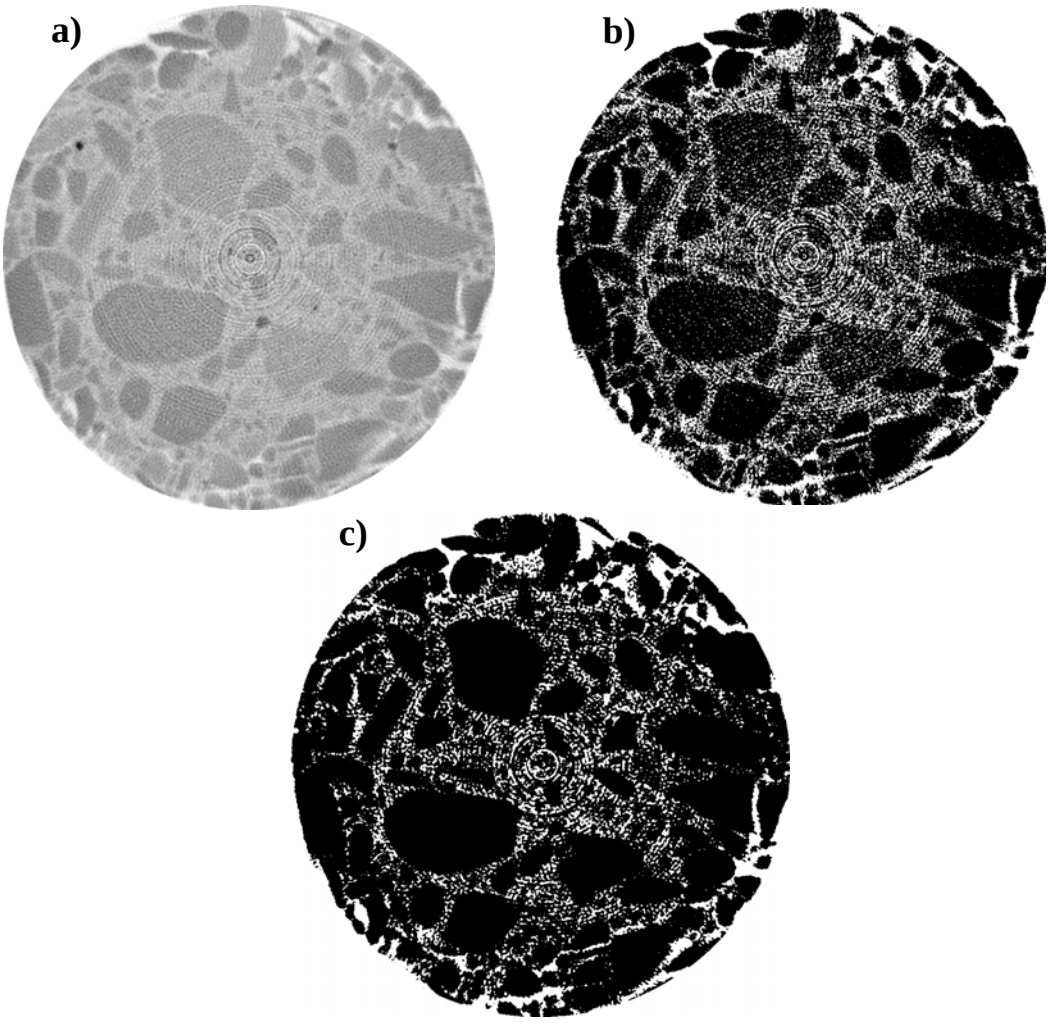

Figure 42. Image processing steps before grain size analysis: a) despeckled image, b) thresholded image, c) image after closing and removal of misclassified void pixels.

Grain size distributions were relatively accurate from the maximum particle size down to approximately 1 or 2 mm, although particles in this size range were represented slightly smaller than indicated by mechanical sieve analysis. This is likely due to some remaining pixels that are misclassified as void. These out-of-place pixels added noise to the images, and if located within a larger particle, caused that particle to be counted as a series of smaller particles. For particle sizes smaller than 1 to 2 mm, the X-ray CT grain

size estimations under-represented the fine particle sizes, as shown in Figure 43. This is likely due to partial volume effects and the closing of images before measuring grain size distribution. The X-ray CT grain size distribution shown in Figure 43 represents the average of the distributions determined for each of the 9 images collected for this sample. X-ray CT grain size distributions for all other samples are provided in Appendix E.

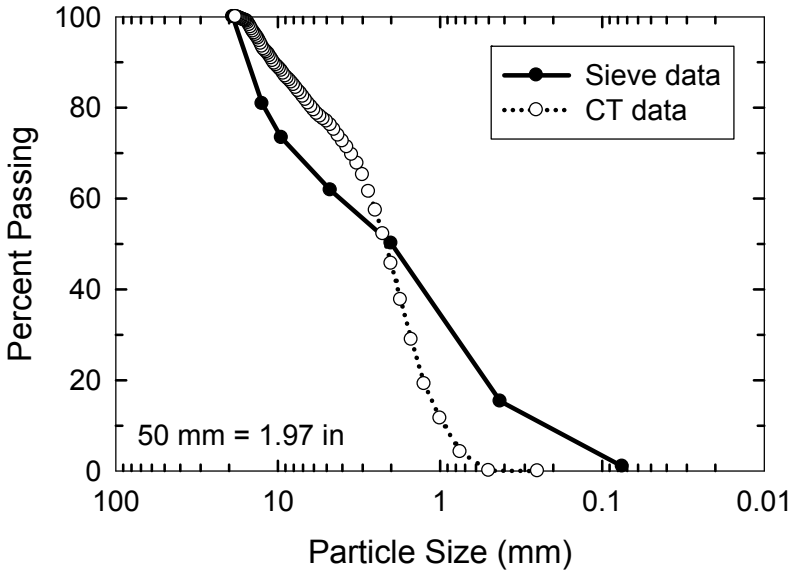

Figure 43. Grain size distributions determined by mechanical sieving and X-ray CT images for the 5A-Missoula sample.

X-ray CT grain size distributions for the 6A-Billings and 6A-Great Falls samples indicated that these samples were segregated and not representative of these materials. Consequently, these materials are not included in Appendix E and have been omitted from the remaining X-ray CT analysis.

Pore Size Analysis

Pore size distributions were calculated from the same thresholded and closed X-ray CT images by inverting the black and white pixels so that pore space was highlighted instead of grain space. The same granulometry and stereology procedures were used. Pore size distributions for 6A, 5A, and 2A samples are shown in Figure 44, Figure 45, and Figure 46, respectively.

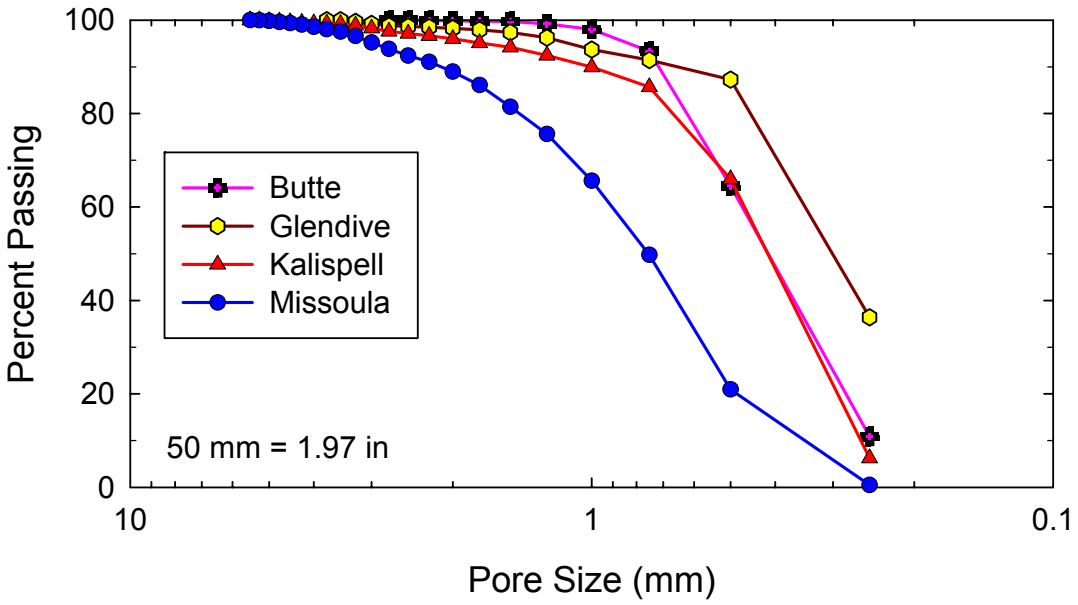

Figure 44. CBC-6A pore size distributions.

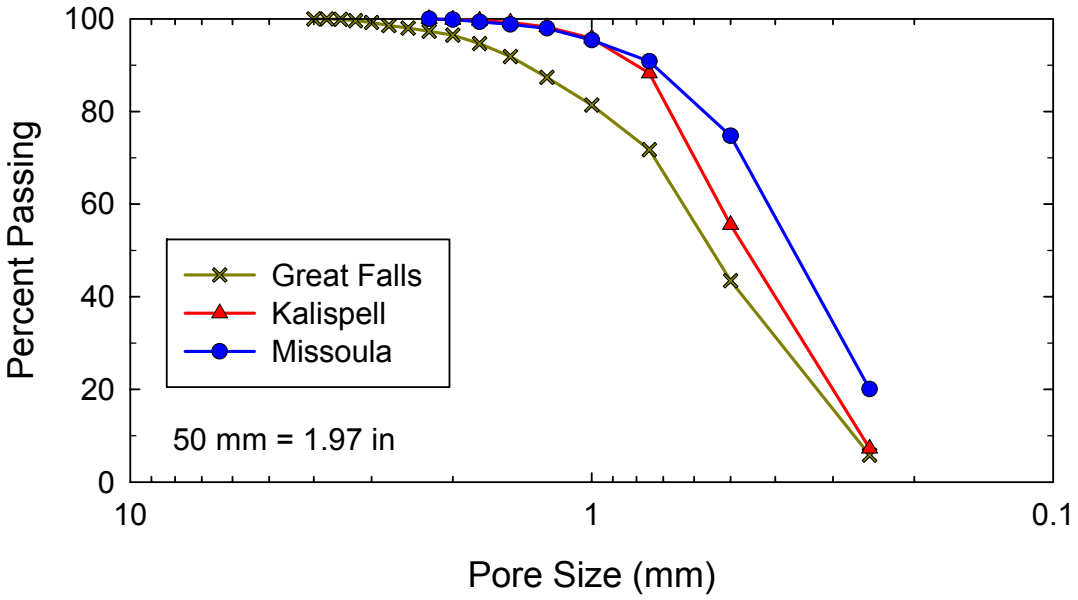

Figure 45. CBC-5A pore size distributions.

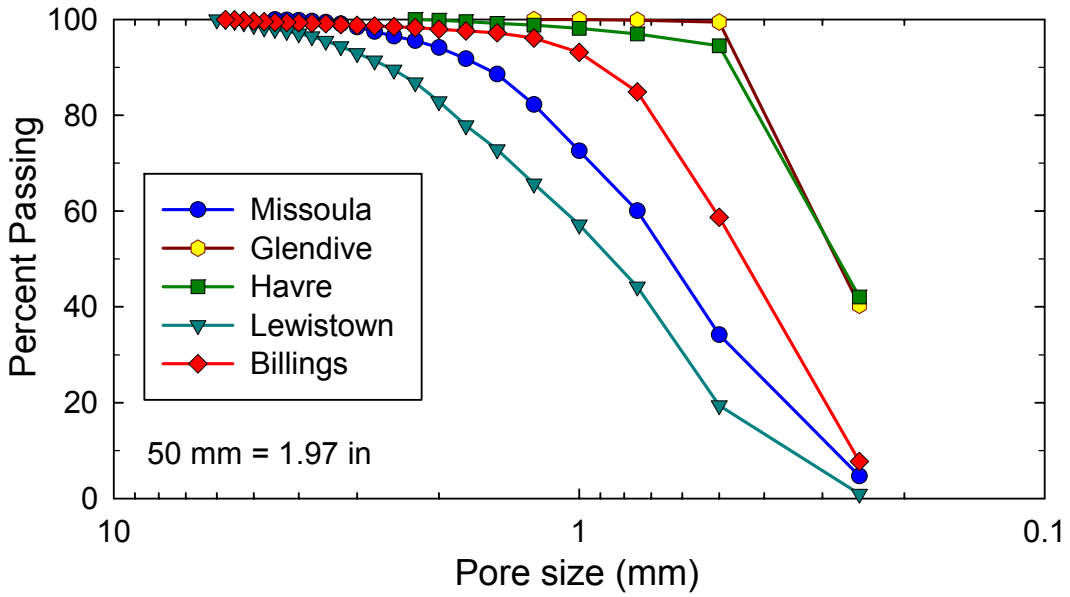

Figure 46. CTS-2A pore size distributions.

No secondary pore size distribution data was available to compare the X-ray CT data with. An abrupt change of slope in many of the pore-size curves occurs at

approximately 0.2 to 0.4 mm. This change of slope is thought to occur largely due to partial volume effects and appears to represent the limit of accuracy for the pore size distributions. This abrupt change of slope can clearly be seen in the following samples: 6A-Glendive, 6A-Butte, 6A-Kalispell, 2A-Havre, and 2A-Glendive. All other samples exhibited pore sizes that were mostly larger than this value and there is consequently no abrupt change of slope visible.

Pore size distributions do not seem to be closely correlated to material type; consequently, no differences based on aggregate type could be discerned.

Estimating Permeability from Pore Size Distribution

Background

Studies by Vervoot (2003) and Cote and Konrad (2003) indicate that pore parameters may exert more influence than grain size parameters on the hydraulic properties of soils. Several attempts have been made at correlating pore size distributions to permeability (Marshall 1958, Garcia-Bengochea 1979). Many of these correlations have been developed for fine-grained soils (particle sizes from clays to sands), but none for open-graded base course aggregates containing few fines. This is attributed to past difficulties in determining pore size distributions for open-graded aggregates containing few fines.

Pore size distributions can be determined for open-graded base course aggregates using relatively recently developed techniques that utilize X-ray CT. Other methods for determining pore size distributions of soils include correlation with the soil water characteristic curve (SWCC) and mercury intrusion. The SWCC method involves

measurement of the relationship between water content and matric suction, and relies on the assumption that matric suction is related to pore radii. This method for determining pore size parameters is not practical for large pore sizes such as those found in base course aggregates because large pores can drain under gravity alone. Mercury intrusion involves introducing mercury into a dry soil specimen and measuring the mercury content of the soil sample under different mercury pressures. This method is no longer used due to the toxicity of mercury.

Results

The pore size of 80% passing (p_{80}) was used for correlation with *k* because this parameter occurred closer to the upper portion of the pore size distributions where data is thought to be more reliable, yet low enough on the curves to be a value that is representative of the entire material sample. The pore size of 80% passing correlates well with *k*, as shown in Figure 47. Permeability values presented in Figure 47 are averages of the three *k* tests performed on each sample. Data from the 6A-Billings and 6A-Great Falls samples were not included in this correlation because they represented dramatic outliers. These outliers likely occur because particle sizes larger than 19.1 mm (0.75 inches) were screened off of the 6A samples for CT scanning, thereby significantly altering the properties of these aggregate samples.

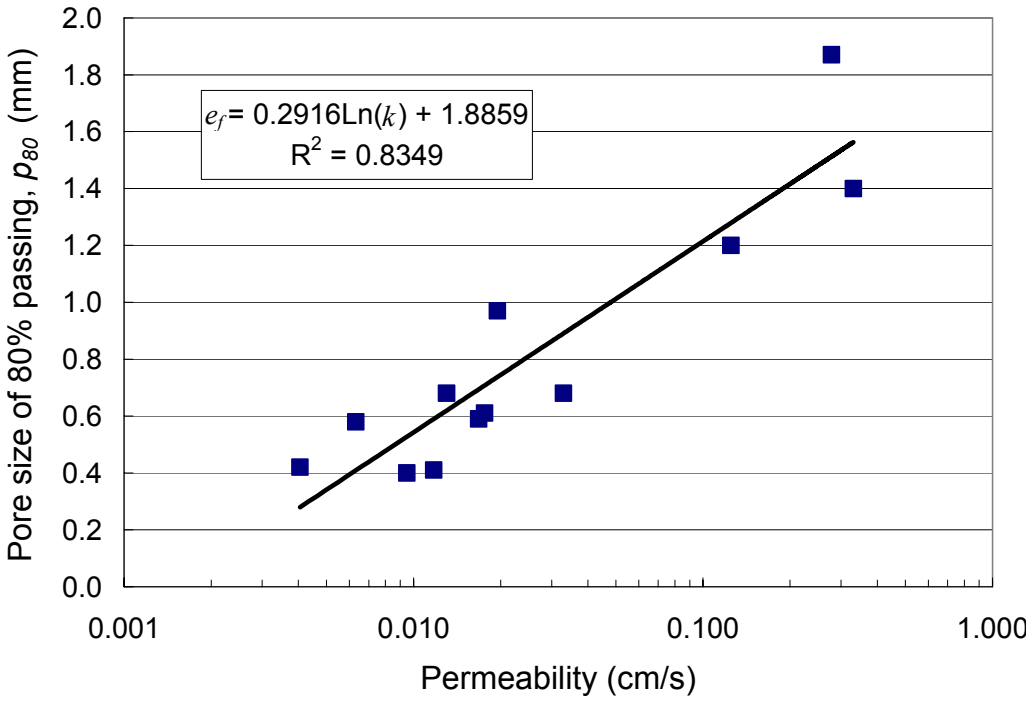

Figure 47. Pore size of 80% passing (p_{80}) versus permeability (k) plot.

Several other pore size parameter correlations were examined including the pore size of 90% passing and the percent passing the No. 10 and No. 40 sieve sizes. These pore size parameters were near the upper end of the pore size distributions, where data for all of the samples was considered most reliable. Some distributions did not produce reliable data for sizes any smaller than approximately the No. 40 sieve size. It is hypothesized that this correlation could be improved if smaller pore information could be included. Based on the data evaluation shown in Figure 47, the following equation is presented for estimating k for base course materials used by MDT:

$$\ln k = \frac{p_{80} - 1.89}{0.29} \qquad (12)$$

where p_{80} is in mm and k is in cm/s. This equation could be useful for making approximate comparisons of k between different MDT crushed aggregates, or for estimating k for out-of-specification materials.

The p_{80} correlation presented in Figure 49 has an even better R^2 value (0.84) than the e_f correlation presented in Figure 39, which had and R^2 value of 0.62. This indicates that using the p_{80}, which is derived from the pore size distribution, is more strongly correlated to hydraulic properties than e_f. While e_f is related to pore information, it is derived from weight-volume and grain size information. The correlations presented here relating k to pore parameters also provide significantly better correlations than the published equations that were evaluated in Figure 32, Figure 33, and Figure 34, which rely largely on grain size information. This shows that the hydraulic properties of crushed base course aggregates (with few fines) depend more on pore parameters than grain parameters.

Summary

Major achievements of the X-ray CT testing are listed below:

- An objective means of thresholding X-ray CT soil images was developed that was based on a histogram of pixel intensities for 2D images.
- Relatively accurate grain and pore size information was produced from 2D X-ray CT images.
- No differences based on aggregate type could be discerned between the pore size distributions.
- Pore size information was found to be very useful in understanding the hydraulic properties of these aggregates.

SUMMARY & CONCLUSIONS

This report details a laboratory analysis of three different grades of MDT aggregates. Two of these grades were crushed base course materials (CBC-6A and CBC-5A) and the other grade was a crushed top surfacing material (CTS-2A). CTS materials have smaller maximum particle sizes than CBC materials because they are intended for different uses. CBC materials are used as full depth base course aggregate layers, while CTS materials are typically used in relatively thin lifts over the CBC aggregate layer to provide a smooth flat surface for the placement of asphalt concrete.

The primary goal of this laboratory analysis was to quantify differences in engineering properties of these three material types. This information will be used to alleviate confusion among designers and materials personnel regarding customary practices, and to provide valuable information to construction personnel when faced with requests by contractors to change or substitute aggregate types.

The engineering properties examined in this study were: compaction, durability, strength, stiffness, and drainage. These properties were quantified by synthesizing and analyzing results from the following laboratory tests:

- Geotechnical index tests
- Direct shear
- R-value
- Permeability
- X-ray CT
- Los Angeles abrasion/degradation

Statistical analyses of average values based on material type were conducted using the two sample t-test to determine if apparent trends in measured laboratory test results represented true differences between aggregate types.

Direct shear tests were performed to quantify the strength and stiffness of the materials. Several parameters were quantified during this testing including the initial stiffness (k_i), the secant stiffness (k_u), and the effective friction angle (ϕ'). Another test that is used to quantify the strength and stiffness of a material is the R-value test. The R-value test is used by MDT to evaluate the stiffness, strength, and stability of subgrade and base materials. All R-value tests were completed by MDT at their Helena materials testing lab. Trends in comparing average values of these various strength/stiffness parameters based on material type are summarized in Table 16.

Table 16. Summary of Key Test Results

k_i	k_u	ϕ'	**R-value**	**Permeability**
6A > 5A	6A > 5A	6A = 5A	6A = 5A	6A > 5A
6A > 2A	6A > 2A	6A > 2A	6A > 2A	6A = 2A
5A = 2A	5A = 2A	5A = 2A	5A > 2A	5A < 2A

In summary, the CBC-6A aggregates generally exhibited the highest strength and stiffness of the three material types. The CBC-6A aggregates exhibited higher k_i and k_u values than both the CBC-5A and CTS-2A material types. On average, the CBC-6A aggregates exhibited higher ϕ' values and higher R-values than the CTS-2A materials. In terms of strength parameters measured from direct shear tests, there was no statistically significant difference between CBC-5A and CTS-2A materials. The CBC-6A and 5A materials exhibited similar average R-values, which were both slightly greater than the

CTS-2A materials. Overall, the CTS-2A materials generally exhibited the lowest average strength and stiffness. Although this material was the poorest performer when compared to the two CBC materials, it still exhibited relatively high strength and stiffness.

Drainage capacity was quantified using saturated constant head permeability (k) tests. There was some scatter in the measured k results; however, trends based on material type averages could still be statistically discerned, as summarized in the last column of Table 16. The CBC-6A and CTS-2A materials exhibited the highest average k values, while the CBC-5A materials exhibited the lowest. Permeability was shown to depend more on the fine fraction void ratio (e_f) than on aggregate type or maximum particle size. A method of predicting k based on e_f was developed, which will allow MDT designers to estimate k based on gradation and state of compaction. This equation could be useful for comparing the hydraulic properties of base course aggregates, for estimating the hydraulic properties of materials that are out of specification, or to determine the maximum amount of material passing the No. 10 sieve to achieve a particular minimum k.

X-ray CT scanning was performed to acquire pore size distributions of the materials. No differences between aggregate types could be discerned from the CT images, but it was determined that hydraulic properties are highly on the pore properties of aggregates. The pore size of 80% passing (p_{80}) was correlated to k, and an equation was presented for this correlation. This equation could be useful for predicting k of crushed base course materials with relatively few fines, if pore size information is available. Additionally, an equation was presented for thresholding 2D X-ray CT soil

images. This equation could be applied in future studies to help reduce the subjectivity of the thresholding process.

Hydraulic properties of open-graded crushed base course materials with relatively few fines were found in this study to depend almost entirely on pore properties. The relationship between e_f and k is convenient because it can be determined from the grain size distribution and compaction information, which are both easily determined in the laboratory. If pore properties can be measured directly, an even better prediction of hydraulic properties can be realized. In this study, p_{80} was found to be strongly correlated to k.

LA abrasion testing was performed to quantify the durability of the aggregates. CBC-5A-Missoula and CTS-2A-Havre did not meet MDT durability specifications based on LA Abrasion testing. Results from the LA abrasion tests did not show any trends with regard to material type. It is hypothesized that the durability measurement in this test depends heavily on the mineralogy of the aggregate.

Based on the results from strength, stiffness, and drainage testing, the CBC-6A materials were generally the best performers in this study. The CBC-5A aggregates generally exhibited the second highest strength and stiffness, but also had the lowest drainage capacity. The CTS-2A aggregates generally exhibited the lowest strength and stiffness, but had relatively good drainage capacity. The ability to substitute CTS-2A material for CBC aggregates depends on the relative importance that is assigned to strength, stiffness, and drainage in the pavement design model.

REFERENCES

AASHTO (American Association of State Highway Transportation Officials) (1993). "AASHTO Guide for Design of Pavement Structures." Washington, D.C.

Alramahi, B.A. and Alshibli, K.A. (2006). "Applications of Computed Tomography (CT) to Characterize the Internal Structure of Geomaterials: Limitations and Challenges." *Proceedings*, GeoShanghai Conference - Site and Geomaterial Characterization, Geotechnical Special Publication, No. 149, pp. 88-95.

Alshibli, K.A., Sture, S., Costes, N.C., Frank, M.L., Lankton, M.R., Batiste, S.N., and Swanson, R.A. (2000). "Assessment of Localized Deformations in Sand Using X-Ray Computed Tomography." *Journal of Geotechnical Testing*, Vol. 23, No. 3, pp. 274-299.

Arnold, J.R., Testa, J.P., Friedman, P.J., and Kambic, G.X. (1982). "Computed Tomographic Analysis of Meteorite Inclusions." *Science*, Vol. 219, pp. 383-384.

Atkinson, J.H. and Bransby, P.L. (1978). "The Mechanics of Soils: An Introduction to Critical State Soil Mechanics." McGraw-Hill, New York, 375 pp.

Bowles, J.E. (1992). "Engineering Properties of Soils and their Measurement." 4th Ed., McGraw-Hill, New York, 241 pp.

Carman, P.C. (1937). "Fluid Flow Through a Granular Bed." *Transactions*, Institution of Chemical Engineers, Vol. 15, p. 150, London, England.

Carrier, W.D. (2003). "Goodbye, Hazen; Hello, Kozeny-Carman." *Journal of Geotechnical and Geoenvironmental Engineering*, Vol. 129, No. 11, pp. 1054-1056.

Chapuis, R. P. (2004). "Predicting the Saturated Hydraulic Conductivity of Sand and Gravel using Effective Diameter and Void Ratio." *Canadian Geotechnical Journal*, Vol. 41, No. 5, pp. 787-795.

Cislerova, M. and Votrubova, J. (2002). "CT Derived Porosity Distribution and Flow Domains." *Journal of Hydrology*, Vol. 267, No. 3-4, pp. 186-200.

Conroy, G.C. and Vannier, M.W. (1984). "Noninvasive Three-Dimensional Computer Imaging of Matrix-Filled Fossil Skulls by High-Resolution Computed Tomography." *Science*, Vol. 226, pp. 456-458.

Cote, J. and Konrad, J.M. (2003). "Assessment of the Hydraulic Characteristics of Unsaturated Base-Course Materials: A Practical Method for Pavement Engineers." *Canadian Geotechnical Journal*, Vol. 40, No. 1, pp. 121-136.

Das, B.M. (2002). "Principles of Geotechnical Engineering." 5th Ed., Brooks/Cole, CA, 589 pp.

Desrues, J., Chambon, R., Mokni, M., and Mazerolle, F. (1996). "Void Ratio Evolution Inside Shear Bands in Triaxial Sand Specimens Studied by Computed Tomography." *Geotechnique*, Vol. 46, No. 3, pp. 529-546.

Fukahori, D., Sato, A., Sugawara, K. (2006). "Development of a New X-Ray CT Permeation Test System and Application to Porous Rocks." *Proceedings,* GeoCongress 2006: Geotechnical Engineering in the Information Technology Age, p. 49.

Garcia-Bengochea, I., Lovell, C.W., and Wood, L.E. (1979). "Use of Pore Size Distribution Parameters to Predict Permeability." *Proceedings*, European Conference on Soil Mechanics and Foundation Engineering, Vol. 2, pp. 49-56.

Hazen, A. (1911). Discussion of "Dams on Sand Foundations." by A.C. Koeing, *Transactions*, ASCE (American Society of Civil Engineers), Vol. 73, pp. 199-203.

Holtz, R.D. and Kovacs, W.D. (1981). "An Introduction to Geotechnical Engineering." Prentice-Hall, New Jersey, 733 pp.

Huang, Y.H. (2004). "Pavement Analysis and Design." 2nd Ed., Pearson Prentice Hall, New Jersey, 775 pp.

Ketcham, R.A. and Carlson, W.D. (2001). "Acquisition, Optimization and Interpretation of X-Ray Computed Tomographic Imagery: Applications to the Geosciences." *Computers & Geosciences*, Vol. 27, pp. 381-400.

Kozeny, J. (1927). "Uber kapillare Leitung des Wassers in Boden," *Sitzungsberichte der Wiener Akademie der Wessenschaften,* Vol. 136, Part 2A, pp. 271-306 (in German).

Kutay, M.E., Ahmet, H.A., and Harman, T. (2006). "Dynamic Hydraulic Conductivity (Permeability) of Asphalt Pavements." *Proceedings*, GeoCongress 2006: Geotechnical Engineering in the Information Technology Age, pp. 230-236.

Marshall, T.J. (1958). "A Relation Between Permeability and Size Distribution of Pores." *Journal of Soil Science*, Vol. 9, No. 1, pp. 1-8.

Moulton, L.K. (1980). "Highway Subdrainage Design." Report No. FHWA-TS-80-224, Federal Highway Administration.

Nielsen, B.D. and Mokwa, R.L. (2004). "Non-Destructive Soil Testing Using X-Ray Computed Tomography." Final Research Report for the Western Transportation Institute, Bozeman, Montana, 126 pp.

PCA (Portland Cement Association). (1966). "Thickness Design for Concrete Pavements."

Russ, J.C. (2002). "The Image Processing Handbook." 4th Ed., CRC Press, Florida, 732 pp.

Shahabi, A.A., Das, B.M., and Tarquin, A.J. (1984). "An Empirical Relation for Coefficient of Permeability of Sand." *Proceedings*, Fourth Australia-New Zealand Conference on Geomechanics, Vol. 1, pp. 54-57.

Steude, J.S., Hopkins, F., and Anders, J.E. (1994). "Industrial X-Ray Computed Tomography Applied to Soil Research." Tomography of Soil-Water-Root Processes, Soil Science Society of America (SSSA) Special Publication, No. 36, pp. 29-41.

Terzaghi, C. (1925). "Principles of Soil Mechanics: III-Determination of Permeability of Clay." *Engineering News Record*, Vol. 95, No. 21, pp. 832-836.

Thornton, S.I. and Toh, C.L. (1995). "Permeability of Pavement Base Course." Report No. MBTC FR 1010, Arkansas Highway and Transportation Department, Little Rock, Arkansas, and Mack-Blackwell National Rural Transportation Study Center, University of Arkansas, Fayetteville, 66 pp.

Van Til, C.J., McCullough, B.F., Vallerga, B.A., and Hicks, R.G. (1972). "Evaluation of AASHO Interim guides for Design of Pavement Structures." Report No. NCHRP 128, Highway Research Board.

Vervoort, R.W. and Cattle, S.R. (2003). "Linking Hydraulic Conductivity and Tortuosity Parameters to Pore Space Geometry and Pore-Size Distribution." *Journal of Hydrology*, Vol. 272, No. 1-4, pp. 36-49.

APPENDICES

APPENDIX A

MDT GRAIN SIZE DISTRIBUTION ANALYSIS PLOTS

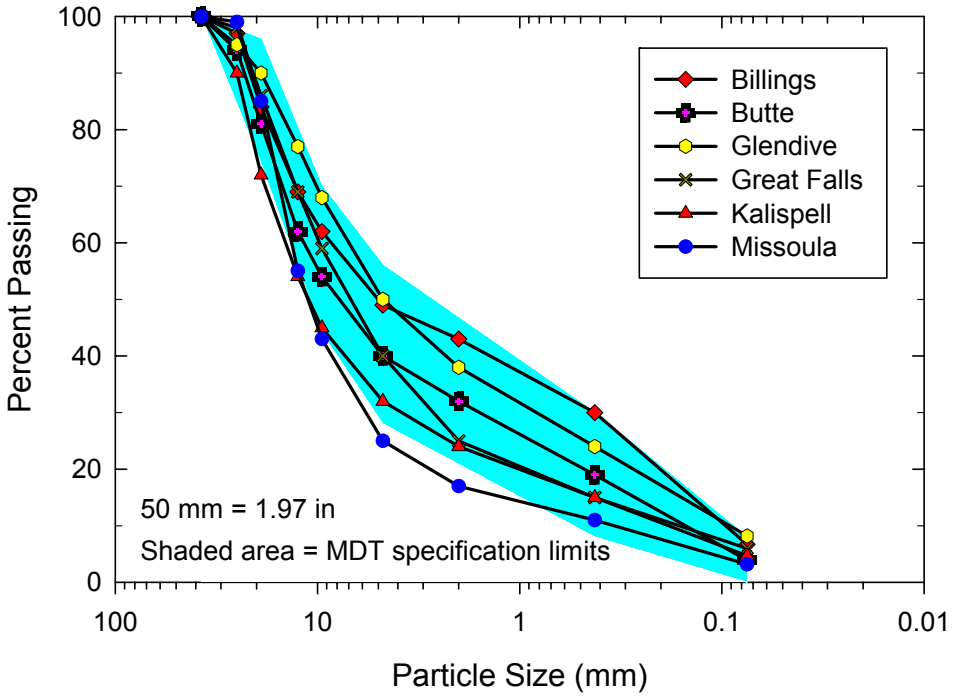

Figure A 1. CBC-6A gradation results from MDT soils lab.

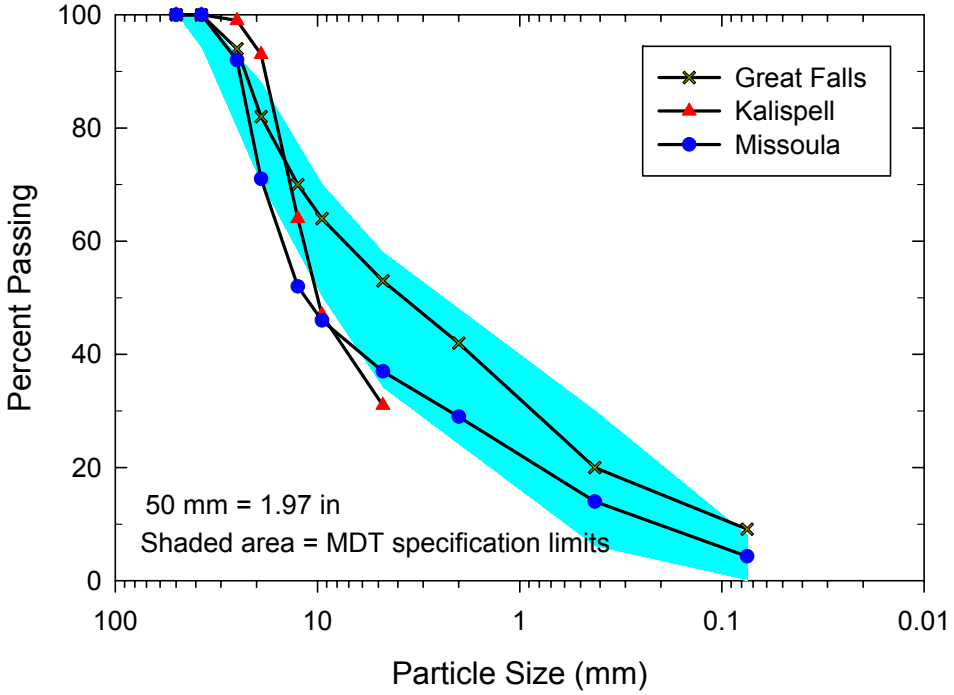

Figure A 2. CBC-5A gradation results from MDT soils lab.

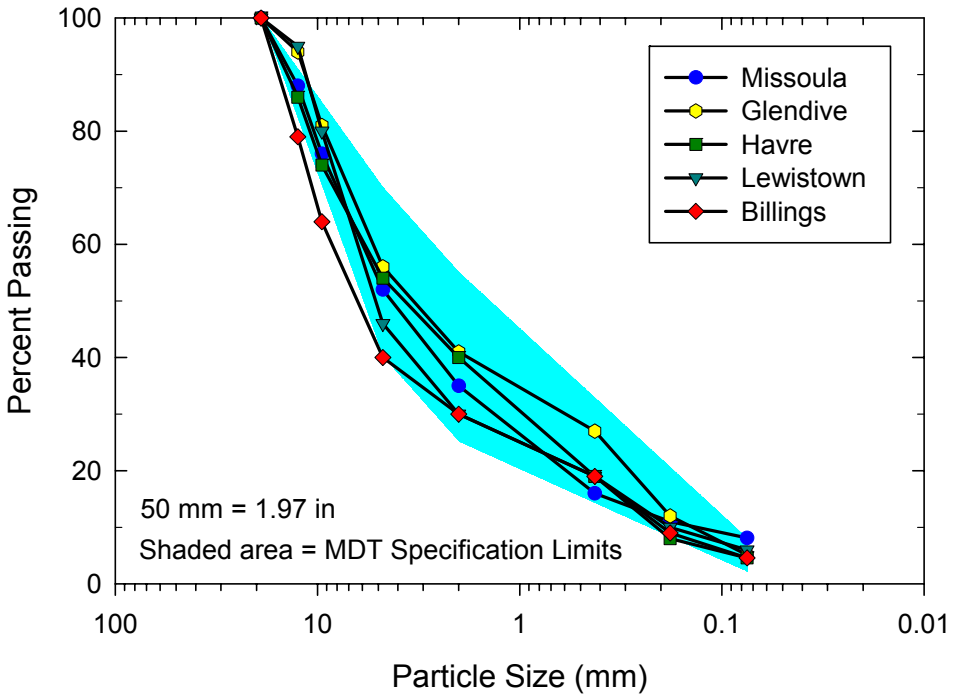

Figure A 3. CBC-2A gradation results from MDT soils lab.

APPENDIX B

R-VALUE TEST REPORTS

R-VALUE TEST REPORT

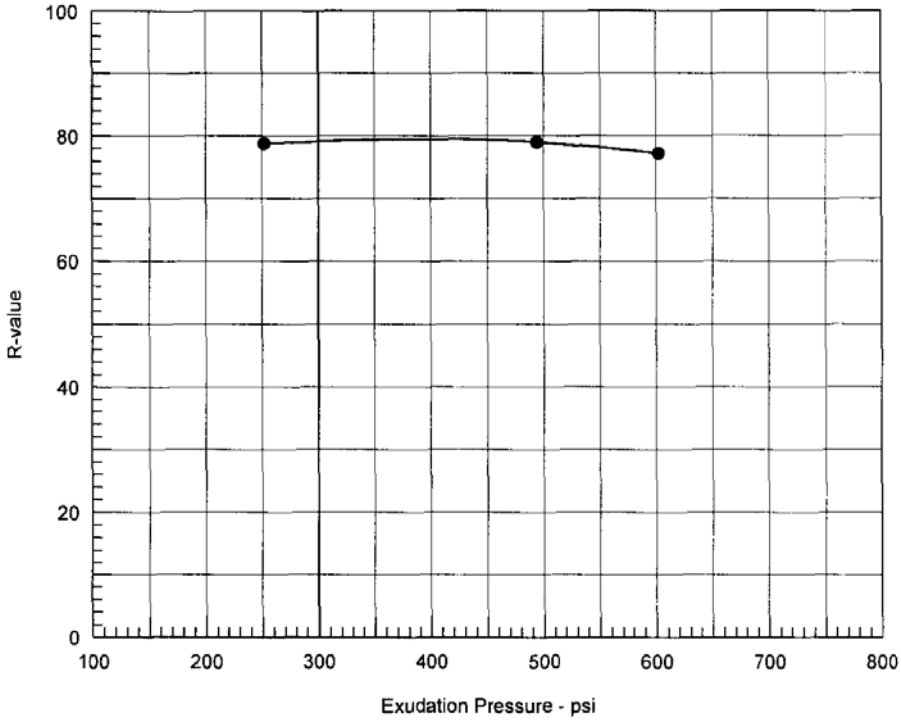

Resistance R-Value and Expansion Pressure - AASHTO T 190

No.	Compact. Pressure psi	Density pcf	Moist. %	Expansion Pressure psi	Horizontal Press. psi @ 160 psi	Sample Height in.	Exud. Pressure psi	R Value	R Value Corr.
1	350	0.0	0.0	0.00	15	2.41	602	78	77
2	350	0.0	0.0	0.00	15	2.53	252	79	79
3	350	0.0	0.0	0.00	16	2.47	494	79	79

Test Results	Material Description
R-value at 300 psi exudation pressure = 79	
Project No.: MDT 8117-30 **Project:** Experimental Surfacing Materials **Sample Number:** 865185 **Date:** 3/7/2007	**Tested by:** **Checked by:** **Remarks:**
R-VALUE TEST REPORT **MONTANA DEPARTMENT OF TRANSPORTATION**	**Figure** ____

Figure B 1. R-value test report for 6A-Missoula.

R-VALUE TEST REPORT

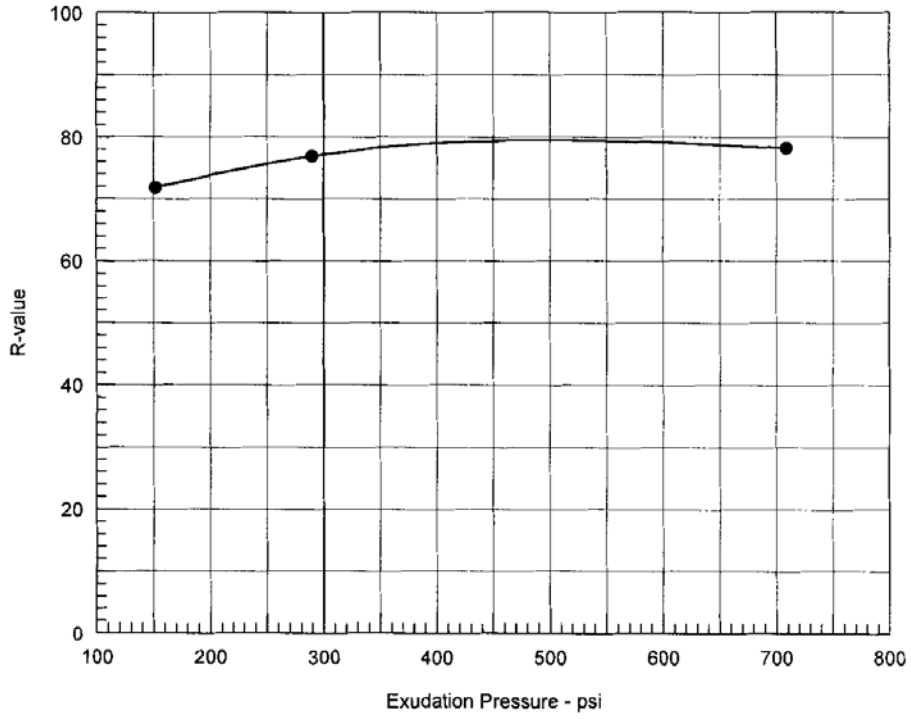

Resistance R-Value and Expansion Pressure - AASHTO T 190

No.	Compact. Pressure psi	Density pcf	Moist. %	Expansion Pressure psi	Horizontal Press. psi @ 160 psi	Sample Height in.	Exud. Pressure psi	R Value	R Value Corr.
1	350	0.0	0.0	0.00	18	2.45	709	78	78
2	350	0.0	0.0	0.00	28	2.58	152	70	72
3	350	0.0	0.0	0.00	23	2.43	290	78	77

Test Results	Material Description
R-value at 300 psi exudation pressure = 77	

Project No.: MDT 8117-30
Project: Experimental Surfacing Materials
Sample Number: 865181

Date: 3/7/2007

Tested by:
Checked by:
Remarks:

R-VALUE TEST REPORT
MONTANA DEPARTMENT OF TRANSPORTATION

Figure ____

Figure B 2. R-value test report for 6A-Glendive.

R-VALUE TEST REPORT

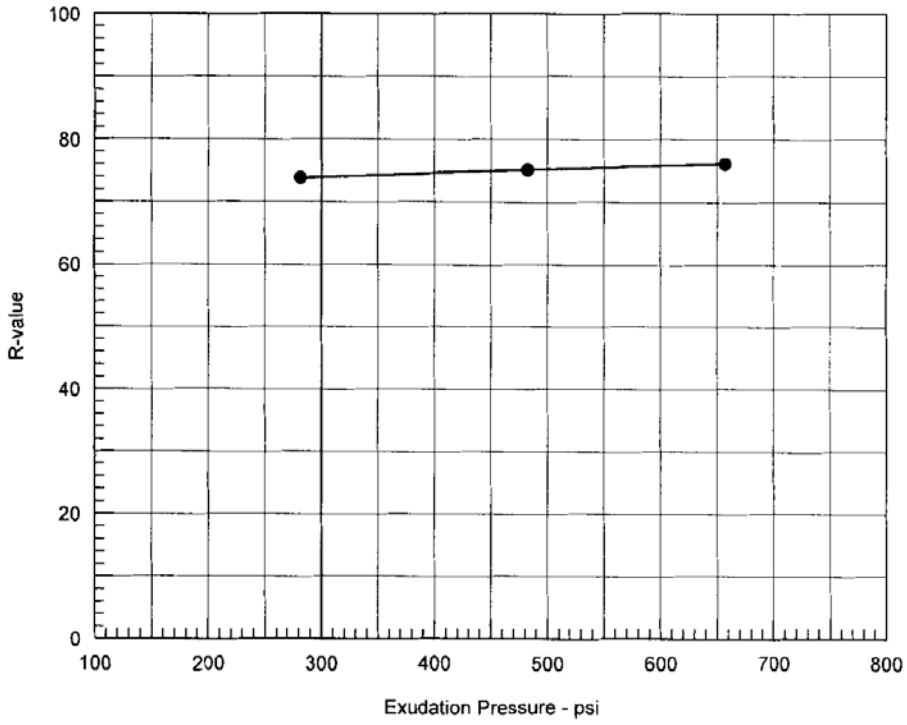

Resistance R-Value and Expansion Pressure - AASHTO T 190

No.	Compact. Pressure psi	Density pcf	Moist. %	Expansion Pressure psi	Horizontal Press. psi @ 160 psi	Sample Height in.	Exud. Pressure psi	R Value	R Value Corr.
1	350	0.0	0.0	0.00	24	2.50	281	74	74
2	350	0.0	0.0	0.00	21	2.50	657	76	76
3	350	0.0	0.0	0.00	23	2.57	483	74	75

Test Results	Material Description
R-value at 300 psi exudation pressure = 74	

Project No.: MDT 8117-30
Project: Experimental Surfacing Materials
Sample Number: 865180

Date: 3/7/2007

Tested by:
Checked by:
Remarks:

R-VALUE TEST REPORT
MONTANA DEPARTMENT OF TRANSPORTATION

Figure ____

Figure B 3. R-value test report for 6A-Billings.

R-VALUE TEST REPORT

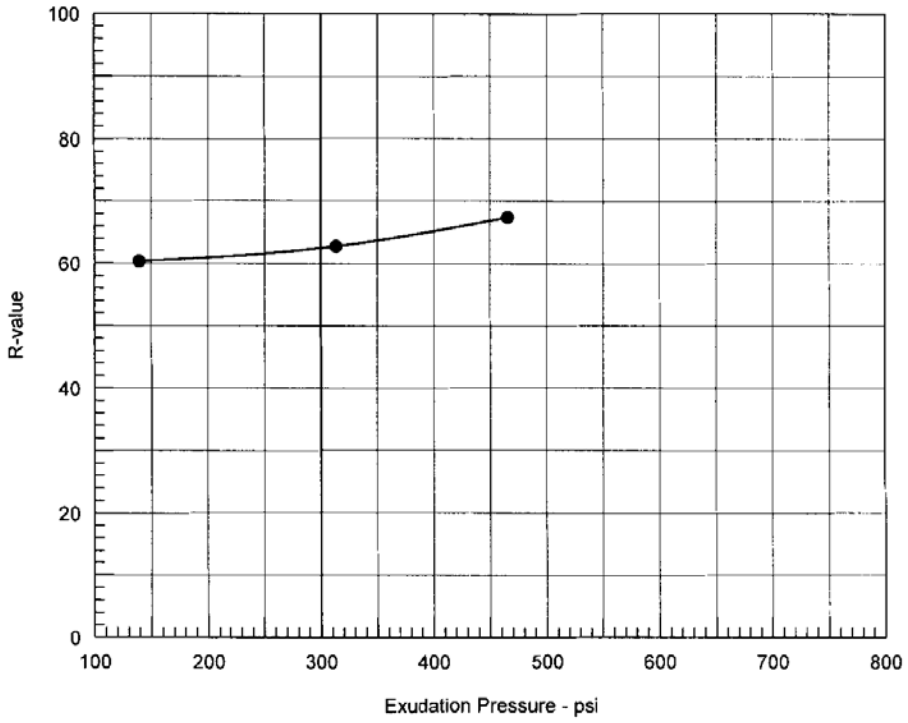

Resistance R-Value and Expansion Pressure - AASHTO T 190

No.	Compact. Pressure psi	Density pcf	Moist. %	Expansion Pressure psi	Horizontal Press. psi @ 160 psi	Sample Height in.	Exud. Pressure psi	R Value	R Value Corr.
1	350	0.0	0.0	0.00	25	2.48	466	67	67
2	350	0.0	0.0	0.00	30	2.38	140	63	60
3	350	0.0	0.0	0.00	27	2.31	314	67	63

Test Results	Material Description
R-value at 300 psi exudation pressure = 62	
Project No.: MDT 8117-30 **Project:** Experimental Surfacing Materials **Sample Number:** 865163 **Date:** 3/7/2007	**Tested by:** **Checked by:** **Remarks:**
R-VALUE TEST REPORT **MONTANA DEPARTMENT OF TRANSPORTATION**	**Figure** ____

Figure B 4. R-value test report for 6A-Great Falls.

R-VALUE TEST REPORT

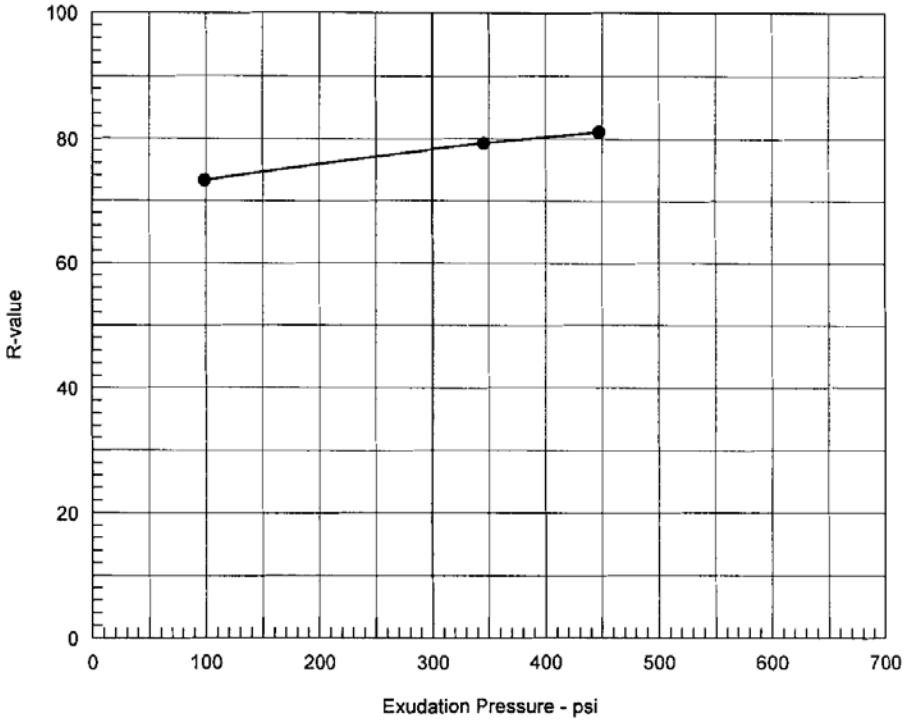

Resistance R-Value and Expansion Pressure - AASHTO T 190

No.	Compact. Pressure psi	Density pcf	Moist. %	Expansion Pressure psi	Horizontal Press. psi @ 160 psi	Sample Height in.	Exud. Pressure psi	R Value	R Value Corr.
1	350	0.0	0.0	0.00	21	2.52	99	73	73
2	350	0.0	0.0	0.00	16	2.57	345	78	79
3	350	0.0	0.0	0.00	17	2.52	447	81	81

Test Results	Material Description
R-value at 300 psi exudation pressure = 78	

Project No.: MDT 8117-30
Project: Experimental Surfacing Materials
Sample Number: 865386

Date: 3/7/2007

Tested by:
Checked by:
Remarks:

R-VALUE TEST REPORT
MONTANA DEPARTMENT OF TRANSPORTATION

Figure _____

Figure B 5. R-value test report for 6A-Butte.

R-VALUE TEST REPORT

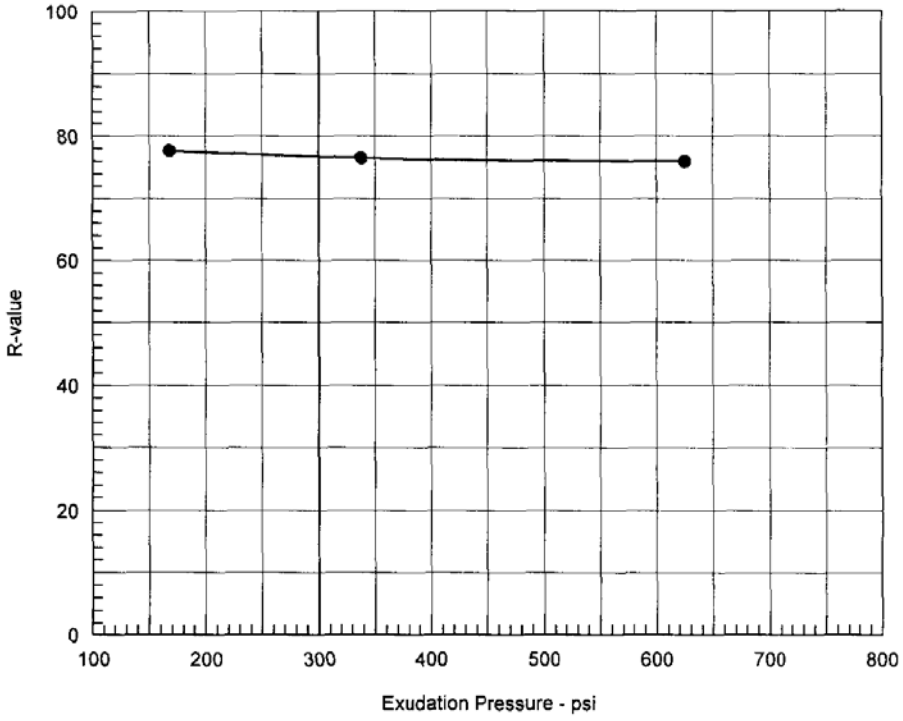

Resistance R-Value and Expansion Pressure - AASHTO T 190

No.	Compact. Pressure psi	Density pcf	Moist. %	Expansion Pressure psi	Horizontal Press. psi @ 160 psi	Sample Height in.	Exud. Pressure psi	R Value	R Value Corr.
1	350	0.0	0.0	0.00	17	2.32	625	79	76
2	350	0.0	0.0	0.00	18	2.42	338	78	76
3	350	0.0	0.0	0.00	17	2.41	168	79	78

Test Results	Material Description
R-value at 300 psi exudation pressure = 77	
Project No.: MDT 8117-30 **Project:** Experimental Surfacing Materials **Sample Number:** 865251 **Date:** 3/7/2007	**Tested by:** **Checked by:** **Remarks:**
R-VALUE TEST REPORT **MONTANA DEPARTMENT OF TRANSPORTATION**	**Figure** ____

Figure B 6. R-value test report for 6A-Kalispell.

R-VALUE TEST REPORT

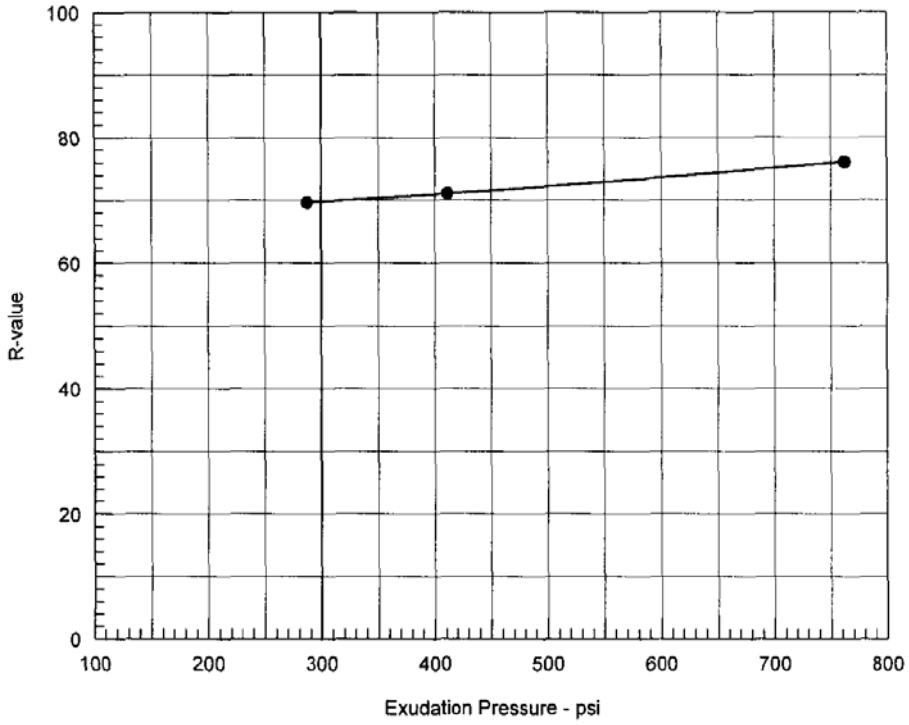

Resistance R-Value and Expansion Pressure - AASHTO T 190

No.	Compact. Pressure psi	Density pcf	Moist. %	Expansion Pressure psi	Horizontal Press. psi @ 160 psi	Sample Height in.	Exud. Pressure psi	R Value	R Value Corr.
1	350	0.0	0.0	0.00	22	2.50	762	76	76
2	350	0.0	0.0	0.00	23	2.51	411	71	71
3	350	0.0	0.0	0.00	25	2.54	287	70	70

Test Results	Material Description
R-value at 300 psi exudation pressure = 70	
Project No.: MDT 8117-30 **Project:** Experimental Surfacing Materials **Sample Number:** 865184 **Date:** 3/7/2007	**Tested by:** **Checked by:** **Remarks:**
R-VALUE TEST REPORT **MONTANA DEPARTMENT OF TRANSPORTATION**	**Figure**

Figure B 7. R-value test report for 5A-Missoula.

R-VALUE TEST REPORT

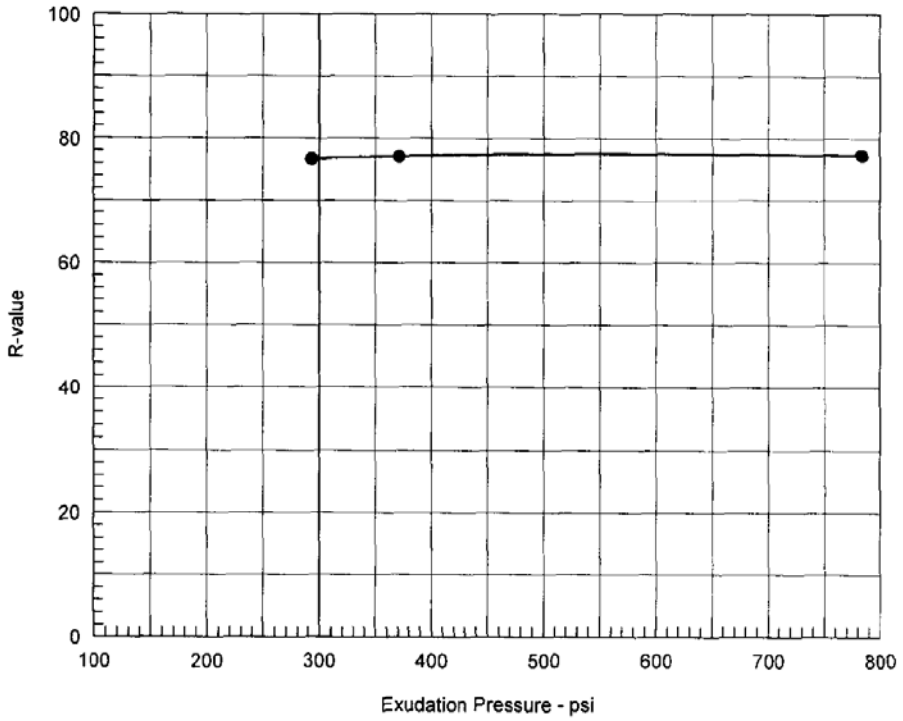

Resistance R-Value and Expansion Pressure - AASHTO T 190

No.	Compact. Pressure psi	Density pcf	Moist. %	Expansion Pressure psi	Horizontal Press. psi @ 160 psi	Sample Height in.	Exud. Pressure psi	R Value	R Value Corr.
1	350	0.0	0.0	0.00	16	2.35	371	79	77
2	350	0.0	0.0	0.00	17	2.48	293	77	77
3	350	0.0	0.0	0.00	16	2.41	783	79	77

Test Results	Material Description
R-value at 300 psi exudation pressure = 77	
Project No.: MDT 8117-30 **Project:** Experimental Surfacing Materials **Sample Number:** 865769 **Date:** 3/7/2007	**Tested by:** **Checked by:** **Remarks:**
R-VALUE TEST REPORT **MONTANA DEPARTMENT OF TRANSPORTATION**	**Figure** _____

Figure B 8. R-value test report for 5A-Kalispell.

R-VALUE TEST REPORT

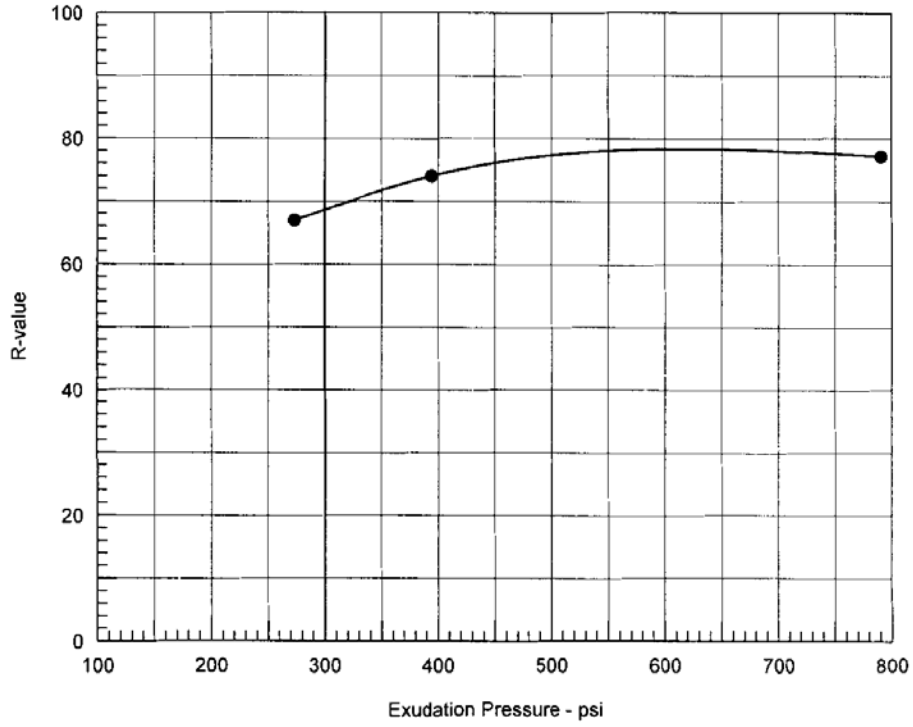

Resistance R-Value and Expansion Pressure - AASHTO T 190

No.	Compact. Pressure psi	Density pcf	Moist. %	Expansion Pressure psi	Horizontal Press. psi @ 160 psi	Sample Height in.	Exud. Pressure psi	R Value	R Value Corr.
1	350	0.0	0.0	0.00	37	2.47	273	67	67
2	350	0.0	0.0	0.00	25	2.41	394	75	74
3	350	0.0	0.0	0.00	21	2.48	791	77	77

Test Results	Material Description
R-value at 300 psi exudation pressure = 69	

Project No.: MDT 8117-30
Project: Experimental Surfacing Materials
Sample Number: 865164

Date: 3/7/2007

Tested by:
Checked by:
Remarks:

R-VALUE TEST REPORT

MONTANA DEPARTMENT OF TRANSPORTATION

Figure _____

Figure B 9. R-value test report for 5A-Great Falls.

R-VALUE TEST REPORT

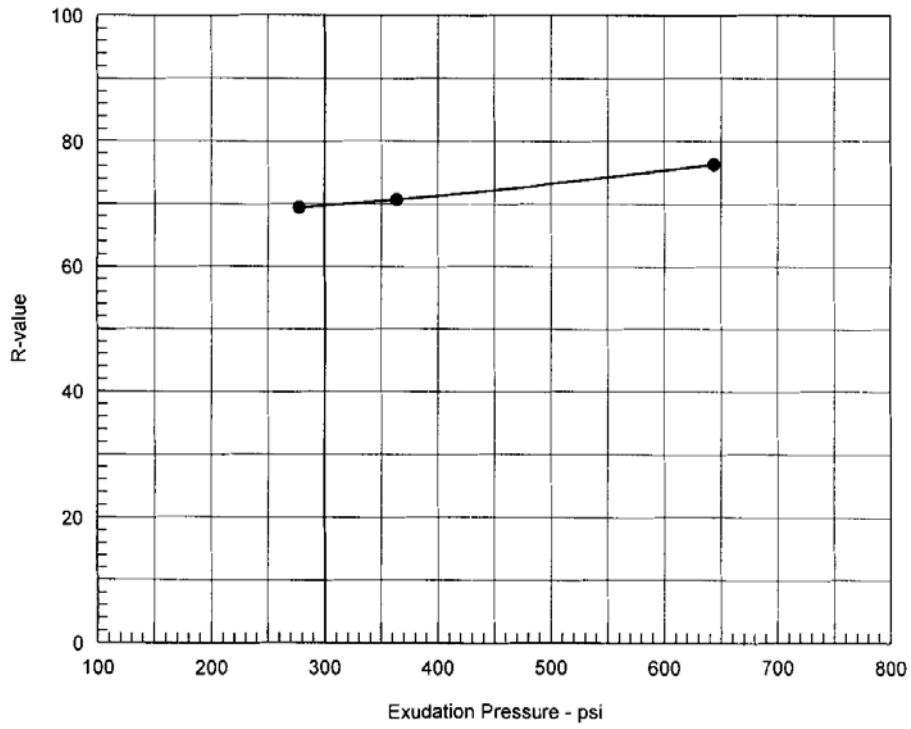

Resistance R-Value and Expansion Pressure - AASHTO T 190

No.	Compact. Pressure psi	Density pcf	Moist. %	Expansion Pressure psi	Horizontal Press. psi @ 160 psi	Sample Height in.	Exud. Pressure psi	R Value	R Value Corr.
1	350	0.0	0.0	0.00	22	2.60	644	75	76
2	350	0.0	0.0	0.00	25	2.50	363	71	71
3	350	0.0	0.0	0.00	26	2.60	278	67	69

Test Results	Material Description
R-value at 300 psi exudation pressure = 70	

Project No.: MDT 8117-30
Project: Experimental Surfacing Materials
Sample Number: 865174

Date: 3/7/2007

Tested by:
Checked by:
Remarks:

R-VALUE TEST REPORT

MONTANA DEPARTMENT OF TRANSPORTATION

Figure _____

Figure B 10. R-value test report for 2A-Havre.

R-VALUE TEST REPORT

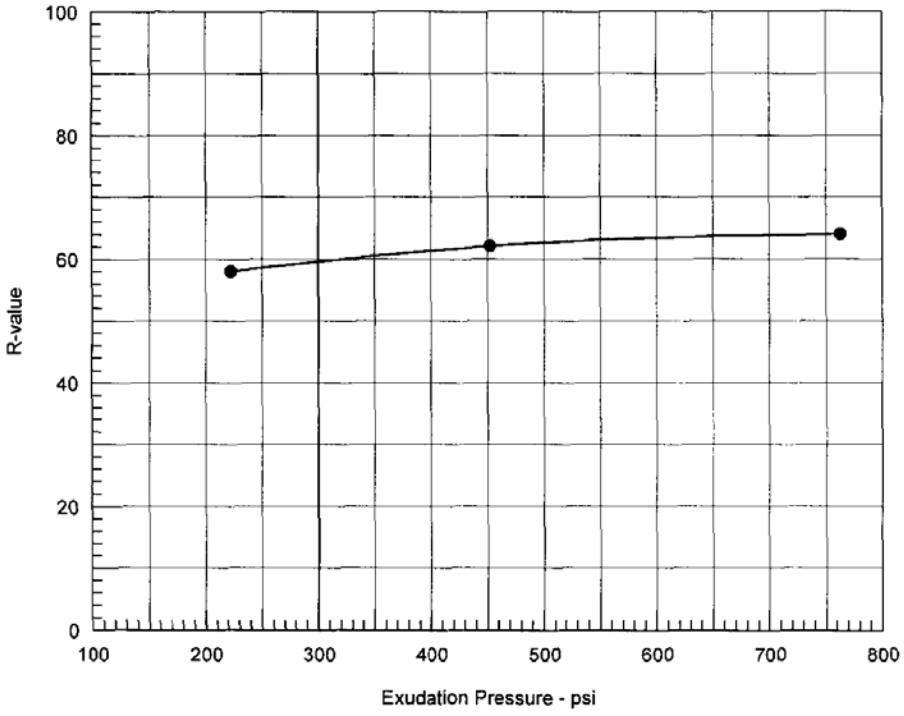

Resistance R-Value and Expansion Pressure - AASHTO T 190

No.	Compact. Pressure psi	Density pcf	Moist. %	Expansion Pressure psi	Horizontal Press. psi @ 160 psi	Sample Height in.	Exud. Pressure psi	R Value	R Value Corr.
1	350	0.0	0.0	0.00	26	2.47	763	64	64
2	350	0.0	0.0	0.00	30	2.59	452	60	62
3	350	0.0	0.0	0.00	30	2.51	223	58	58

Test Results	Material Description
R-value at 300 psi exudation pressure = 60	

Project No.: MDT 8117-30
Project: Experimental Surfacing Materials
Sample Number: 865182

Date: 3/7/2007

Tested by:
Checked by:
Remarks:

R-VALUE TEST REPORT
MONTANA DEPARTMENT OF TRANSPORTATION

Figure ____

Figure B 11. R-value test report for 2A-Glendive.

R-VALUE TEST REPORT

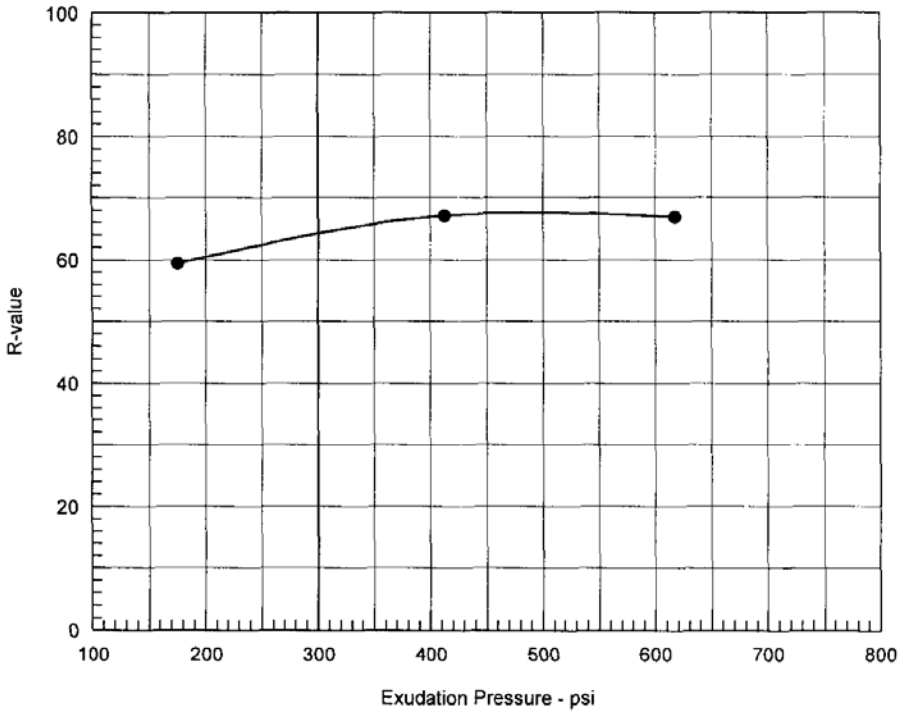

Resistance R-Value and Expansion Pressure - AASHTO T 190

No.	Compact. Pressure psi	Density pcf	Moist. %	Expansion Pressure psi	Horizontal Press. psi @ 160 psi	Sample Height in.	Exud. Pressure psi	R Value	R Value Corr.
1	350	0.0	0.0	0.00	25	2.54	618	67	67
2	350	0.0	0.0	0.00	24	2.46	413	67	67
3	350	0.0	0.0	0.00	29	2.43	175	61	59

Test Results	Material Description
R-value at 300 psi exudation pressure = 64	
Project No.: MDT 8117-30 **Project:** Experimental Surfacing Materials **Sample Number:** 865183 **Date:** 3/7/2007	**Tested by:** **Checked by:** **Remarks:**
R-VALUE TEST REPORT **MONTANA DEPARTMENT OF TRANSPORTATION**	**Figure** ____

Figure B 12. R-value test report for 2A-Missoula.

R-VALUE TEST REPORT

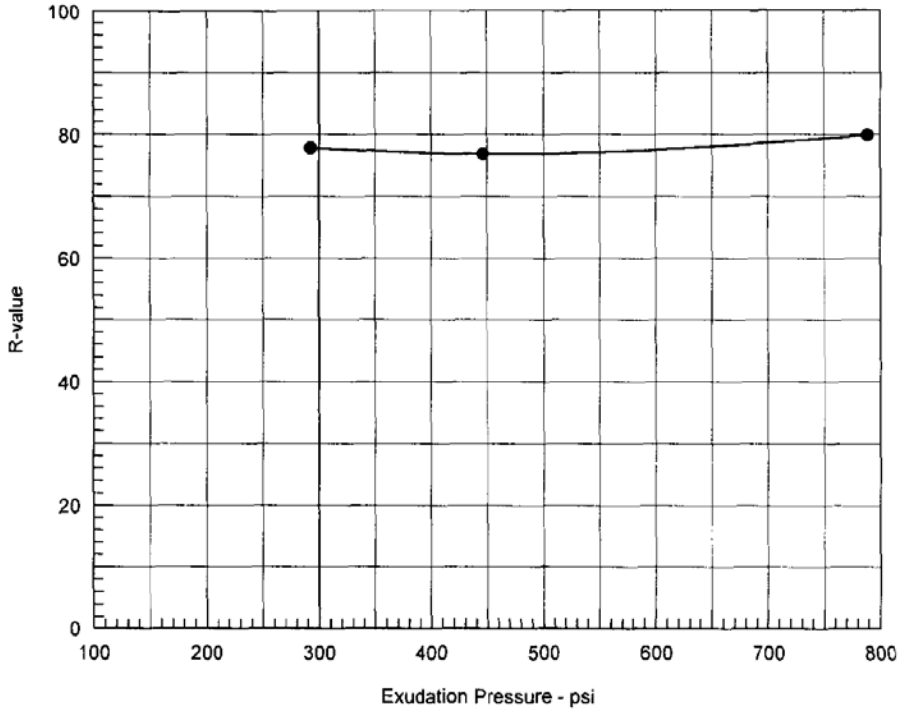

Resistance R-Value and Expansion Pressure - AASHTO T 190

No.	Compact. Pressure psi	Density pcf	Moist. %	Expansion Pressure psi	Horizontal Press. psi @ 160 psi	Sample Height in.	Exud. Pressure psi	R Value	R Value Corr.
1	350	0.0	0.0	0.00	17	2.51	789	80	80
2	350	0.0	0.0	0.00	17	2.31	446	80	77
3	350	0.0	0.0	0.00	17	2.43	292	79	78

Test Results	Material Description
R-value at 300 psi exudation pressure = 78	
Project No.: MDT 8117-30 **Project:** Experimental Surfacing Materials **Sample Number:** 865338 **Date:** 3/7/2007	**Tested by:** **Checked by:** **Remarks:**
R-VALUE TEST REPORT **MONTANA DEPARTMENT OF TRANSPORTATION**	**Figure** ____

Figure B 13. R-value test report for 2A-Lewistown.

R-VALUE TEST REPORT

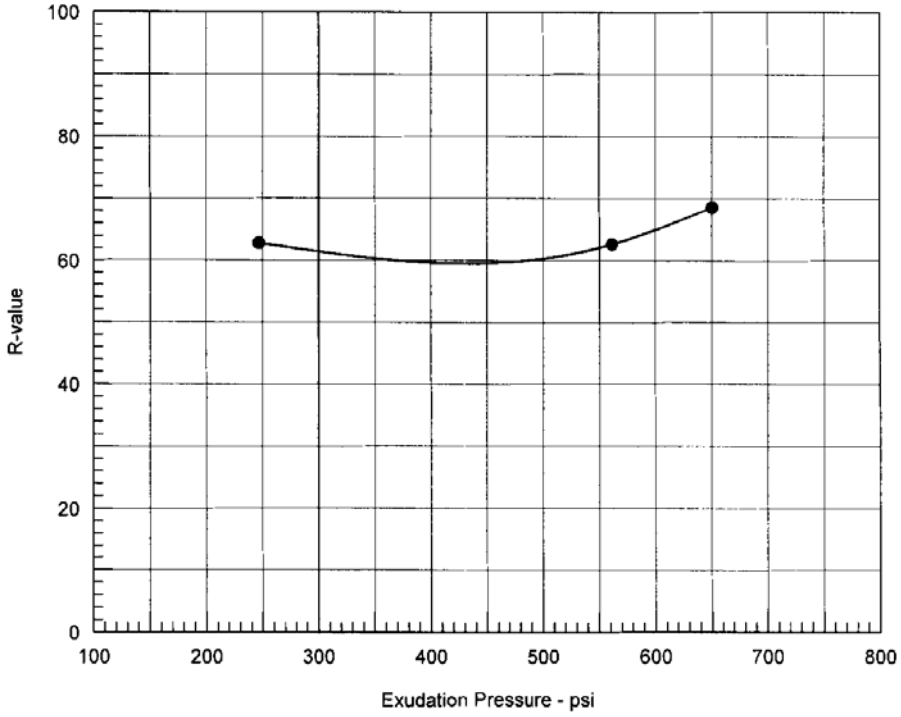

Resistance R-Value and Expansion Pressure - AASHTO T 190

No.	Compact. Pressure psi	Density pcf	Moist. %	Expansion Pressure psi	Horizontal Press. psi @ 160 psi	Sample Height in.	Exud. Pressure psi	R Value	R Value Corr.
1	350	0.0	0.0	0.00	23	2.46	651	69	69
2	350	0.0	0.0	0.00	28	2.49	561	63	63
3	350	0.0	0.0	0.00	25	2.33	247	67	63

Test Results	Material Description
R-value at 300 psi exudation pressure = 61	
Project No.: MDT 8117-30 **Project:** Experimental Surfacing Materials **Sample Number:** 865820 **Date:** 3/7/2007	**Tested by:** **Checked by:** **Remarks:**
R-VALUE TEST REPORT **MONTANA DEPARTMENT OF TRANSPORTATION**	**Figure** _____

Figure B 14. R-value test report for 2A-Billings.

APPENDIX C

SHEAR STRESS-DISPLACEMENT PLOTS

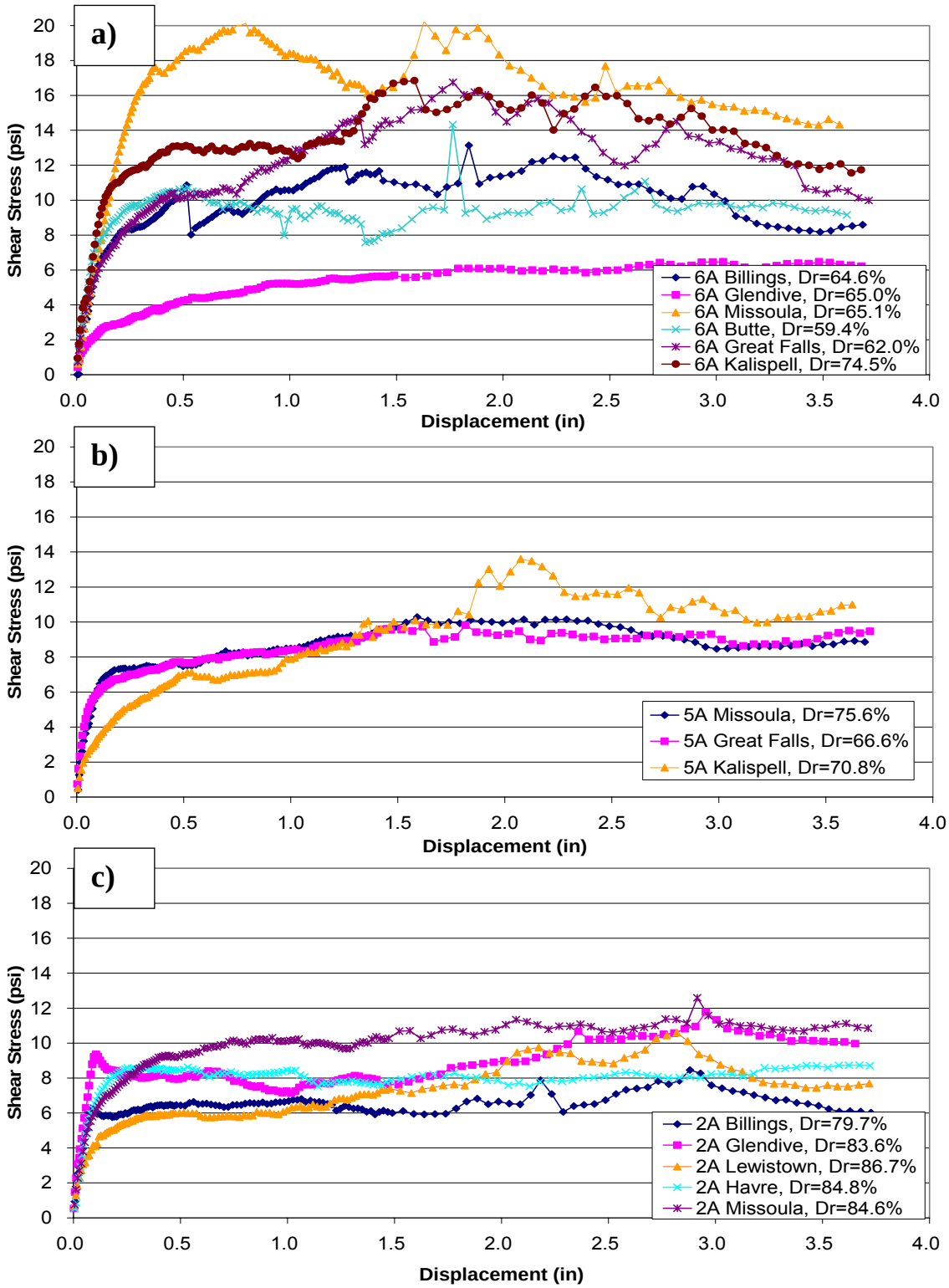

Figure C 1. Shear stress-displacement plots for 5 psi normal stress: a) 6A samples, b) 5A samples, and c) 2A samples.

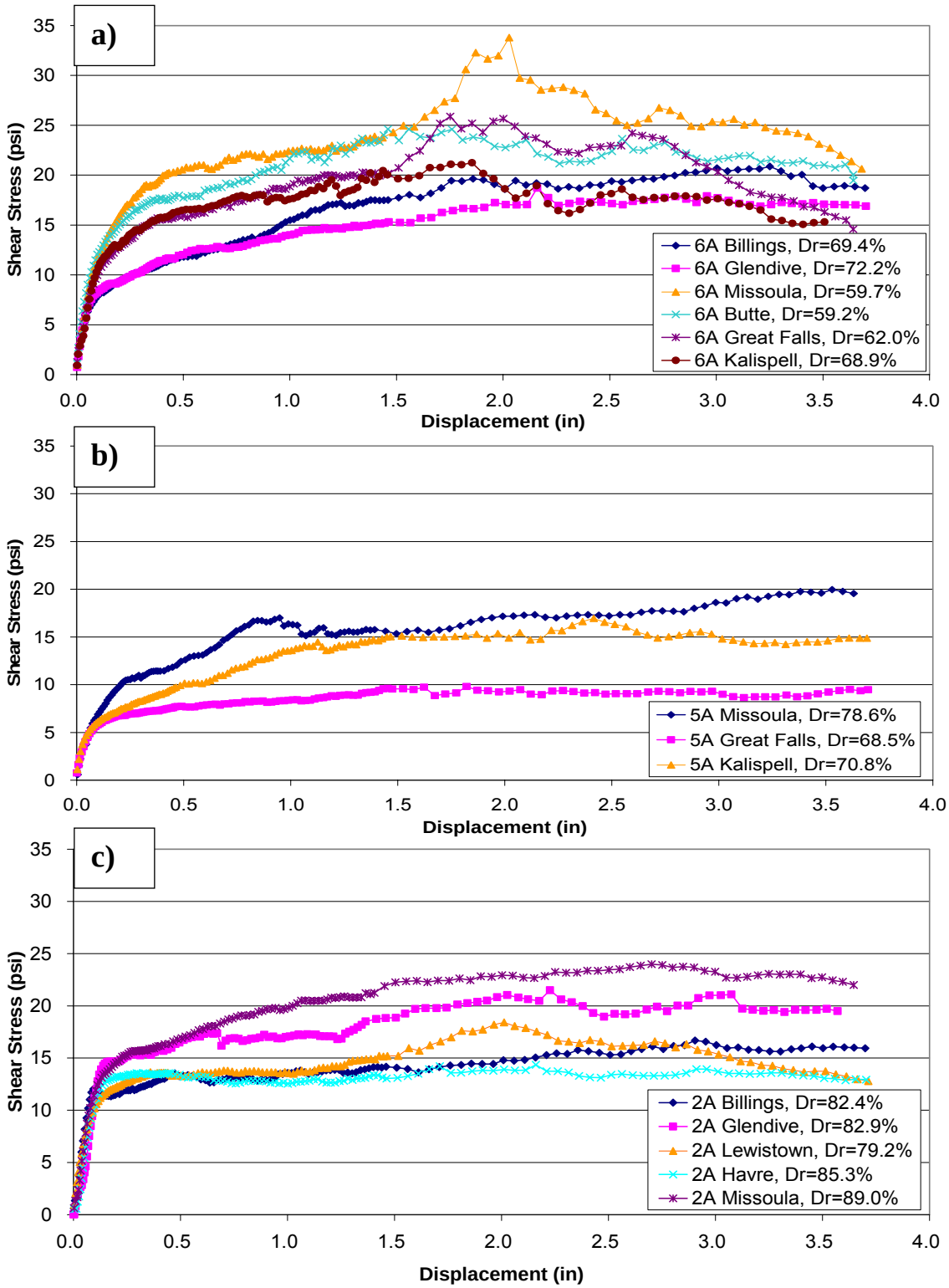

Figure C 2. Shear stress-displacement plots for 10 psi normal stress: a) 6A samples, b) 5A samples, and c) 2A samples.

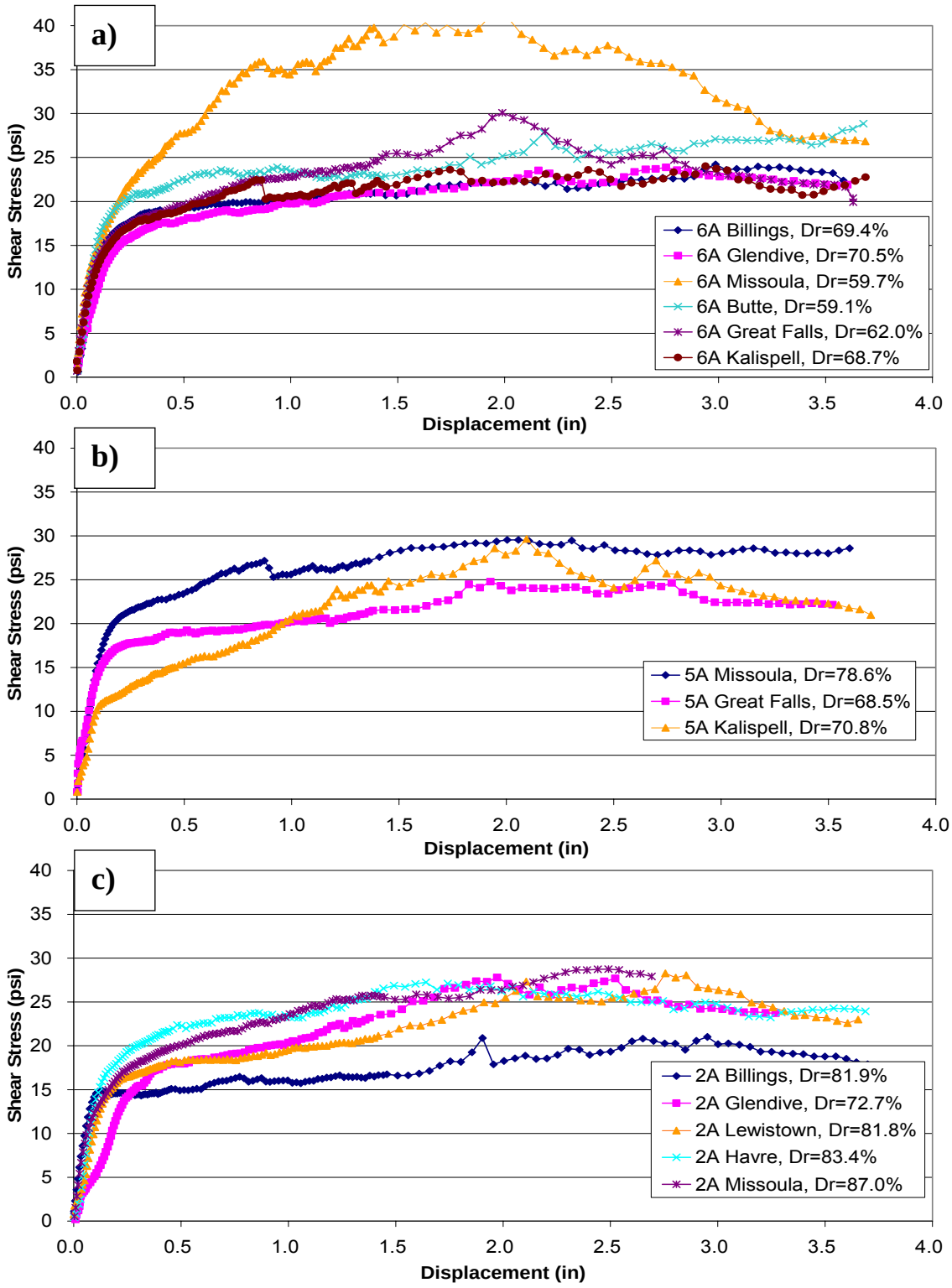

Figure C 3. Shear stress-displacement plots for 15 psi normal stress: a) 6A samples, b) 5A samples, and c) 2A samples.

APPENDIX D

DESPECKLED 2D X-RAY CT IMAGES

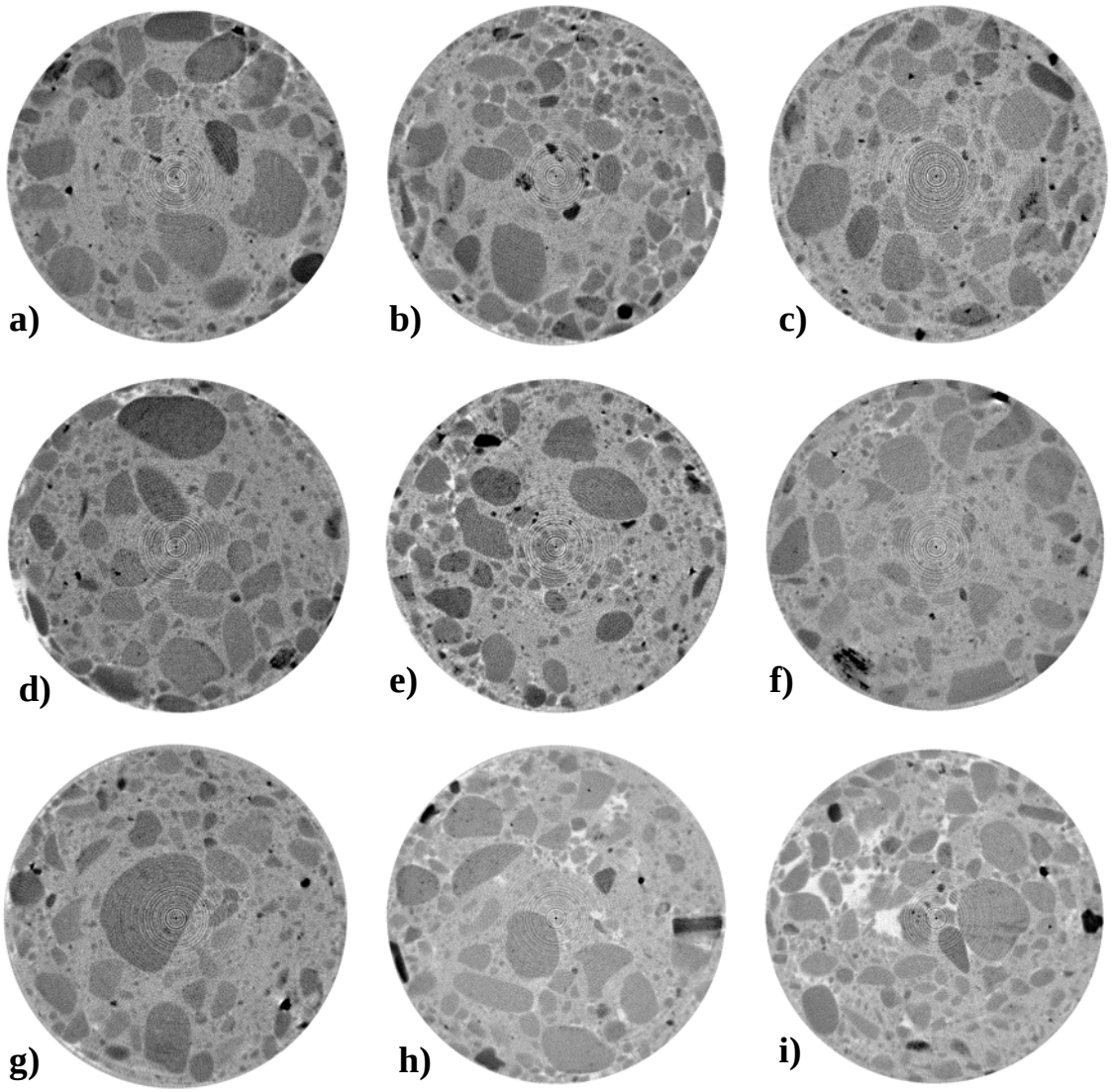

Figure D 1. 6A-Glendive X-ray CT images top (a) to bottom (i) at 9 mm intervals.

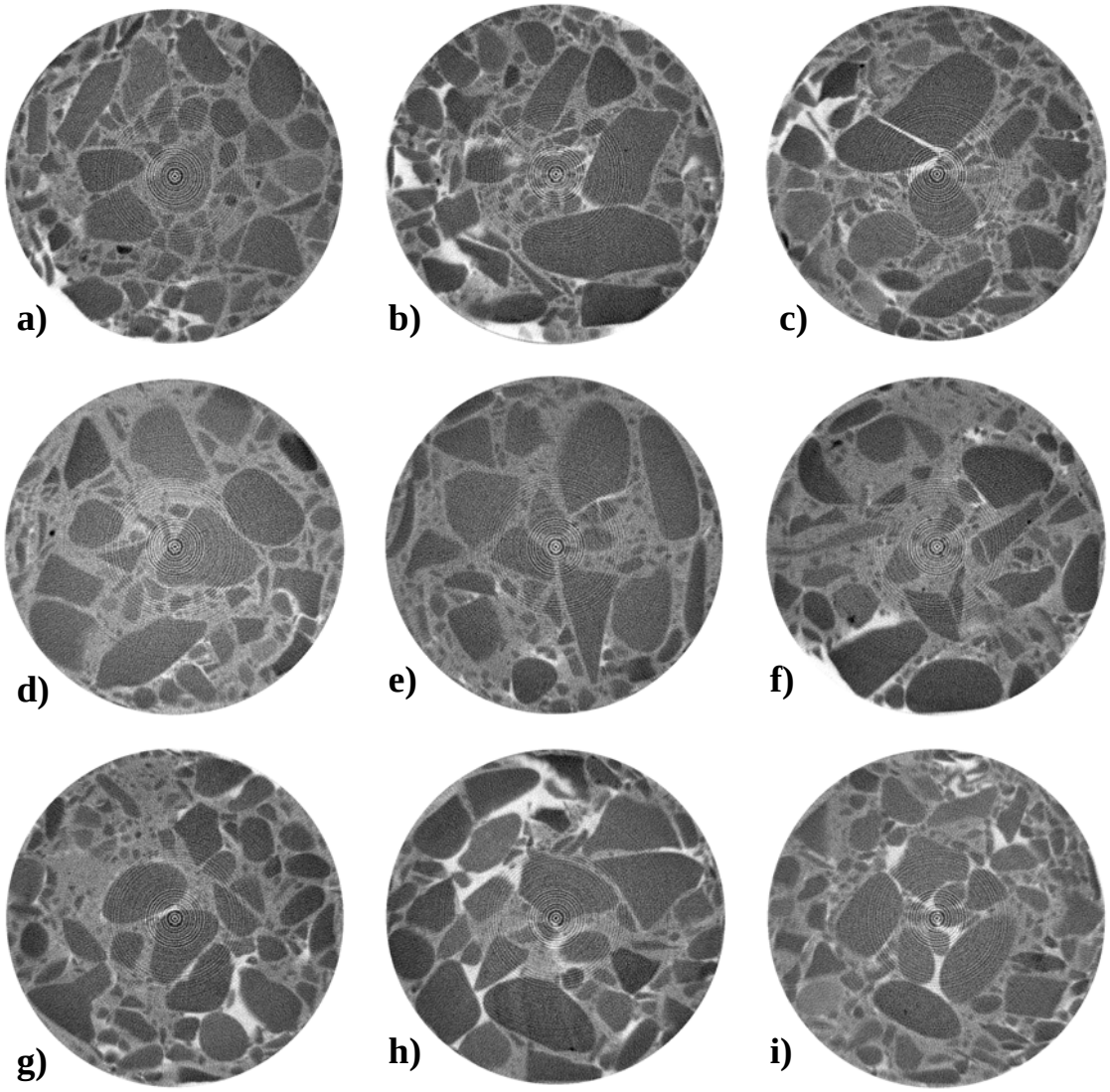

Figure D 2. 6A-Missoula X-ray CT images top (a) to bottom (i) at 9 mm intervals.

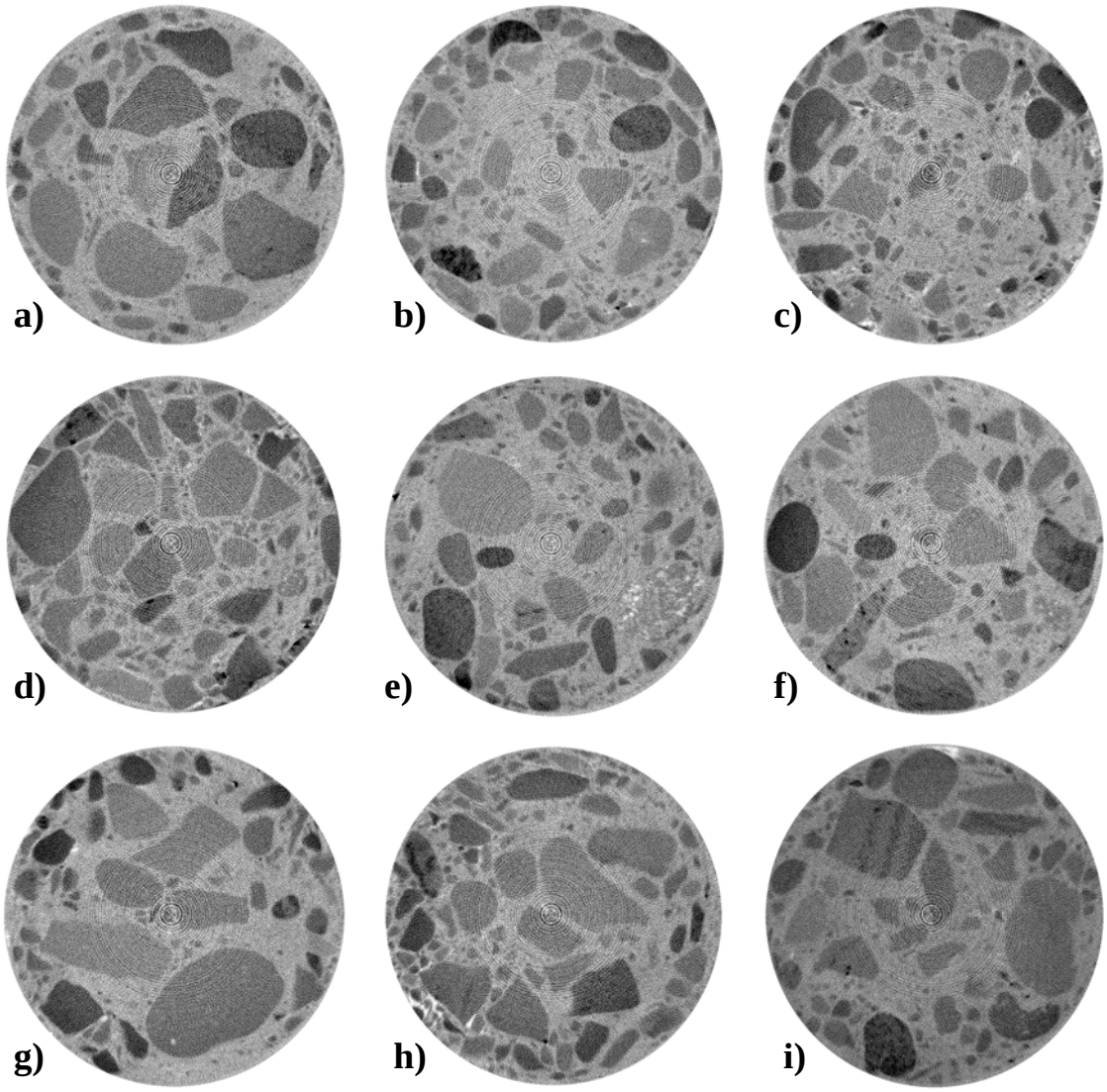

Figure D 3. 6A-Butte X-ray CT images top (a) to bottom (i) at 9 mm intervals.

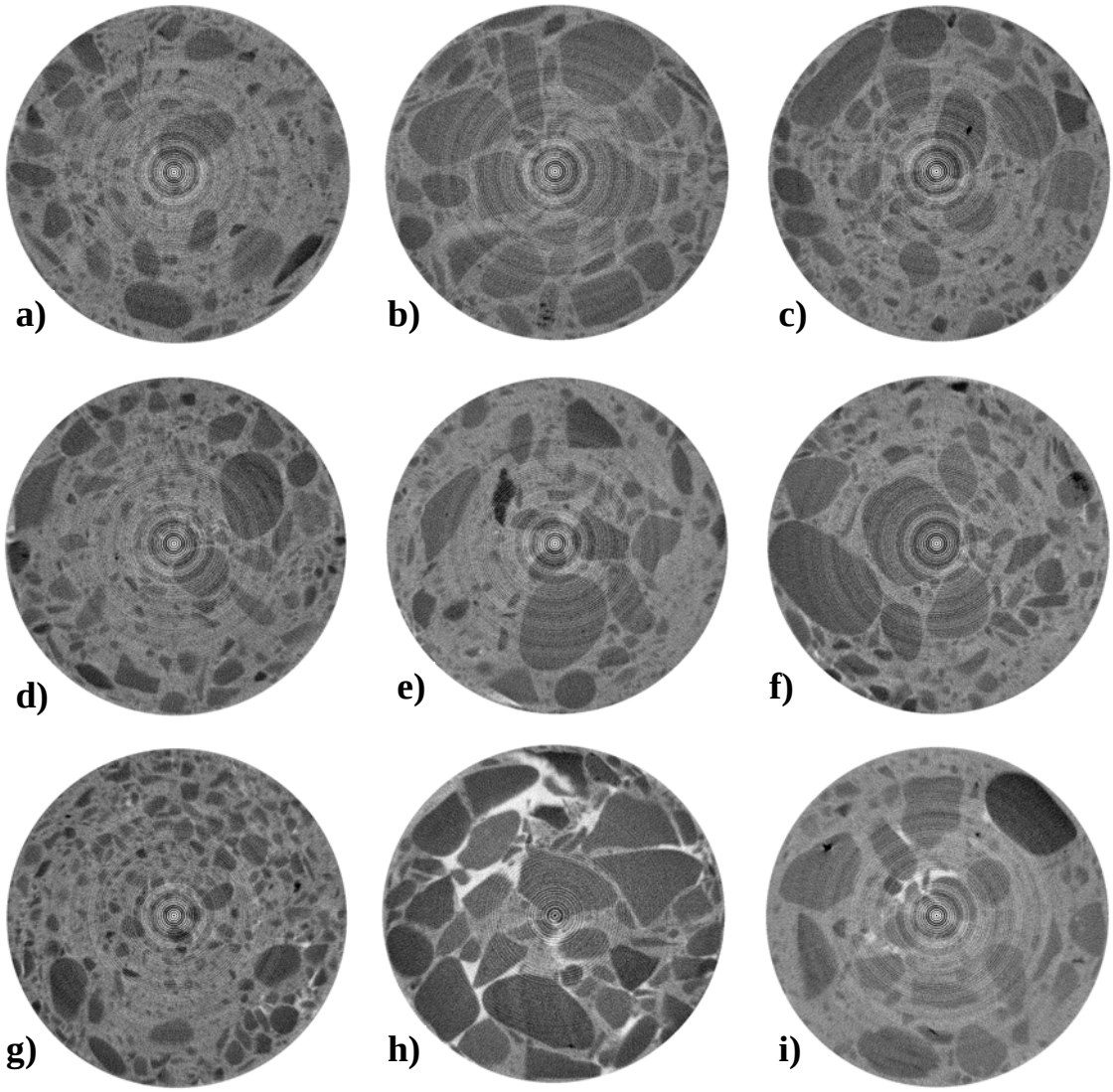

Figure D 4. 6A-Kalispell X-ray CT images top (a) to bottom (i) at 9 mm intervals.

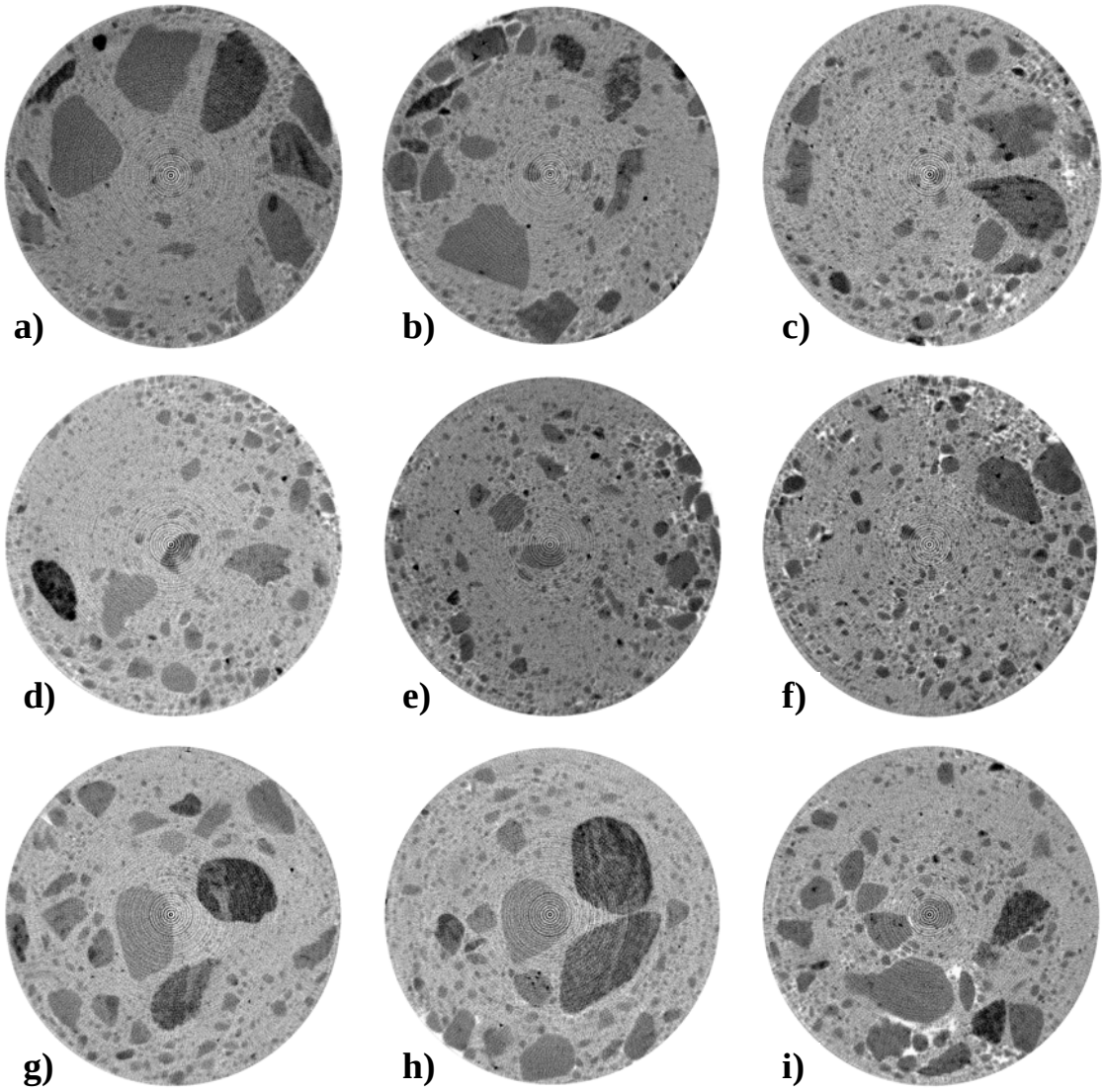

Figure D 5. 5A-Missoula X-ray CT images top (a) to bottom (i) at 9 mm intervals.

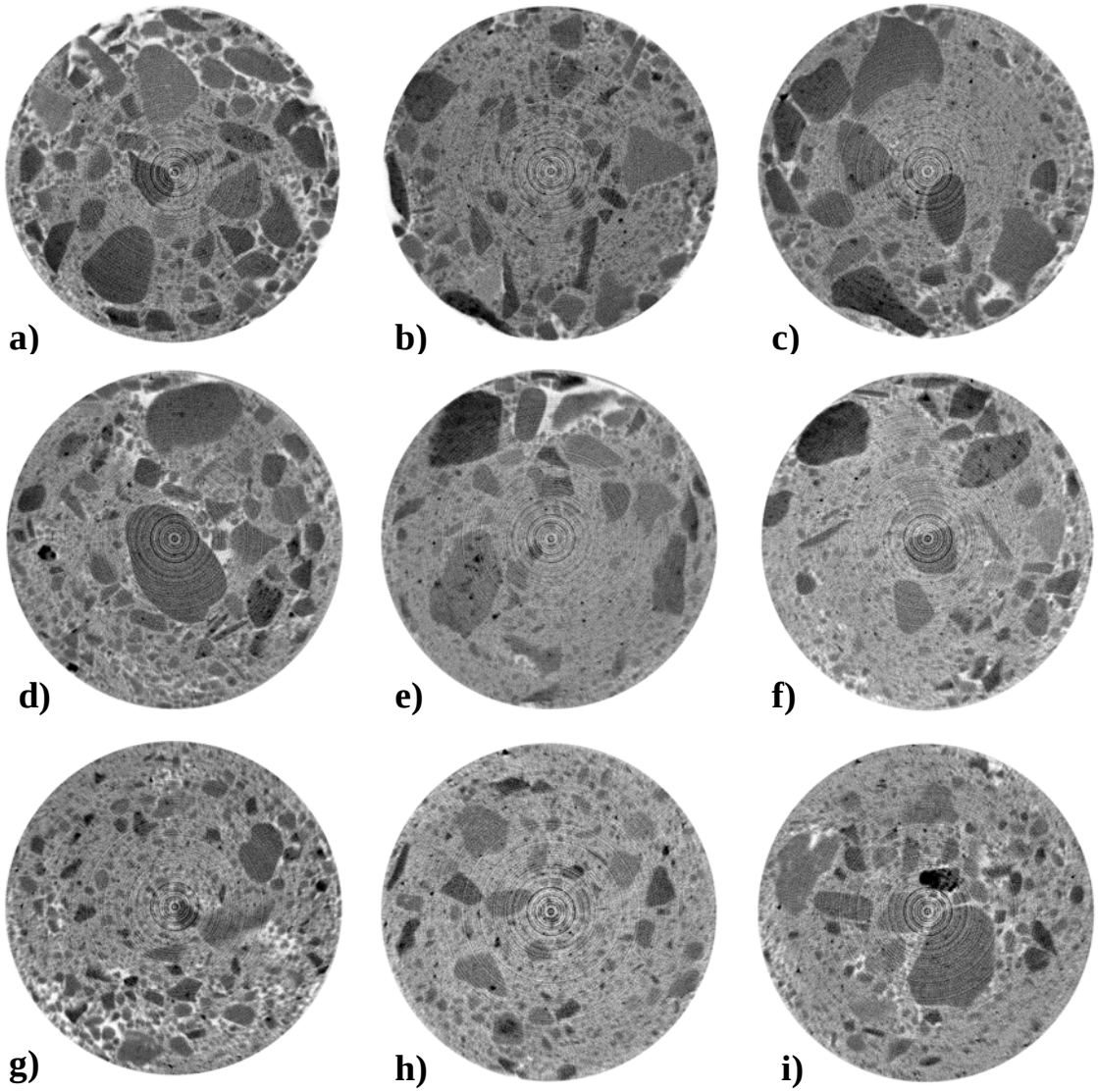

Figure D 6. 5A-Great Falls X-ray CT images top (a) to bottom (i) at 9 mm intervals.

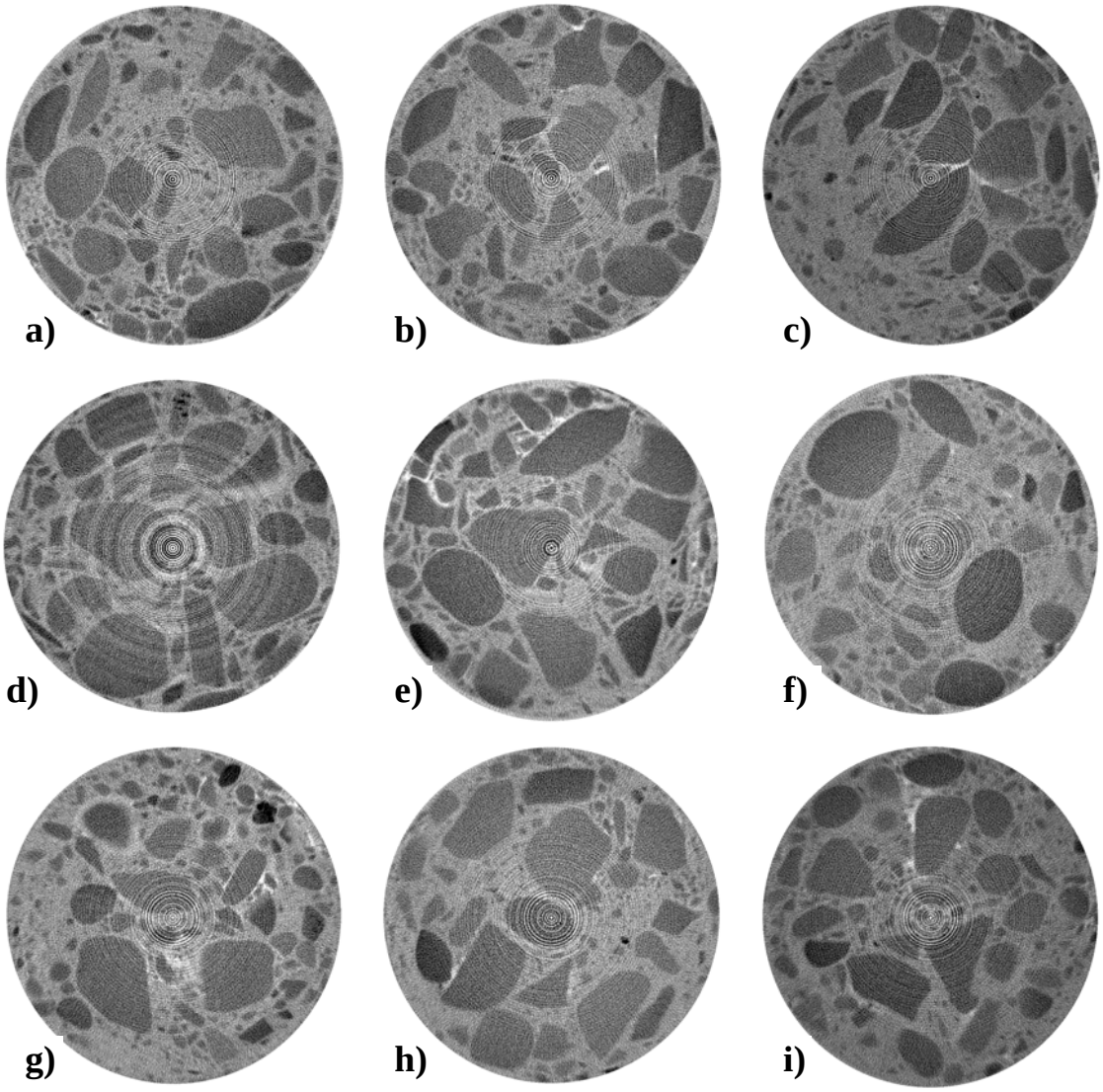

Figure D 7. 5A-Kalispell X-ray CT images top (a) to bottom (i) at 9 mm intervals.

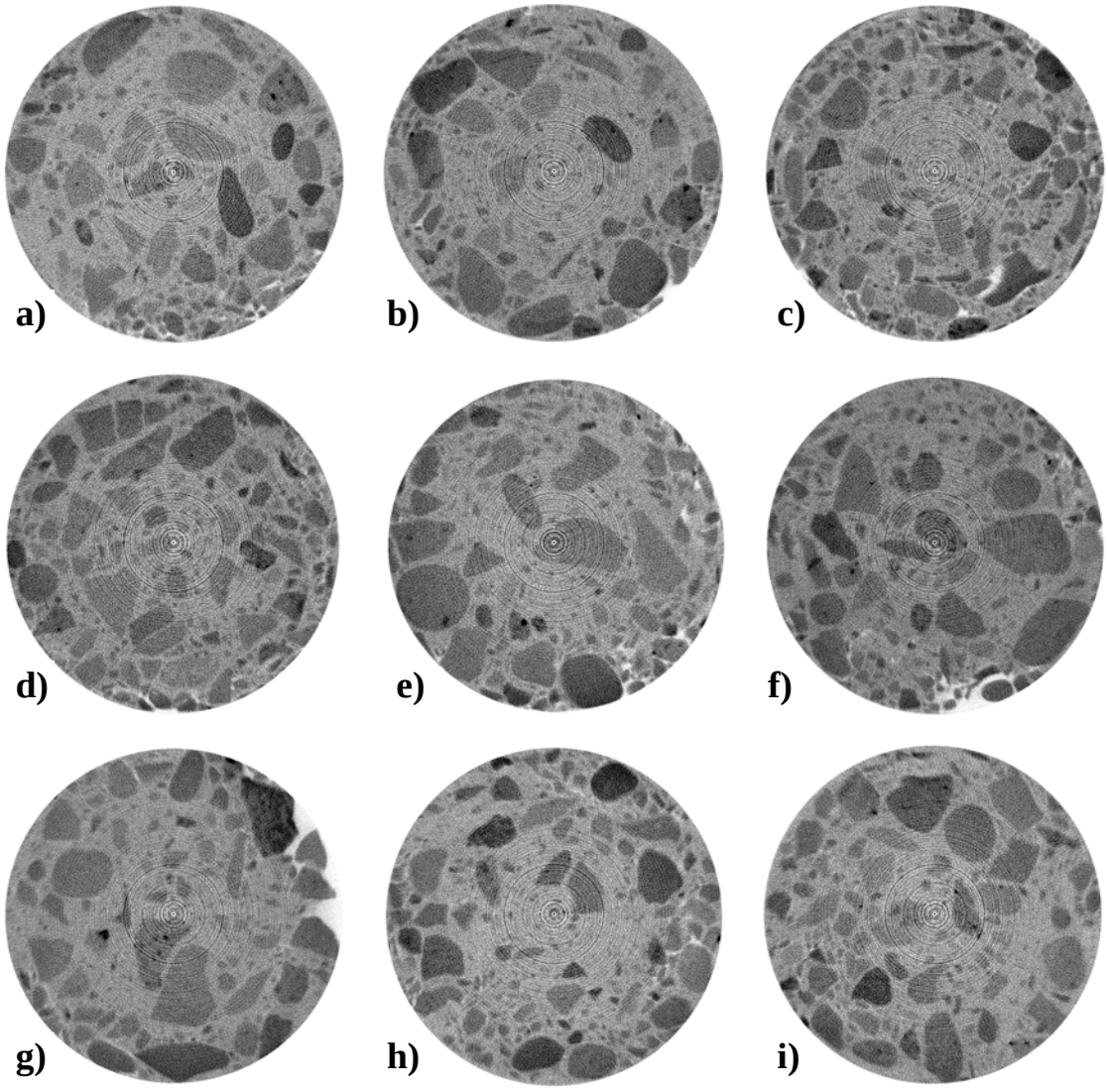

Figure D 8. 2A-Billings X-ray CT images top (a) to bottom (i) at 9 mm intervals.

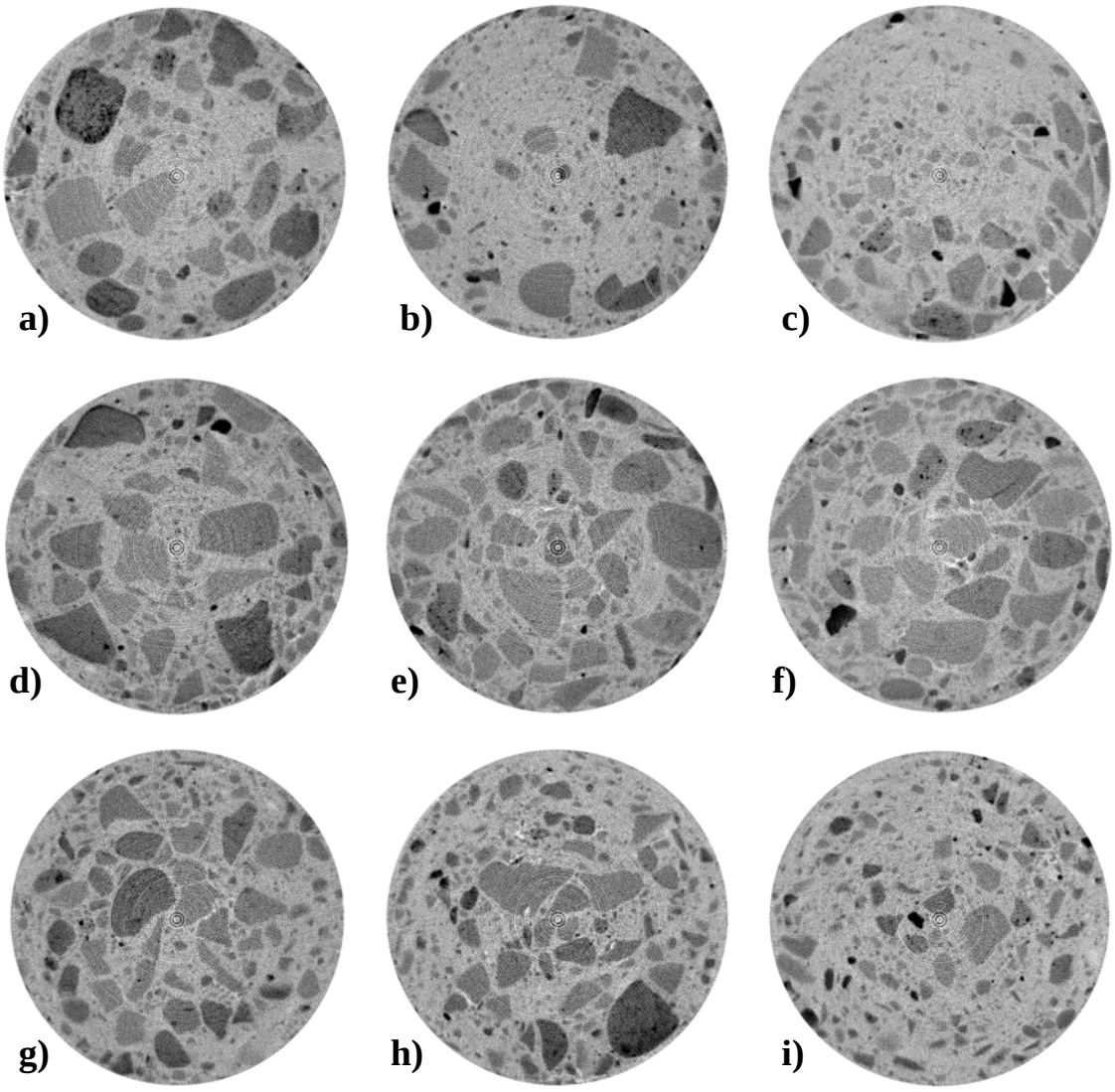

Figure D 9. 2A-Glendive X-ray CT images top (a) to bottom (i) at 9 mm intervals.

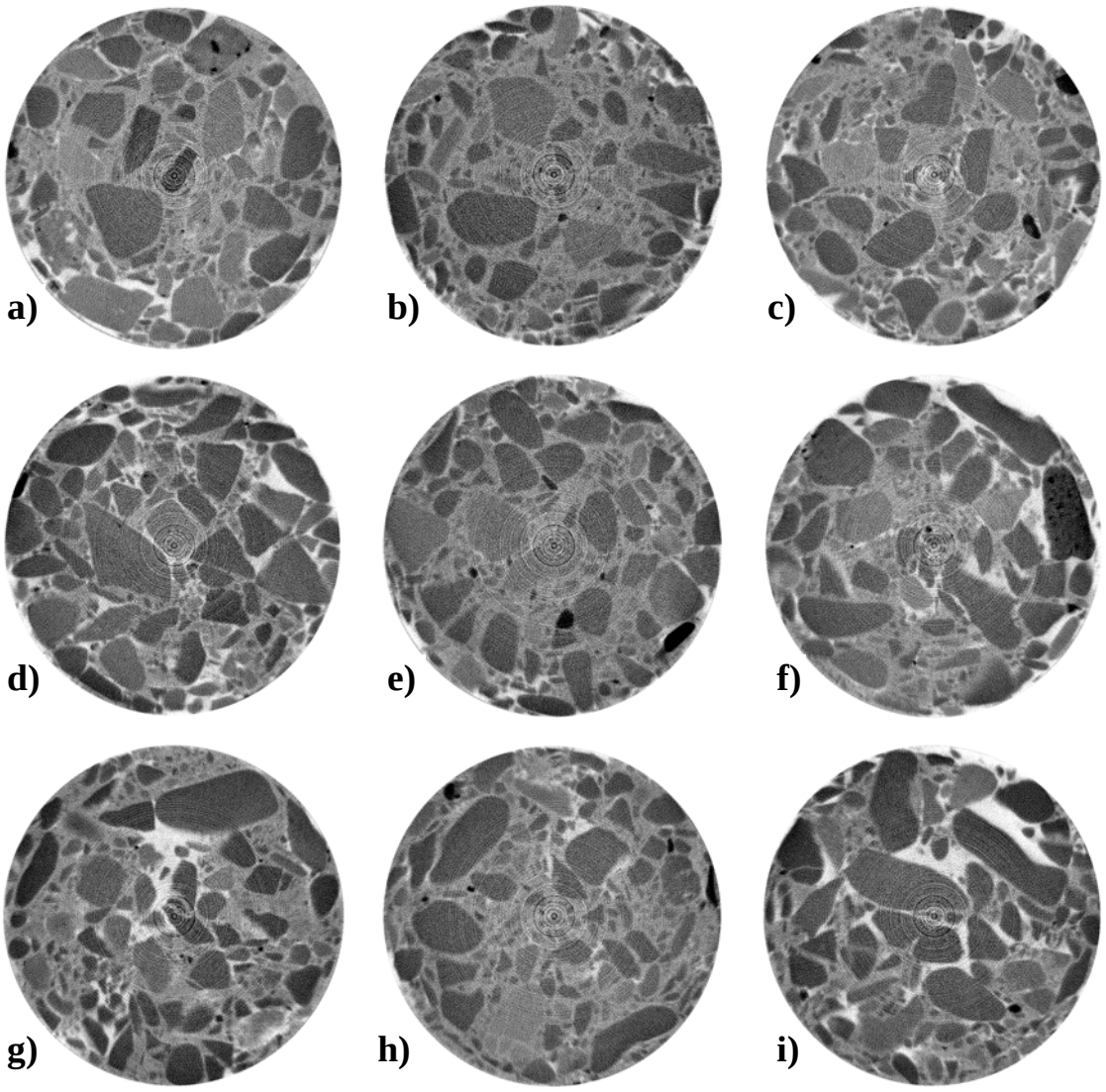

Figure D 10. 2A-Lewistown X-ray CT images top (a) to bottom (i) at 9 mm intervals.

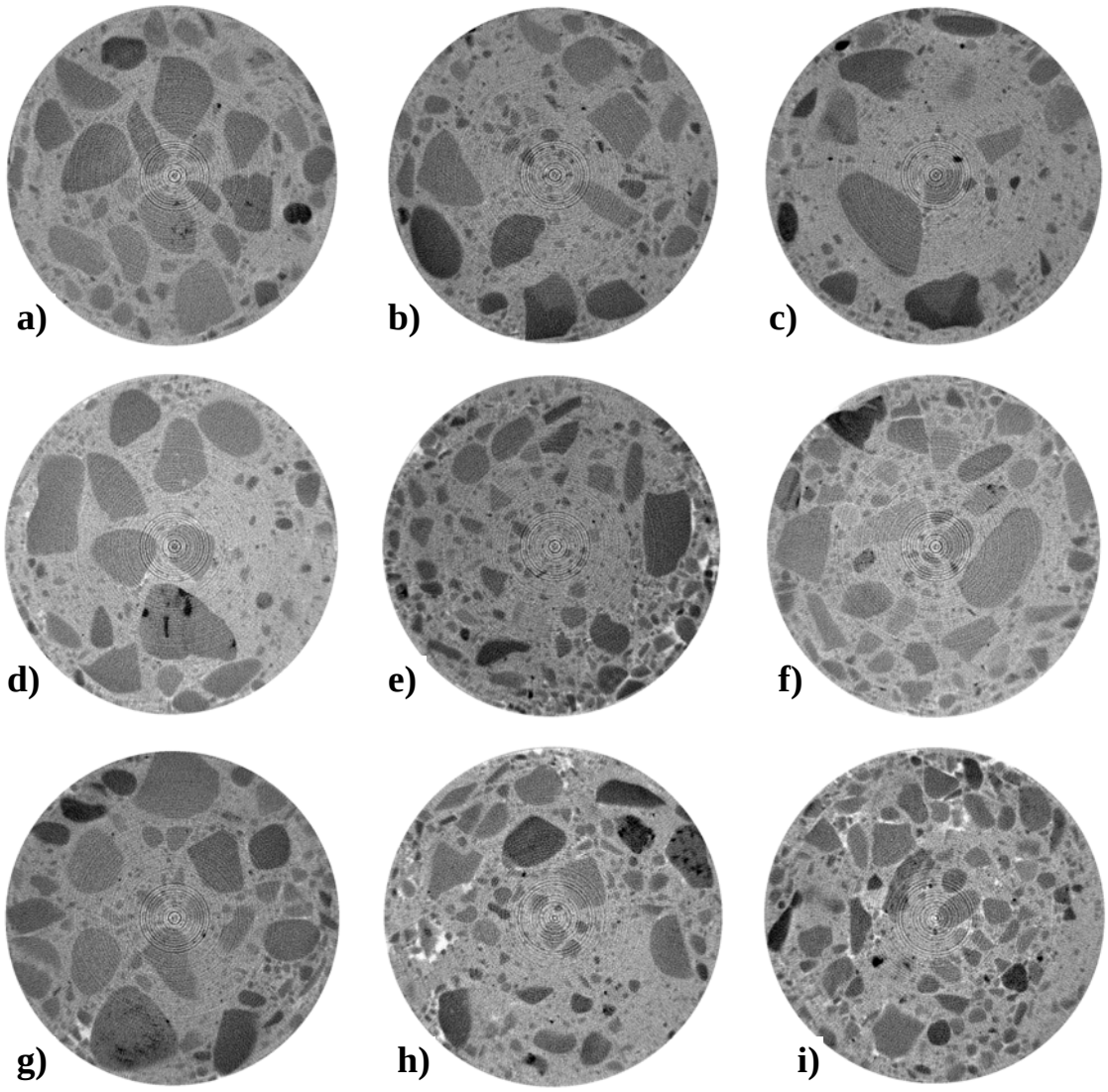

Figure D 11. 2A-Havre X-ray CT images top (a) to bottom (i) at 9 mm intervals.

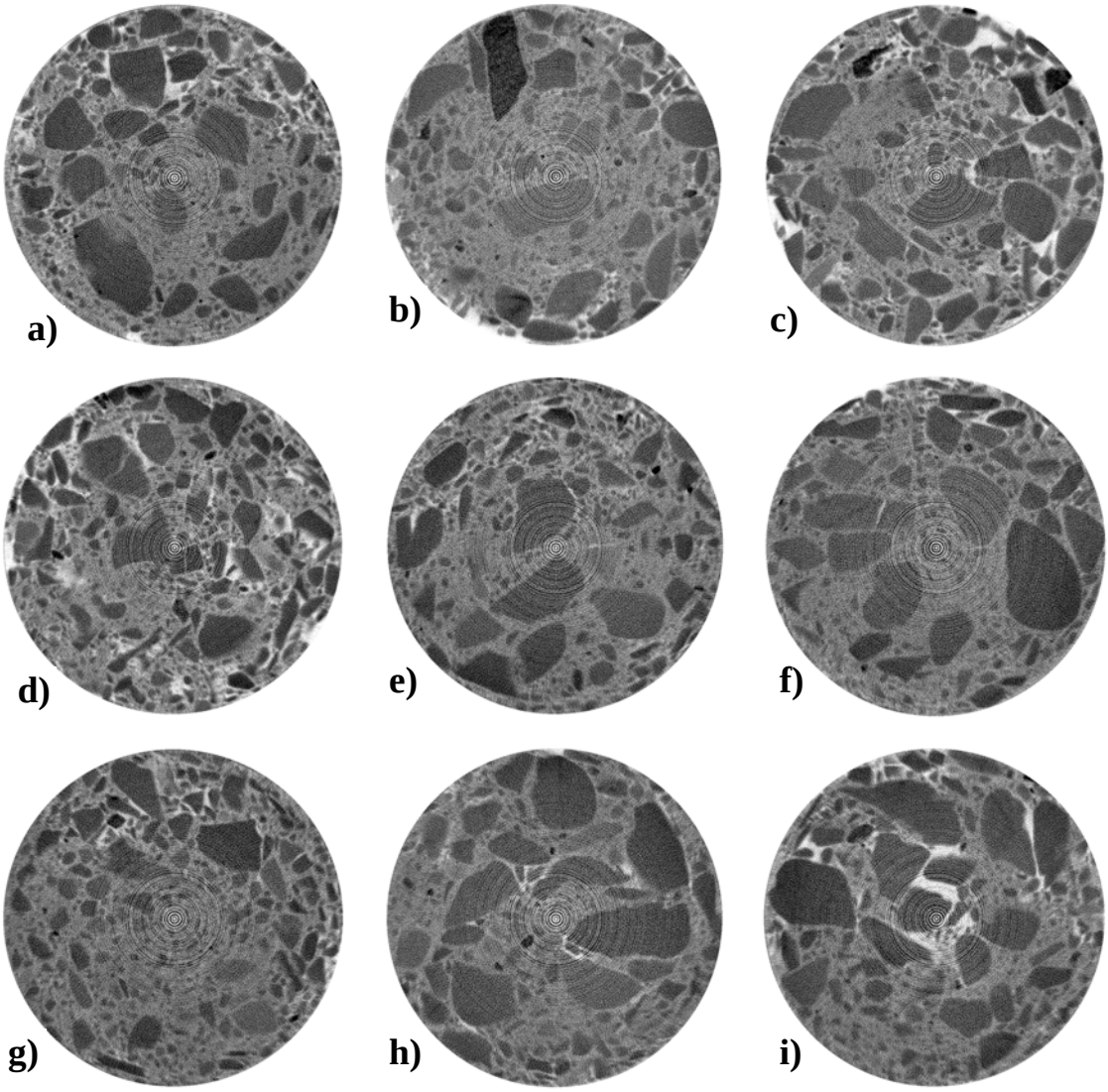

Figure D 12. 2A-Missoula X-ray CT images top (a) to bottom (i) at 9 mm intervals.

APPENDIX E

X-RAY CT GRAIN SIZE PLOTS

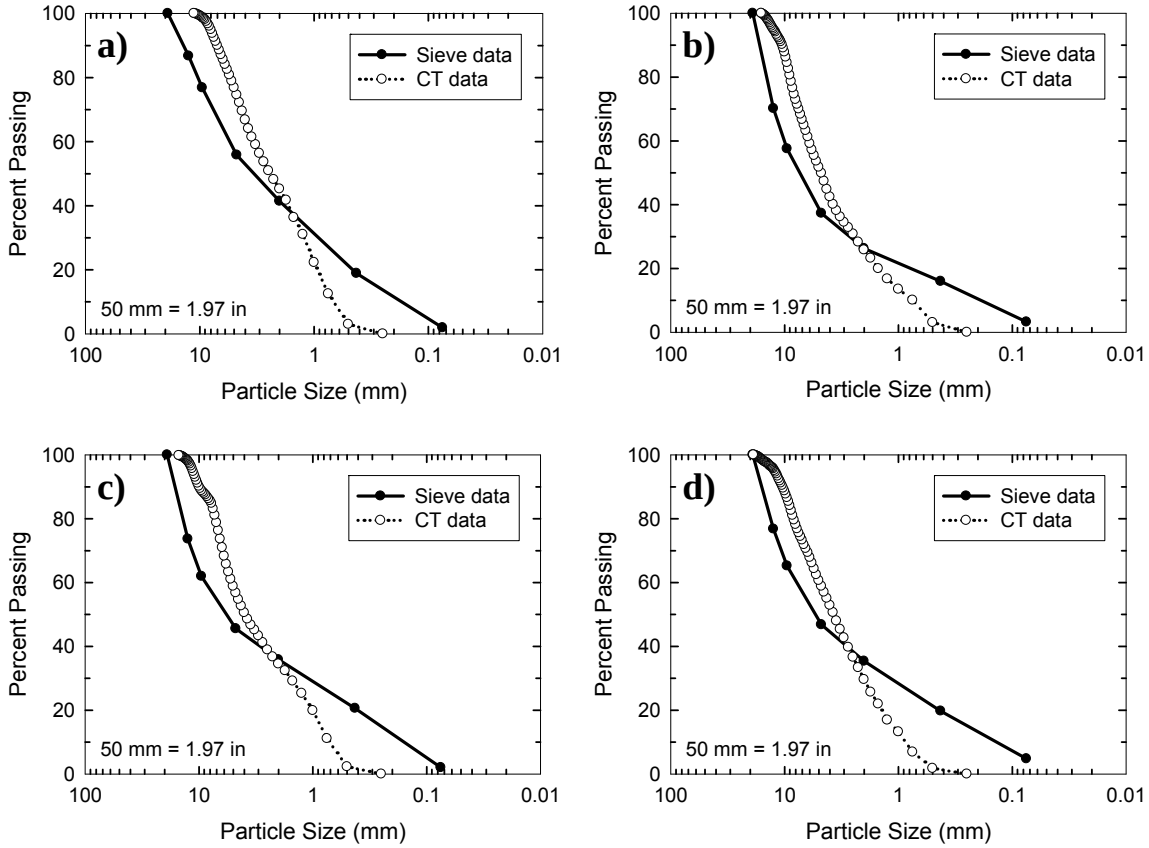

Figure E 1. X-ray CT Derived Grain Size Distributions for CBC-6A Samples: a) Glendive, b) Missoula, c) Butte, and d) Kalispell.

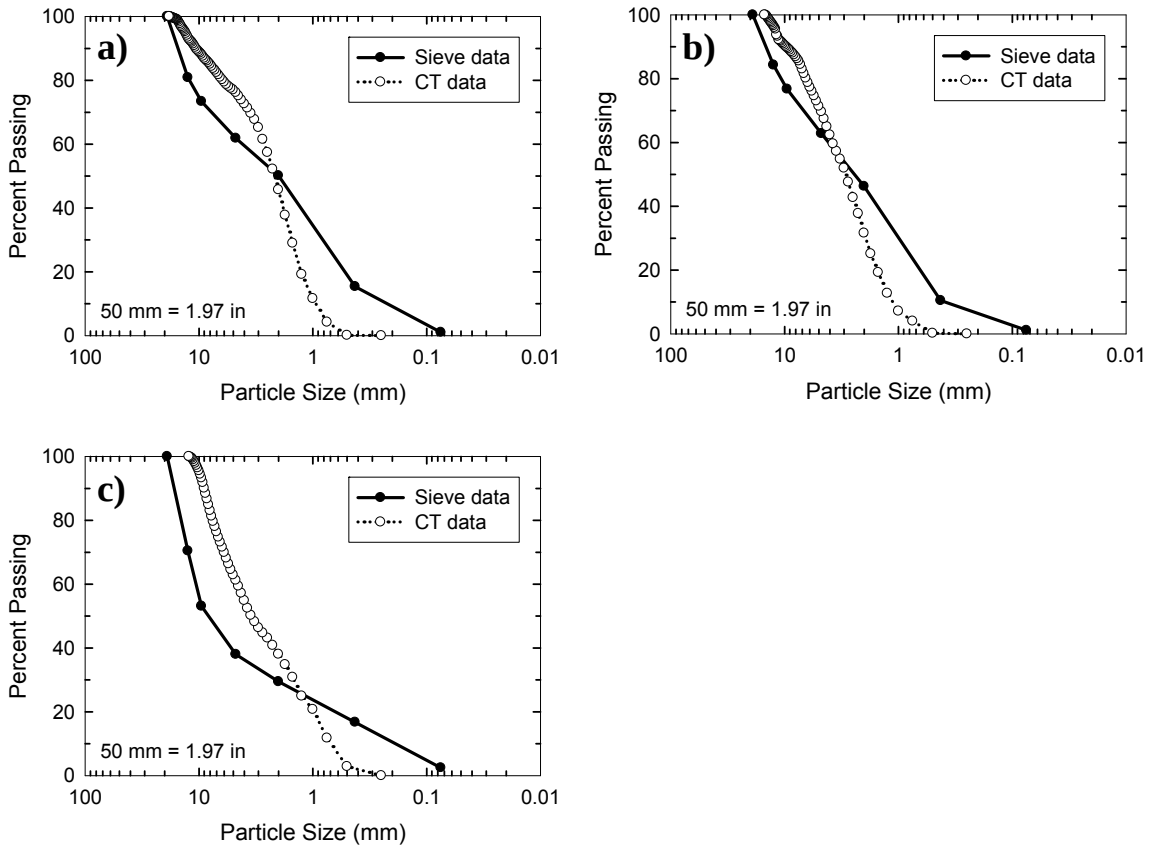

Figure E 2. X-ray CT Derived Grain Size Distributions for CBC-5A Samples: a) Missoula, b) Great Falls, and c) Kalispell.

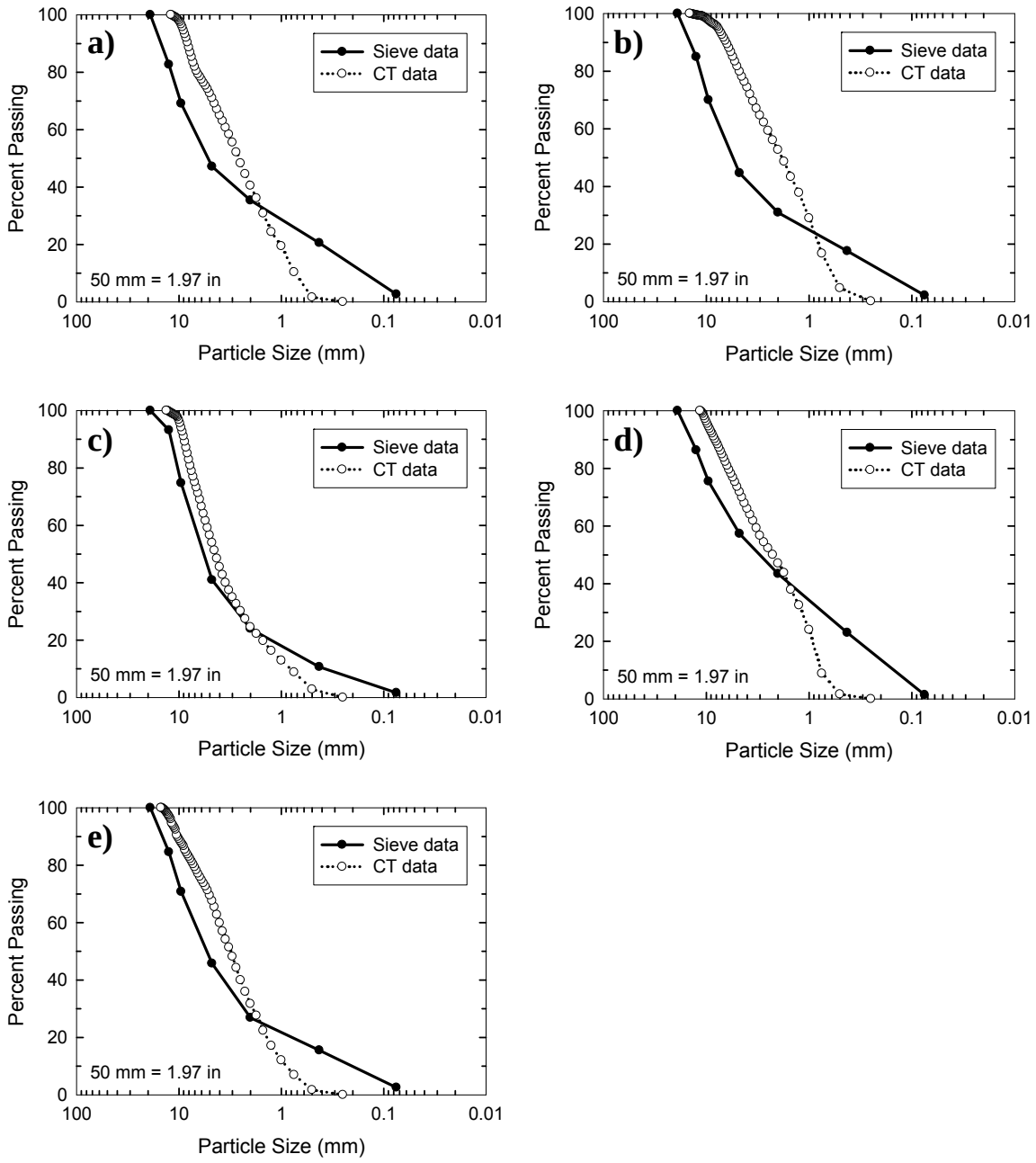

Figure E 3. X-ray CT Derived Grain Size Distributions for CTS-2A Samples: a) Billings, b) Glendive, c) Lewistown, d) Havre, and e) Missoula.